Nedim Radončić

Tunnel design and prediction of system behaviour in weak ground

Doctoral Thesis

Department of Civil Engineering

Graz University of Technology

Reviewers:

O.Univ.-Prof. Dipl.-Ing. Dr.mont. Wulf Schubert

Institute for Rock Mechanics and Tunnelling

Graz University of Technology

Professore Ordinario Dr. Giovanni Barla

Dipartimento di Ingegneria Strutturale e Geotecnica

Politecnico di Torino, Italy

Graz, March 2011

Acknowledgement

I was actually looking forward to writing this section – I saw it as the section of a PhD thesis with the lowest presence of formal constraints. Hence, Dear Reader, please forgive me if some of the following sentences appear cryptic and sound like insider-jokes and remarks: they certainly are, and it is definitely good that way.

Every single day of waking up and going to work at the Institute for Rock Mechanics and Tunnelling under the leadership of Prof. Dr. Wulf Schubert was tremendous fun and great privilege[1]. By a twist of fate, I was sitting in the rock mechanics lecture (as a student) in Spring 2003 and listening to this bearded, athletic and tall guy with a gravely voice talking about tunnel construction, common sense and Q nonsense. The assistants at the institute appeared to be laid back and competent at the same time. One day later, I was visiting every lecture and thinking that should I ever write a PhD thesis, I would like to do it at Prof. Schubert's Institute. Three years later, I dropped by to ask them for a favour: Charly had an interesting idea for my geotechnics project, and the idea turned out to be everything else but trivial. In addition, I was also utterly unmotivated that time – having finished the work on my master thesis. So I claimed that I need more time, but I would like to finish my studies and I PROMISE I will complete my work after the final exam. Sincerely: this DEFINITELY does not sound like a competent and reliable student. Three weeks later they offered me a job. Never figured out why (I wouldn't give it to me myself). So here I am: Wulf, thank You for being a great mentor, kommandante and colleague throughout the last five years. All in all, they have been the best five years of my life. My loyalty will never fail my vast gratitude.

Prof. Dr. Giovanni Barla immediately struck me as an elegant and competent presenter, doing excellent research into issues quite relevant for my thesis. He showed a great amount of interest and enthusiasm for our research work at the Institute. Thank You.

"When we're good, we're good, when we're bad, we're better" Gang: attentive eyes see that Carlos Grande Forrester (alias Dr. Karl Grossauer) is also briefly mentioned above. He really has a lousy butterfly swimming style, HOWeffer! he is very good in everything else. And he is particularly good at being my friend, although he constantly insinuates at my Balkan and his northern Balkan origins. I am also very proud that we wrote the article called "The influence of the global spherical coordinate system on measurement data interpretation difficulties and male cranial baldness" together, which is currently under review for "Nature".

---

[1] Apart from the days following meeting Dr. Pötsch, Dr. Grossauer and Dr. Pilgerstorfer for "one single beer" to "discuss some rock mechanics issues" at Rosy/Trudl's.

Abstract

The use of yielding elements in order to create a ductile support system gradually becomes international state-of-the-art in alpine tunnels in weak ground. In a stark contrast to their ever-increasing application and development of the element types, the design methods allowing a simple and reliable prediction of their influence on the system behaviour are still rudimentary.

The thesis addresses this issue, with a strict separation into three thematic units. The first part focuses on reviewing the currently available research and practical experience associated with tunnelling in weak ground, and attempts to make a clear classification of the causes for ground deformations and their interaction with the support. Subsequently, a novel method for predicting the system behaviour in case of full-face excavation and top heading - bench advance is presented, capturing the effects of the ground conditions, shotcrete rheology, support kinematics and yielding element behaviour within a relatively simple framework. Finally, a numerical case study with the goal of examining the influence of the currently available yielding element types on the system behaviour is conducted. The used numerical model is calibrated on the displacement measurement data from the exploratory tunnel Paierdorf, ensuring that the comparison is based on reliable input parameters.

Kurzfassung

Der Einsatz von Stauchelementen zur Erschaffung eines duktilen Ausbaus stellt, bis auf wenige Ausnahmen, den internationalen Stand der Technik im alpinen Tunnelbau bei verformungsfreudigem Gebirge dar. In einem starken Gegensatz zum breiten Einsatz der Elemente und ihrer intensiven Entwicklung sind die Entwurfsmethoden zur schnellen Abschätzung ihres Einflusses auf das Systemverhalten eher rudimentär.

Diese Arbeit konzentriert sich auf genau diese Fragestellung, mit strikter Teilung auf drei thematische Einheiten. Als erstes wird eine Recherche der gegenwärtigen Forschungsergebnisse und Erfahrungen durchgeführt, um eine Klassifikation der Ursachen und Mechanismen, die das Auftreten großer Verschiebungen verursachen und begleiten, vorzunehmen. Danach werden zwei neue Methoden vorgestellt, die eine Prognose des Systemverhaltens bei Vollausbruch und Kalottenvortrieb ermöglichen. Sie erfassen gleichzeitig die Einflüsse und Wechselwirkungen von Gebirgsverhältnissen, rheologischen Eigenschaften von Spritzbeton, den Stauchelementen und der Ausbaukinematik in einem einfachen Rahmenwerk. Schließlich wird eine numerische Fallstudie durchgeführt, mit dem Ziel der Untersuchung vom Einfluss der verschiedenen, zur Zeit am Markt verfügbaren Stauchelemente auf das Systemverhalten. Das verwendete numerische Modell und die angenommenen Gebirgseigenschaften wurden an den Messdaten aus dem Erkundungstunnel Paierdorf kalibriert, um sicherzustellen, dass die Ergebnisse des Vergleichs auf möglichst zuverlässigen Annahmen basieren.

Contents

1 Introduction

The ongoing expansion of European and world-wide infrastructure and the recent increase in realizing ambitious hydropower projects dictate the construction of numerous tunnelling projects. Due to their frequent position as "base tunnels" and their length, they frequently have to cross numerous tectonic faults under high overburden. Such geotechnical conditions inevitably are associated with loads unsustainable by conventional support concepts. This usually leads to severe damage of the lining and costly reshaping works in order to comply with the required structural integrity and clearance profile. The idea of using support measures featuring high ductility and thus developing support pressure in a controlled manner while deforming was presented as early as 1930 (Lenk, 1930) and extended to shotcrete linings in 1950 (Rabcewicz, 1950). In practice, a support concept featuring open shotcrete gaps and dense rock bolting was successfully applied in many alpine tunnels constructed in the nineteen seventies and nineteen eighties of the past century (Pöchhacker, 1974), beginning with the construction of the "Tauern Tunnel".

Following the "Galgenberg Tunnel" collapse (Riedmüller & Schubert, 1993), the awareness for advantages of a truly ductile support system, featuring a fully controlled development of the support pressure, was considerably raised and lead to application of low-cost yielding steel elements. With time, various yielding element types with improved mechanical characteristics have been developed internationally.

In contrast to the relatively intensive development of the yielding elements and their application, the theoretical framework for tunnel design has lagged behind. While the design requirements posed by the respective geotechnical conditions and rheological properties of the shotcrete are well known, the calculation methods allowing fast assessment of all relevant aspects of the system behaviour are currently rudimentary. This thesis deals with tunnel pre-design methods, presenting a set of novel methods and extensions to already established methods.

1.1 Symbols and abbreviations

1.1.1 Vectors and matrices

a	– fitting parameter vector
K	– Stiffness matrix
q	– load vector
q$_{err}$	– nodal unbalanced force vector
u$_{CP}$	– displacement vector of the control points
u$_\varphi$	– vector of nodal tangential displacements
$\Delta\boldsymbol{\varepsilon}_d$	– reversible creep strain increment tensor
$\boldsymbol{\varepsilon}_d$	– accumulated creep strain increment tensor
$\Delta\boldsymbol{\varepsilon}_{sh}$	– change of strain tensor due to shrinkage
$\Delta\boldsymbol{\sigma}$	– change of stress tensor
$\Delta\boldsymbol{\sigma}_{sh}$	–stress tensor correction due to shrinkage
$\boldsymbol{\varepsilon}$	– strain tensor
$\Delta\boldsymbol{\varepsilon}_{Dev}$	– deviatoric portion of the strain tensor increment
$\Delta\boldsymbol{\varepsilon}_{CR}$	– Creep strain increment tensor in the power-law implementation
$\boldsymbol{\sigma}$	– stress tensor
$\boldsymbol{\sigma}_D$	– deviatoric portion of the stress tensor

1.1.2 Scalars

$\dot{\varepsilon}_{CR}$	– specific creep rate (axial elongation and shear)
A	– power-law creep function parameter
A'	– flow rate method creep function parameter
A_{RB}	– cross-section area of rock bolts
A_{shot}	– cross-section area of the shotcrete lining
a	– advance rate
$C_{d\infty}$	– flow-rate creep parameter
c	– ground cohesion
$E(t)$	– Time – dependent Young's modulus
E_0	– Reference Young's modulus (no confinement)
E_{28}	– secant modulus of shotcrete at age of 28 days
E_i	– confinement corrected Young's modulus
E_{rb}	– Young's modulus of rock bolts
E_{shot}	– shotcrete Young's modulus
F^i	– force in truss element i
$f_i(x)$	– arbitrary function
F_N	– normal force
F_{rb}	– axial rock bolt force
$F_{rb,i}$	– shear force of the rock bolt at the i-th node
$F_{shear,i}$	– shear force at the i-th node

$F_{unbal,i}$	– unbalanced force at node i
F_{YE}	–Yielding element force
G	– shear modulus
H^*	– critical overburden function parameter
H_0	– critical overburden function parameter
H_{crit}	– critical overburden defining failure of conventional support
K	– bulk modulus
K_{abut}	– Abutment stiffness
K_{arm}	– Arm stiffness
K_{ass}	– Assembly stiffness
K_{CB}	– Beam stiffness
K^i	– stiffness of the i-th truss element
$k_{r,i}$	– correction factor for radial displacements, i-th control point
$K_{rb,shear,i}$	– shear stiffness of the i-th rock bolt
K_{RM}	– rock mass stiffness
K_{YE}	– Yielding element stiffness in the initial stages
$k_{\varphi,i}$	– correction factor for tangential displacements, i-th control point
L^i	– element of the i-th truss element
L_{seg}	– Length of the shotcrete segment
L_{YE}	– Length of the yielding element
L_{rb}	– Length of the rock bolt
m	– number of nodes associated with the lining discretization
n	– Janbu's parameter
N_C	– ratio between σCM and p0, indicating squeezing (according to Jethwa)
n_{gaps}	– number of yielding element gaps
n_{rb}	– number of installed rock bolts
n_{TE}	– number of truss elements (representing the lining)
n_{YE}	– number of yielding elements
$o(\lambda)$	– objective function describing dissimilarity between 3D and 2D displacement field at the moment of face passage
p_0	– primary stress level (according to Jethwa, 1984)
p_1	– primary stress level
p_a	– Atmospherical pressure
p_{Bolts}	– rock bolt support pressure contribution
$p_{L,max}$	– pressure associated with the maximum thrust in the lining
p_{Lining}	– support pressure contributed by the lining
$p_{max}(t)$	– maximum allowable lining support pressure
p_{sup}	– support pressure
p_{tot}	– overall support pressure
Q	– flow-rate creep parameter.
R	– tunnel radius

$r(x)$	– arbitrary reference function
R_{arm}	– Arm radius
R_{pl}	– plastic radius
$R_{pl,eq}$	– plastic radius at the equilibrium point
t	– time
t_{init}	– initial shotcrete age before it is subjected to loading
t_{shot}	– lining thickness
$u(x)$	– radial displacement at the face distance x
u_0	– radial displacement at face passage
$u_{0,i}$	– displacement of the i-th point at the moment of face passage
$u_{3D,r,i}$	– radial displacement from the 3D simulation, i-th control point
$u_{r,i}$	– radial displacement of the i-th point
$u_i(x)$	– displacement of the i-th point at the face distance x
u_{max}	– final radial displacement (no support pressure)
$u_{max,i}$	– displacement at infinite face distance, i-th point
$u_{n,corr}$	– normal displacement correction
$u_{n,tot}$	– total normal displacement
u_{rad}	– radial displacement
u_s	– shear displacement
U_{shot}	– Specific shotcrete energy density
$u_{\varphi,i}$	– tangential displacement of the i-th node
$u_{\varphi,i,RM}$	– rock mass tangential displacement at the i-th node, counted from shotcrete segment middlepoint
$u_{\varphi,tot}$	– tangential shortening of a shotcrete half-segment
V	– deformation modulus
W	– external work of the ground (general)
$W_{diss,int}$	– dissipation work on the intact rock material
$W_{diss,joint}$	– dissipation work on the joints
W_{full}	– external work of the ground in case of full-face excavation
w_k	– weight factor at k-th point
W_{sup}	– external work of the support (general)
W_{TH}	– external work of the top heading's upper arch
x	– face distance or general function variable
X	– Sulem's displacement function paramer
$z(x,y)$	– fitting surface
α	– shotcrete utilisation
β_{28}	– uniaxial shotcrete strength at the age of 28 days
$\beta(t)$	– time-dependent shotcrete strength
$\Delta C(t)$	– Time – dependent plastic creep rate
Δt	– time interval
Δt_{ex}	– time required for round excavation
Δt_{sup}	– time required for support installation

$\mathit{\Delta U}$	– internal change of the energy in the ground
$\mathit{\Delta U_{FOOT}}$	– work performed by "translation" of the top heading and settlement of the top heading feet
$\mathit{\Delta U_{lin}}^{i}$	– work performed by deforming the truss element i of the lining
$\mathit{\Delta U_{RB}}^{i}$	– work performed on the rock bolt at node i
$\mathit{\Delta U_{YE}}^{i}$	– work performed by deforming the yielding elements
$\mathit{\Delta W_{shear,i}}$	– dissipative work performed by frictional sliding between the lining and the rock mass, calculated nodewise
$\Delta\varepsilon_d$	– Increment of reversible creep strain
$\Delta\varepsilon_{sh}$	– Increment of shrinkage strain
$\mathit{\Delta\Pi}$	– change of the elastic potential
$\mathit{\Delta\Pi_{grav}}$	– change of the gravitic potential
ε	– radial strain in unsupported case
ε_{vol}	– volumetric portion of the strain tensor
ε_0	– critical overburden function parameter
ε_1	– axial strain at the time "1" (begin of interval)
ε_2	– axial strain at the time "2" (end of interval)
$\varepsilon_{sh\infty}$	– final shrinkage strain of shotcrete
ε_{yield}	– yield strain of rock bolts
λ	– stress relaxation factor
ν	– Poisson's ratio
σ_1	– axial stress at the time "1"
σ_2	– axial stress at the time "2"
σ_{CM}	– uniaxial rock mass strength (according to Jethwa, 1984)
$\sigma_{cont,i}$	– contact stress between shotcrete and ground, node i
σ_{rad}	– local radial stress in the shotcrete-ground contact surface
σ_{yield}	– yield stress of rock bolts
σ_θ	– hoop stress
φ	–friction angle of the ground
$\phi(\mathbf{a})$	– objective function
φ_{cont}	– friction angle in the shotcrete-ground contact surface

1.1.3 Abbreviations

MLS	– Moving Least Squares
NATM	– New Austrian Tunnelling Method.

2 State of the art

In order to obtain a safe and economical solution, the design of a ductile lining has to incorporate a plethora of geomechanical and structural influences. A brief review of the influences and an attempt of their classification is presented here, in order to enable a clear definition of the thesis' objectives and lay foundation for the discussion of results presented in the course of the thesis. The review deliberately follows the methodology presented in the "Guideline for the geotechnical design of underground structures with conventional excavation" (Austrian Society for Geomechanics, 2008), thus trying to address the following issues:

1. The description of the geotechnical properties of the ground;

2. The anticipated response of the ground to the excavation and summary of mechanisms "behind" the observed response;

3. Summary of support measures and construction methods applicable under the described circumstances;

4. Summary of the currently available calculation methods for predicting the system behaviour.

2.1 Structural and geotechnical features of tectonic faults

Since the construction of tunnels under high overburden in neogenous and weak ground of sedimentary origin is highly unlikely, the tectonic faults represent the most relevant type of geological formations in which large displacements can be expected. However, the material found in tectonic faults can be highly similar to sedimentary materials. Due to its origin, its structure can be highly complex and highly heterogeneous (Riedmüller et al., 2001). It possesses a set of structural and geomechanical characteristics which have to be kept in mind when trying to predict and/or interpret the system behaviour of underground structures in respective conditions.

2.1.1 Genesis and geological features

By definition, tectonic faults are planar geological dislocation structures, along which relative movement of the adjacent rock masses has happened. They are caused by brittle failure processes associated with low confinement pressures in the upper Earth's crust, in contrast to ductile shearing processes in its lower parts (Sibson, 1977; Riedmüller et al., 2001). The process of fault generation results in an internal structure of interlacing shear planes, tensile fractures and

heterogeneous fault rocks. The rock mass encountered in the fault is usually composed of the following two components:

1. Damage zone

   The damage zone is characterised by a dense fracture network and minor sets of veins filled with finely grained material. The transition from the parent rock is usually gradual.

2. Cataclastic rock mass

   The cataclastic rock mass is formed by intense fracturing. It is usually characterised by its fractal structure, thus featuring self-similarity of the grain size distribution on all scales (Figure 1, left). Simply put, no sharp boundary between "blocks" and "matrix" can be drawn, since "grains" of similar lenticular shape and *all* sizes can be found. The rock mass is usually intertwined with planes of strongly sheared material following the overall alignment of blocks (Figure 1, right).
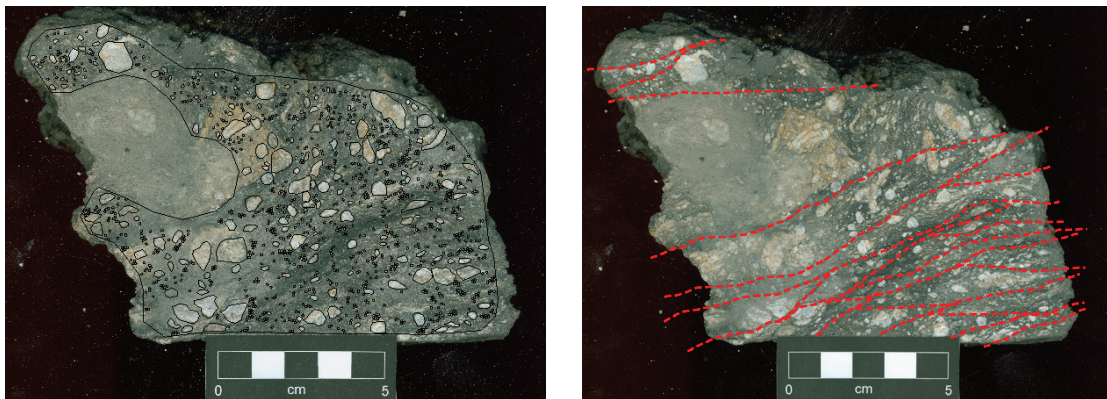
Figure 1. Left: Larger grains ("blocks") embedded in the matrix
Right: strain concentrations – "shear bands"
(courtesy of Dipl.-Ing. Florian Fasching, 3G)

The internal structure is usually asymmetrical with regard to the fault boundaries, and various qualitative and quantitative combinations of the components listed above are possible. The lenticular cataclasite grains are usually oriented in accordance to the predominant general direction of shearing (Figure 2).
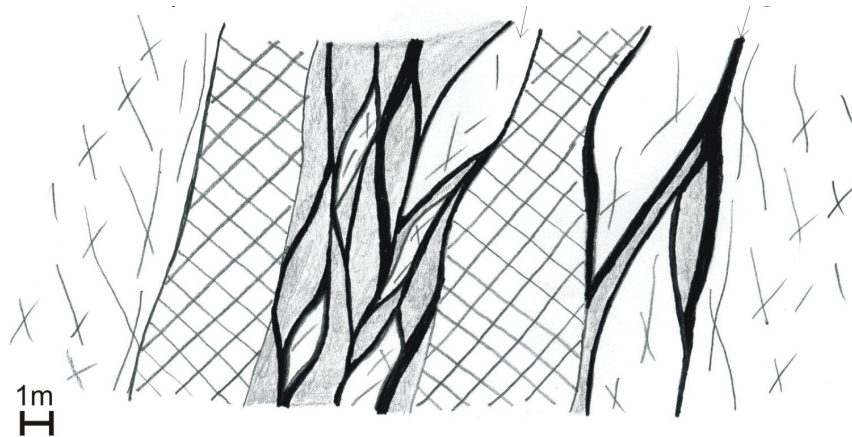
Figure 2. Above: Sketch of a fault structure composed of alternating zones of
intense fracturing and blocks embedded in finely and/or coarsely
grained cataclastic material (courtesy of 3G and ÖBB (3G, 2008))

Due to the variation of geological circumstances under which the fault was
created and on-going hydro/geo/chemical processes in a fault, it is hard to define
a generally applicable model. Many of the components listed above can be
completely missing, thus resulting in zones ranging from meter – wide densely
jointed areas to hundreds of meters – wide major faults consisting of extremely
weak fault material (Schubert, 1993; Dalgic, 2002).

2.1.2 Geomechanical properties

By the virtue of the heterogeneous and anisotropic structure described above, an
appropriate assessment of the fault zones' mechanical behaviour is challenging.
The retrieval of representative specimen from core drillings is sometimes nearly
impossible, due to the loss (spilling out) of the cohesionless material. In addition,
the laboratory results frequently have to be modified in order to account for the
scale effects and influence of more competent blocks.

Although a considerable amount of research on mechanical behaviour and
geomechanical characterisation of the block-in-matrix rocks has been performed
in the past (Medley & Goodman, 1994; Lindquist & Goodman, 1994, Riedmüller
et al., 2001; Sönmez et al., 2004), the peculiarities of a rock mass composed of
lenticular clasts and regularly aligned zones of weakness (shear bands) are not
fully understood yet. In addition, the strength and deformability of the fault rock
mass can be considerably altered by the relatively high primary stresses and
complex hydro chemical processes. Nevertheless, the published research results
draw a clear overall picture, and following statements are found:

1. As with all porous and granular materials, the deformability shows high
    dependency on the stress magnitude (Reinhold und Kudla; 2007,
    Habimana, 2002; Kulhawy, 1975). Disregarding the presence of

competent blocks, the rock mass features increasing stiffness with the increasing hydrostatic portion of the stress state.

2. Due to the relatively low grain competence, the strength envelope of the material is strongly influenced by the stress magnitude as well. Simply put, even if the coarse fractions dominate and high internal friction is anticipated, the grains themselves can fail under sufficient confinement pressure, thus circumventing the grain to grain interlocking and mobilising the cohesion of the grain material itself. With increasing degree of shearing and domination of small grain sizes, the influence of these effects diminishes and the initially curved strength envelope tends to the Mohr-Coulomb criterion (Habimana, 2002).

3. The softening behaviour of the material is still relatively unknown and can range from ductile behaviour (in case of dominating fine grains) to significant strain – softening in presence of more competent, larger particles.

4. The cataclastic rock mass can be (and usually is) highly anisotropic, due to the presence of a general orientation of the structure, caused by unidirectional shearing (Riedmüller et al, 2001). The shape of the blocks embedded in the matrix and the regularity of their orientation can cause strong differences in the dilatant behaviour of the material. Shearing through the blocks leads to relatively high strength properties but low dilatancy. On the other hand, blocks sliding along the weakness planes act like wedges and lead to considerable increase of displacements perpendicular to the sliding direction (Solak, 2006).

5. Both experimental and numerical studies show that the presence of blocks influences the deformability of the rock mass in a favourable manner (Pan et al. 2008; Lindquist & Goodman, 1994). Their influence on the strength properties seems to be complex: while the internal friction is considerably raised, the cohesion of the rock mass drops due to concentrations of shear strains in the matrix between blocks (Irfan & Tang, 1993; Lindquist & Goodman, 1994). However, these findings deal with the "usual" block in matrix rock masses, featuring spherical blocks and low anisotropy. The influence of blocks on the rock mass strength featuring a strongly correlated general alignment has to be examined yet, and is one of the current research foci at the institute (Pilgerstorfer, 2010).

6. The hydrochemical processes can lead to generation of swelling clay materials in faults, causing time – dependent and water – sensitive behaviour (Einstein, 1996).

2.2 Effects of excavation

The ongoing excavation of an underground structure continuously generates a new boundary free of normal stresses. This results in an instantaneous stress re-distribution, which initiates the inward movement of the excavation boundary. While the qualitative description of this simple mechanism is straightforward and intuitive, the quantitative estimation of the resulting displacement field is very challenging and always relies on a certain degree of idealisation and simplification. The process of "converting" changes in the stress field to displacements is governed by the ground strength, creep behaviour, long term – strength (associated with tertiary creep), pore – pressure redistribution and their interactions.

2.2.1 Immediate stress redistribution

The situation of tunnelling under high overburden in weak ground inevitably leads to secondary stresses exceeding the strength of the ground and forming of a deep failure zone around the excavation. This relationship is well understood (Rabcewicz, 1944) and numerous plane-strain closed-solutions for simple constitutive laws have been developed over time (Fenner, 1938; Kastner, 1962; Brown et al., 1984; Feder and Arwanitakis, 1976; Carranza – Torres, 2004). Three-dimensional analysis has proven that, in reality, the failure zone forms well ahead of the tunnel face (Figure 3) and causes gradual development of displacements with the growing face distance (Panet & Guenot, 1982; Barla, 2001; Hoek, 2008; Pilgerstorfer, 2008).
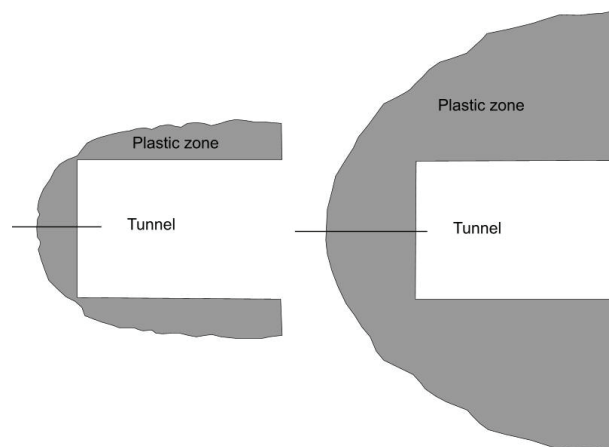
Figure 3. Development of a failure zone around an advancing excavation Left: shallow failure. Right: deep failure of the ground. (taken from Hoek, 2008)

For a long time, this simple three-dimensional effect of face advance was misinterpreted due to the practice of making time – displacement plots while omitting the face position. Simply put, if the longitudinal displacement profile is plotted against *time*, then different displacement characteristics *appear* to exist, even if the basic response is entirely time-independent and only caused by the face advance.

As a demonstration, a simple example is provided: the displacements ahead of the face (pre-displacements), final displacements and the plastic radius are determined by the solutions and relationships proposed by Feder (1976) and Hoek (2008) with the input parameters as presented in Table 1. The applied ground parameters and empirical relationships describe the displacement development due to elato-plastic stress re-distribution and face advance, and completely omit any kind of time-dependent behaviour.

Table 1. Applied ground properties

φ [°]	25
c [MPa]	0,71
E [MPa]	1000
v [-]	0,20
p_I [MPa]	15

In the first step, the longitudinal displacement profile is determined by the relationship proposed by Panet & Gueonot (1982). The relationship between face distance and radial displacement being thus determined, different advance rates are assumed and temporal information is assigned to the respective face positions. After plotting the radial displacements against the thus obtained time data, the ground appears to respond in a completely different fashion to the excavation. The displacements in a rapidly advancing tunnel appear to develop in an acute manner, while the slow progress implies a long and stretched out displacement development.
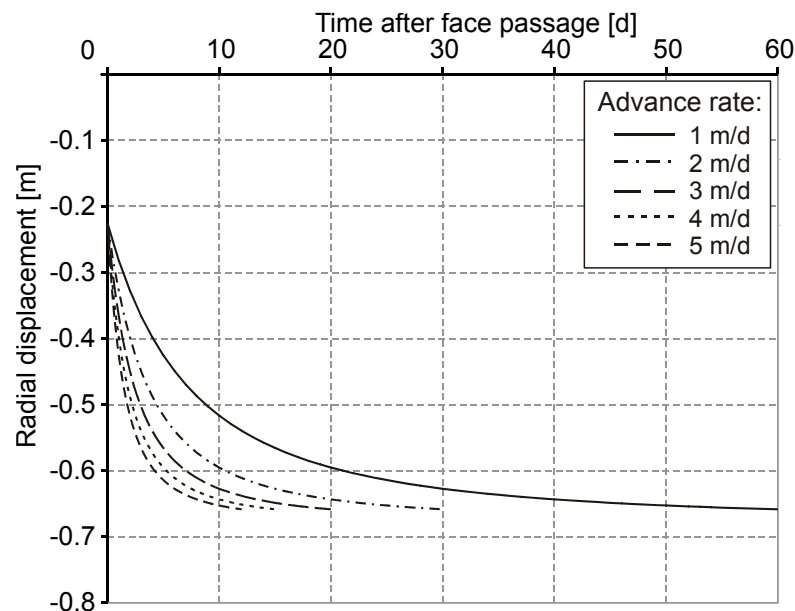
Figure 4. The *apparent* temporal influence on the displacement development

In reality, *all five cases* have been excavated in the *same* ground conditions, and the ground response to *the excavation* is exactly the *same*. Therefore, a proper analysis of the displacement monitoring data and conclusions with regard to the stress – redistribution mechanisms are only possible when spatial and temporal

information about the face position is recorded meticulously. If this information is scarce, it is impossible to differentiate between immediate stress redistribution, viscous behaviour, pore – pressure redistribution and transient processes in the shotcrete lining.

2.2.2 Influence of the structure orientation

As presented previously, tectonic faults usually possess a pronounced structure and anisotropy. Its influence on the ground behaviour and on the transient ground response due to the face advance has been observed by the displacement monitoring data from numerous tunnelling projects. The subsequent numerical calculations with continuum models and anisotropic constitutive laws (Goricki et al., 2005; Rupnik, 2008) and discontinuum models (Pötsch, 2001) have deepened the understanding of the underlying mechanisms. In general, both the ground behaviour and the system behaviour are always dominated by the poor shear stress transfer along the weak planes of intense tectonic shearing. As a consequence, the relative movement within the rock mass (sliding) caused by stress redistribution, almost always happens along these planes. Due to the lenticular shape of the more competent portions and generally intertwined shape of the planes containing the weak material, strong dilatancy occurs usually in the later stages of sliding (Solak, 2006). The displacement monitoring data from Wienerwald tunnel (excavated in flysch, featuring similar anisotropic structure) strikingly demonstrates the described mechanism (Figure 5). The right sidewall (measurement point 5) initially slides downwards in the plane of anisotropy, followed by dilatancy and strong backward and inward (against the direction of excavation) movement.
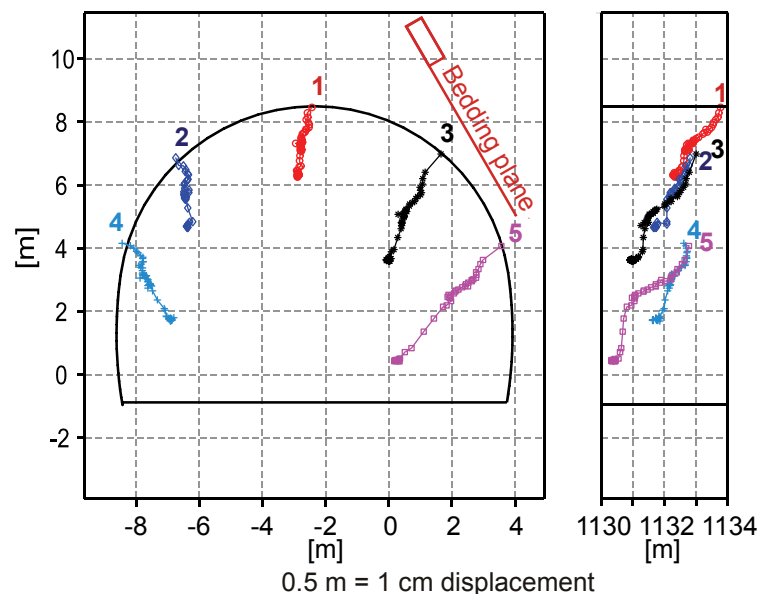
Figure 5. Displacement monitoring data from Wienerwald tunnel, chainage 1130.

In addition, the ground structure strongly influences the longitudinal displacement profile. The excavation perpendicular to the plane of anisotropy causes almost immediate stress redistribution in the cross – section plane, while the stress redistribution in the longitudinal direction is limited by the low shear strength of fine cataclastic material. This results in relatively low displacement magnitudes and a symmetrical displacement field, while the development of the displacements (with advancing excavation) is very acute (Figure 6).
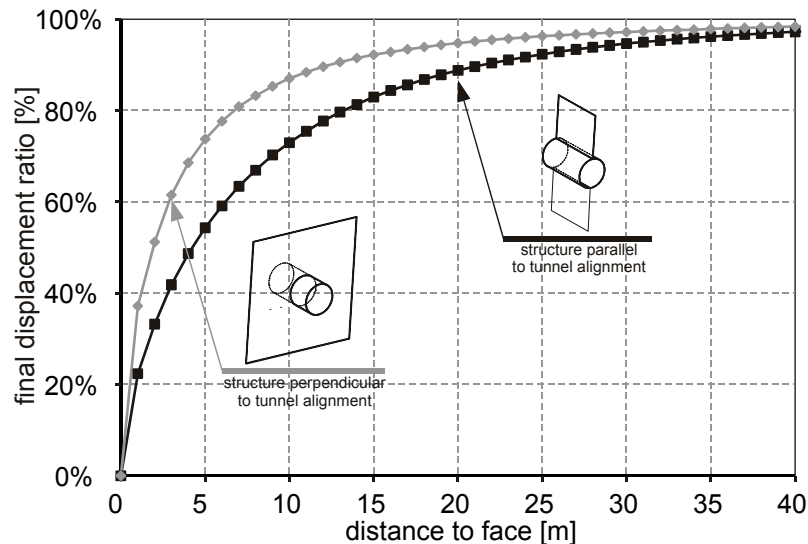
Figure 6. Longitudinal displacement profile normalized with the respective final displacement magnitude (taken from Goricki et al., 2005).

On the other hand, a tunnel alignment sub-parallel to the plane of anisotropy results in an unsymmetrical displacement distribution, long – stretched displacement development and high magnitudes of final displacements (Figure 6 and Figure 7).
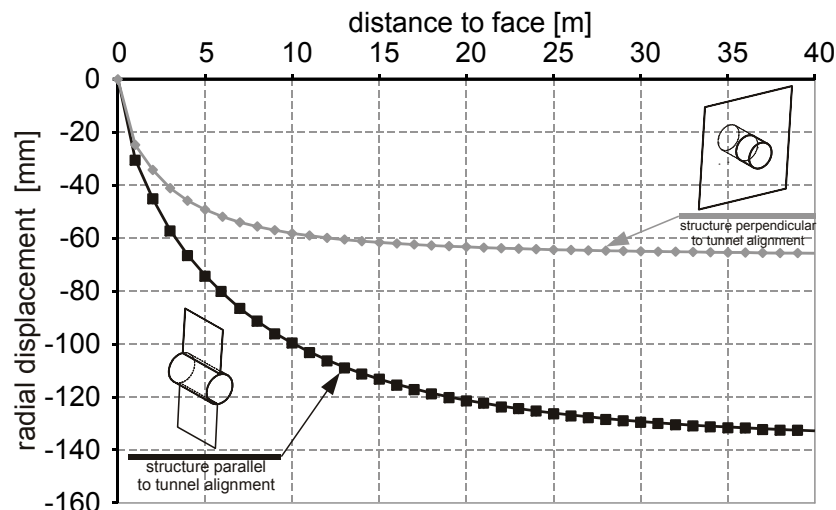
Figure 7. Longitudinal displacement profile for two tunnels in same material and with different relative orientations (Goricki et al., 2005)

2.2.3 Viscous processes

The viscous behaviour of geomaterials is a subject of research for many decades, with creep tests being conducted on soil and rocks as early as middle of the past century (Mitchell et al., 1968). The basic physical mechanisms are not yet fully understood and differ strongly, depending whether the material is porous (for instance: clay creep) or crystalline (metals and rocks). In crystalline materials, creep is caused by complex dislocation, diffusion and crystalline lattice damage processes. The dislocations happen at the atomary scale, and the movement at the microscale is influenced by the stochastic nature of quantum mechanics (Peltham, 1973). This renders creep in crystalline materials strongly dependent on temperature (Cristaceu & Hunsche, 1998), since an increase in temperature raises the amount of inner "movement" in the material. In clays, being composed of extremely fine grains, the grain movement is the dominant mechanism of creep, thus shifting the crystalline lattice dislocations mechanisms (Pusch et al. 2010) to the scale of clay grains.

In both cases, long lasting, time- and load-dependent deformations are the consequence, caused by the arrangement of micro-scale movements in accordance to the external loading. There is general agreement that creep is caused mainly by deviatoric stresses, while specimen loaded by a hydrostatic stress state exhibit practically no creep deformations. Most materials feature three distinct creep "phases" of creep (Figure 9):

1. *Primary creep* is characterised by the growing amount of dislocations and high strain rates. The strain rate decreases gradually with additional creep strains. This is the initial creep process following a change in the stress state, and reversible strains develop.

2. *Secondary creep* (or steady – state creep) follows the primary creep and is characterised by equilibrium between further dislocation generation and the decreasing potential for additional dislocations, with this effect being called work hardening. The creep rate is constant and the materials exhibit linear increase of strain with time.

3. *Tertiary creep* occurs if the stress level nears the short – term strength of material and/or the irreversible creep strain accumulated by the secondary creep reaches a certain threshold. In both cases, the crystalline lattice becomes damaged to such extent (either by excessive loading or by long-lasting secondary creep) that the generation process of additional dislocations in the lattice is unstable and leads to rupture.
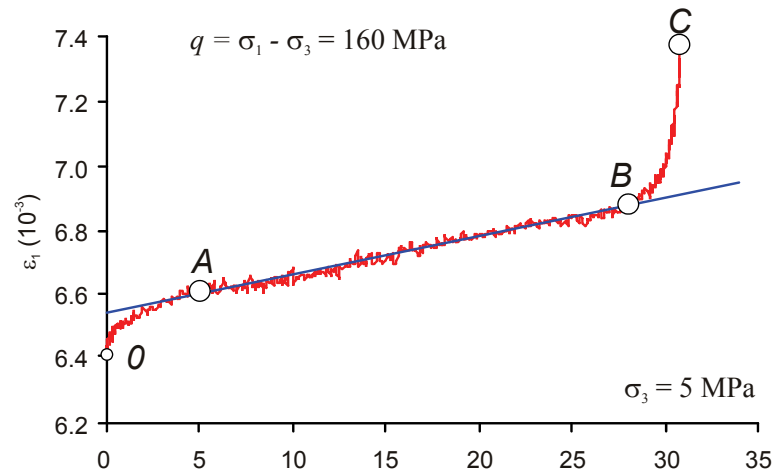
Figure 8. Typical results of a long-term creep tests (taken from Yang & Jiang, 2010) 0 – begin of deviatoric loading; A –transition from primary creep to secondary creep; B – transition to tertiary creep; C – specimen failure

In the recent years, intense research on relatively simple and practically applicable macro-scale models for creep in geomaterials has been conducted by Debernardi & Barla (2009), Bonini et al. (2007), Sterpi & Gioda (2009) and Yang & Jiang, 2010. The research is driven by two main issues:

- Assessment of the long-term behaviour of nuclear waste disposal sites, in order to prevent long-term damage of the support, especially in the view of the increased inner temperatures;

- Tunnelling in weak ground with high overburden, where time – dependent deformations (if occurring) can cause severe damage to the lining, since the shotcrete is usually already "old", featuring very high stiffness and low potential for sustaining additional displacements. In addition, mechanical excavation with a TBM can encounter severe difficulties if the ground continues to deform and locks the shield during a longer standstill (Debernardi & Barla, 2009). Extreme project delays and very costly auxiliary measures in order to free the trapped TBM are the usual consequence.

In general, the creep analysis of a tunnel excavation represents a highly transient problem. The ongoing and relatively fast advance of the face (when compared to the time magnitudes in creep processes) means that the ground is constantly experiencing changes in the stress state, and no steady-state creep is reached in the initial stages after face passage. As a consequence, only three-dimensional numerical analysis yields meaningful results when an assessment of creep effects is required.

Bonini et al. (2007) used the already established viscoelastic – ideally plastic constitutive law to model the time-dependent rock mass behaviour in clay shales occurring in the so-called "Chaotic Complex" of the Raticosa tunnel. Further research work (Debernardi & Barla, 2009) resulted in the development of new

viscous - elastic and viscous – plastic constitutive law (SHELLVIP), based on two concentric Drucker – Prager yield surfaces (one used for detection of the onset of creep, the other for "true" plasticity). In their plenary lecture paper (Barla, 2009), they report a good fit between model response and laboratory data. In addition, it has been successfully applied to predict the system behaviour of the Lyon-Turin access adit, excavated in graphitic phyllites (Figure 9). Unfortunately, the system behaviour was captured by convergence measurements and not by absolute displacement monitoring, thus loosing/blurring a significant amount of information about the influence of rock mass structure. In addition, no information about the recorded relative face position is presented.
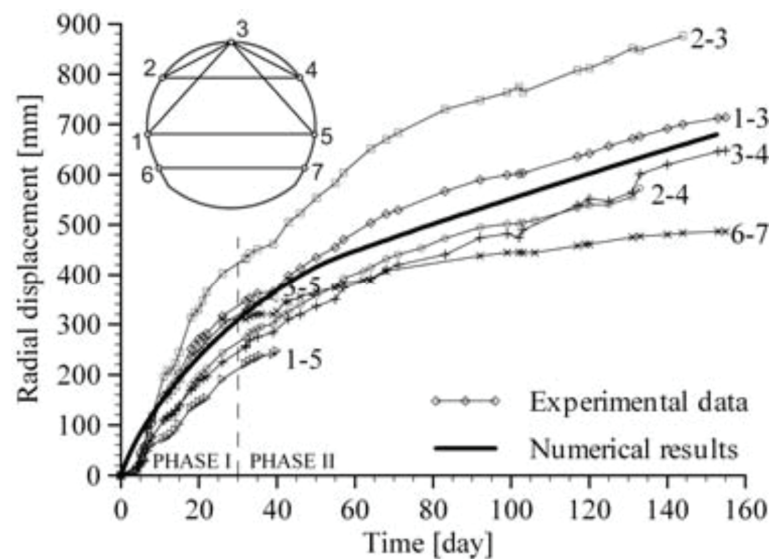
Figure 9. Comparison between convergence measurements and numerical analysis with SHELLVIP (taken from Barla, 2009)

In its current development stage, the SHELLVIP model is neither able to capture tertiary creep processes, nor strain hardening, however the authors stated these issues as goals of future development in their paper (Debernardi & Barla, 2009).

2.2.4 Pore water pressure redistribution effects

The geomechanical influence of pore water pressure re-distribution are well known for over half a century (Biot, 1941) and are being regularly applied in the engineering practice related to near - surface structures in soil. The main effects of the pore water subjected to a pore volume change due to disturbance in the stress field (excavation) can be simply described. In a highly permeable ground, the water is allowed to equalize the pressure gradient by movement (flow) and the grains are allowed to close the pores. This results in immediate deformation of the ground and full mobilisation of the ground strength. On the other hand, impermeable ground leads to pore water pressure build-up and water beginning to actively *bear* the additional volumetric stress. Since water has no shear resistance, this leads to an extreme decrease of the perceived ground strength: the normal stresses between the grains remain unchanged during the loading, but at

the same time, the grain structure has to deal with the full deviatoric stress. The macroscopic effect of such circumstances is that the angle of internal friction is perceived as equalling zero.

In reality, the ground permeability lies somewhere between the two bracketing cases mentioned above. The lower the ground permeability is, the longer lasts the pore pressure equalization processes (consolidation) and the ground becomes increasingly sensitive to sudden changes in loading.

In comparison to the soil mechanics engineering practice, examples of application of the consolidation theory to deep, alpine tunnels are very scarce. The heterogeneity of the ground and the limited knowledge of its properties make a sound hydromechanical characterisation a very difficult task. The existence of joints and their effect as aquifers renders the generally accepted fluid flow rules based on the assumptions of isotropic and homogenous material meaningless. True coupled calculations with discontinuum models capturing both the geomechanical and hydraulic behaviour of discontinuities and the interaction between discontinuity aperture, normal stress and its conductivity are very rare and usually represent academic examples. Even if the ground is assumed isotropic and homogenous, realistic results can be obtained only if a fully coupled geomechanical – hydromechanical three – dimensional analysis is performed. The excavation of the tunnel generates a continuously moving zero-pressure boundary, thus causing both a continuously changing stress field and changing boundary conditions for the fluid flow analysis. If the effect of the drainage ahead of the face is disregarded and an undrained analysis is performed, the results are too pessimistic and conflict the past centuries' experience in tunnel design and construction. On the other hand, complete neglecting of the pore water and consolidation effects leads to unsafe simplifications (Amberg, 2009; Anagnostou, 2009).

Additional problems associated with ground water are caused by the heterogeneity of tectonic faults. The fine cataclastic material usually features low permeability, while the strongly jointed zones may contain large amounts of pore water and high permeability. A tunnel heading through the fault gouge (low permeability) into an intensely fractured zone can result in extreme water and debris inflow, since the effect of advance drainage is hampered by the impermeable material (Leitner & Müller, 2007). The amount of research work on such effects is currently scarce, and the process is usually described only in qualitative way.

2.3 Tunnel construction in squeezing conditions

The construction of a tunnel in weak ground and high primary stresses is, in its most simplified form, nothing more than a problem of two pre-loaded, constrained springs. Over the past decades, the rock mechanics community established the term "squeezing conditions" in order to describe such circumstances. In this chapter, review and discussion of the proposed definitions for "squeezing" and criteria allowing identification of squeezing conditions is presented, along with construction methods which have been proposed and/or successfully executed.

2.3.1 Defining "squeezing"

There is general consent that „squeezing" occurs when secondary stresses are much higher than the ground strength, causing deep-seated failure of the ground and high displacement magnitudes. However, most criteria proposed for squeezing differ in the nature of the variables used for defining the boundaries. Two most common suggestions are the definition of a „critical strength ratio", defined as a ratio between uniaxial compressive strength of the ground and hoop stress at the excavation boundary, and the notion of a „critical strain" – representing a size-independent measure of deformations resulting in support failure. However, type and properties of the supports are not defined, leading to a useless criterion. In addition, several criteria based on application of empirical classification systems have been suggested as well.

Singh et al. (1992) presented a clear line in a diagram spanned by the Q-value of the ground and the overburden H (Figure 10).
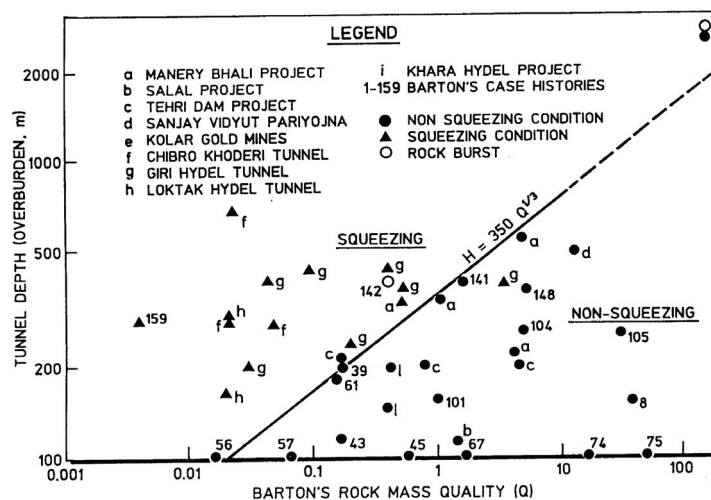
Figure 10. The Q-H diagram defining squeezing (Singh et al., 1992)
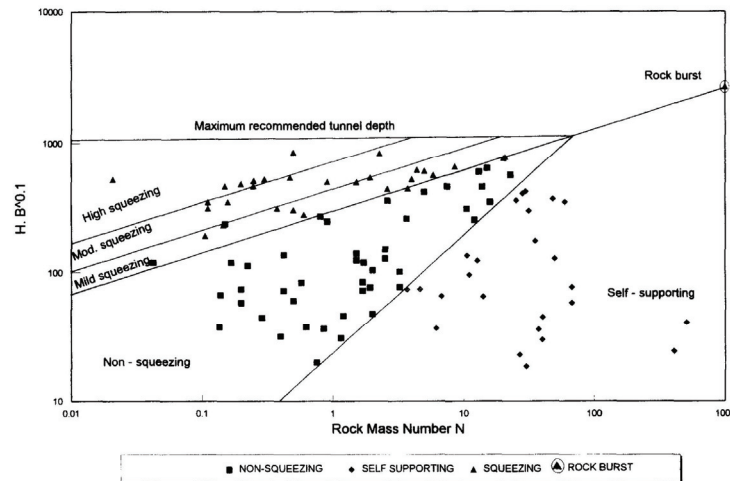
Figure 11. Q-H diagram defining boundaries of squeezing after Goel et al.,1995, with a corrected SRF (taken from Singh et al., 1997)

A similar criterion has been established by Goel et al. (1995) with a fixed SRF factor in order to circumvent severe causality problems associated with it (Figure 11). The notion of first determining the mechanical behaviour of the ground (by estimating the SRF-value) and then using the Q value to estimate the mechanical behaviour of the ground (by determining whether squeezing will occur or not) is obviously against common sense. However, even if this problem has been thus avoided, the Q system has been custom-tailored for jointed and massive rock mass, and most of its "ingredients" cannot be easily quantified in rock masses where high deformations occur. Simply put: a strongly tectonized fault gauge has neither a joint condition factor, nor a joint roughness coefficient, sometimes not even a uniaxial compressive strength (since it is often cohesionless) (Figure 3), thus making a serious treatment by an empirical classification system requiring these input values a futile effort. For these reasons, and for the sake of a sound and transparent engineering reasoning, the criteria based on empirical classification systems are not further treated or referred to within the scope of this thesis.

Figure 12. Core sample from a tectonic fault in the Koralm massif. Most of the fine material has been spilled out during the core drilling. Q value?

Jethwa (1984) defines a ratio between the uniaxial compressive strength of the rock mass σ_{cm} and primary stress level p_0 (Equation 1), and proposes that squeezing occurs when N_C is below 0.4.

$$N_C = \frac{\sigma_{cm}}{p_0}$$ **Equation 1**

This is a rough threshold, since it neglects both the deformability of the ground and the absolute level of the primary stresses. For example, a tunnel under 100 m of overburden (thus having a primary stress level of approximately 2.80 MPa), if excavated in a neogenic siltstone with a UCS of approximately 1.00 MPa, would have to feature very high deformations and high support loading. This is in direct conflict with many experiences from tunnelling projects under similar conditions.

Hoek (2001) and Aydan (1995) define levels of radial strain (calculated for an unsupported cavity and including pre-displacements) and associate them with different intensities of squeezing (Figure 13).
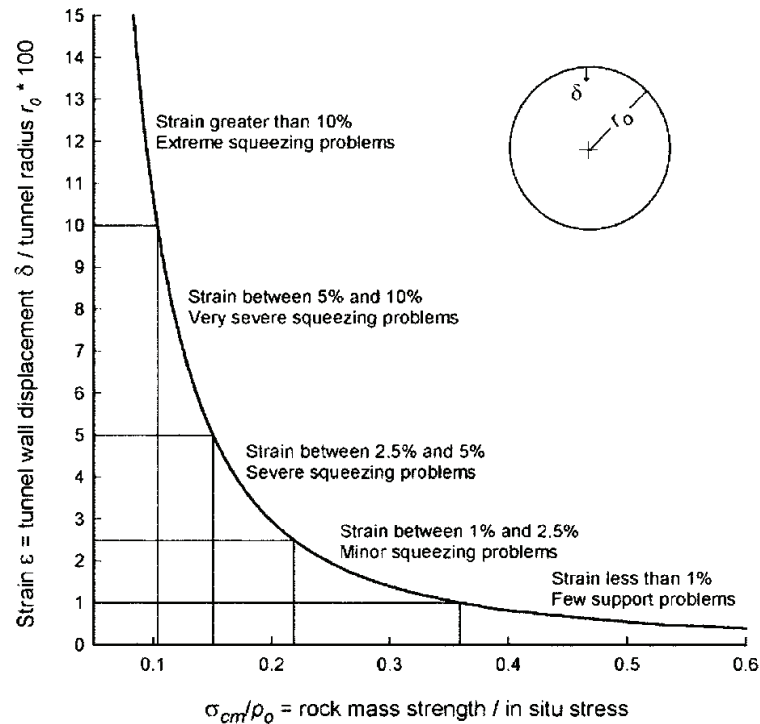
Figure 13. Tunnelling problems associated with different levels of radial strain according to Hoek (2001)

The thresholds defined by both authors are very similar and regard radial strains of approx. 1% as onset of "squeezing" and approx. 2% as a threshold for "severe squeezing problems". This is reasonable and agrees well with many theoretical considerations. However, it still does not take the absolute magnitude of primary stresses into account. For a relatively shallow tunnel in weak ground, 2% of radial strain in an unsupported state is nothing unusual, and can still be easily coped with by utilising a conventional stiff support. A deep tunnel featuring the same level of final deformations would result in the failure of the support in most cases.

Barla (2001) gives the following qualitative definition: "*Squeezing stands for large time – dependent convergence during tunnel excavation*", and in the further course of the paper, adds that "*The magnitude of tunnel convergence, the rate of deformation and the extent of the yielding zone around the tunnel depend on the geological and geotechnical conditions, the in-situ state of stress relative to rock mass strength, the groundwater flow and pore pressure, and the rock mass properties. Squeezing is therefore synonymous with yielding and time-dependence; it is closely related to the excavation and support techniques which are adopted.*" This is a holistic (and somewhat vague) definition; however it is thoroughly in line of reasoning presented in the course of this thesis and clearly states all influencing factors. Remarkably enough, it is the only definition mentioning the (extremely important) aspect of the installed support. Explicitly said: whether or not squeezing will be observed during the tunnel construction merely depends on the support capacity. If the support measures standing at our

disposal would have infinite load capacity and stiffness, then nobody would have ever observed "squeezing behaviour". The criteria for squeezing have to clearly incorporate the current support capacity limits. With time, as better support measures are available, the criteria would have to be updated as well.

2.3.2 Summary of support concepts

The traditional solution used for dealing with large displacements in mining is the application of TH – sets with sliding joints. The drawbacks of this concept are the low support capacity, uncontrolled behaviour when subjected to an unsymmetric displacement field and strong loosening of the rock mass due to high displacements and strains occurring. As already presented in the introduction, Rabcewicz (1950) proposed a segmented lining with wooden "yielding elements" as a modification to the emerging NATM support concept of shotcrete lining and rock bolts.
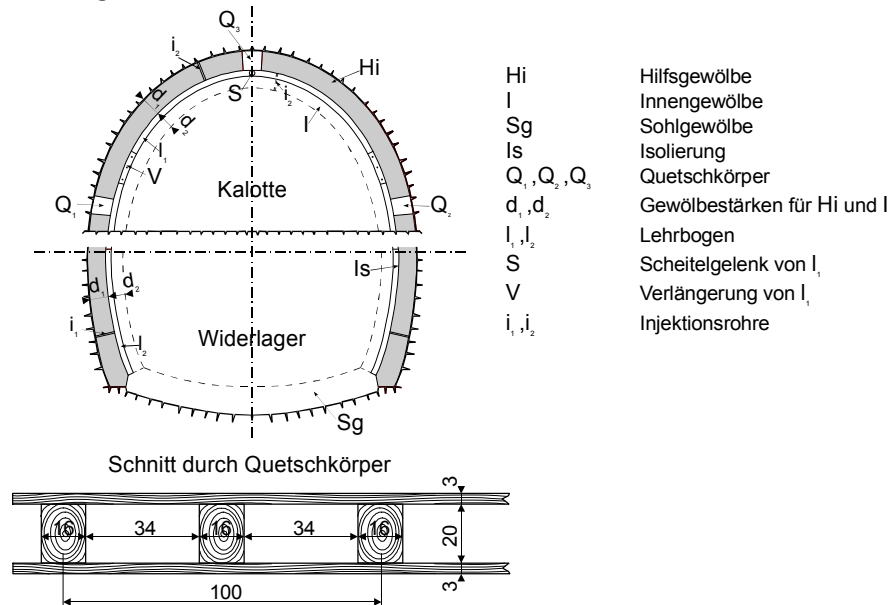
Figure 14. "Die Hilfsgewölbebauweise" as proposed by Rabcewicz (after Rabcewicz, 1950).

Over the time, numerous additional support concepts for dealing with large displacements have been developed. The concepts differ strongly due to the differences in design "philosophy" (resistance principle vs. yielding principle) and due to the requirements posed by the applied method of excavation. The applied support measures for conventional tunnelling can be roughly divided into:

- *Massive shotcrete lining*, featuring very thick shotcrete linings and dense rock bolting. Increasing the support capacity until compatibility between the support resistance and occurring displacements is reached appears, at the first look, as an intuitive and straightforward approach to the problem.

Unfortunately, the loading caused by the deforming ground is usually one order of the magnitude higher than the economically and technically obtainable support capacity. In the best case, the advance of the tunnel is very slow and expensive due to the sheer amount of support installed. In addition, a stiff support is only obtainable by a full face excavation and immediate ring closure or by utilising a temporary top heading invert. This results in either a significantly increased amount of face support measures and massive construction machinery (due the dimensions of the cross section) or in an *a priori* statically unfavourable shape of the lining (if applying a temporary invert). Sudden and spectacular failures as depicted in Figure 15 and extreme project delays are a regular consequence (Mahmutoglu et al., 2006; Schubert, 2008a; Hoek, 2009).

Figure 15. Excavation of the remains of the TBM, Yacambu Tunnel, Venezuela (taken from Hoek, 2009)

Another, very adverse aspect of a stiff support is the suppressing of displacements as a measured quantity, being the most direct indicators of the system behaviour. The interpretation of well-gathered displacement monitoring data allows not only directly assessing stability, but also predicting the ground conditions ahead (Schubert & Budil, 1996; Steindorfer, 1996; Schubert, 2002). Massive support results in low displacement magnitudes per default, rendering the analysis of system behaviour by the techniques mentioned above almost impossible.

- *Segmented shotcrete lining*, featuring dense systematic bolting and open gaps between shotcrete segments (Figure 16).
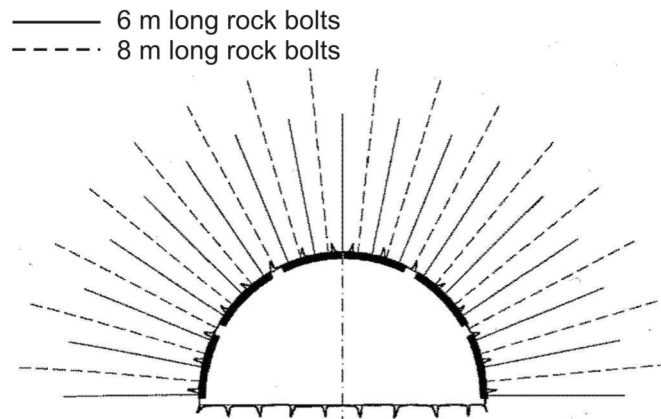
Figure 16. Typical support applied at the Inntal tunnel, taken from Schubert (1993)

This pragmatic solution was successfully applied in the Tauern tunnel (Pöchhacker, 1974), Arlberg tunnel (John, 1980), Karawanken tunnel (Schubert & Marinko, 1989), and Inntal tunnel (Schubert, 1993). The approach relies on gaps allowing for large deformations to take place without damage to the shotcrete lining, and a certain amount of support resistance being mobilized by the dense bolting and the dowel action between rock bolts and shotcrete segments (Pöttler, 1996; Schubert 1996, John & Mattle, 2008; Radoncic et al., 2009). Due to the fact that the concept deliberately avoids support resistance mobilisation, it was only used in a top heading advance without temporary invert. The subsequent construction of the bench has proven to be rather uncomplicated, since the major part of stress redistribution has taken place during top heading advance (Radoncic & Schubert, 2010). The drawbacks of this support system lie in a generally low support mobilisation, low utilisation of the shotcrete lining accompanied with large displacement magnitudes and reliance on rock bolts for overall stability and support resistance before the gaps are closed. As demonstrated in a rather tragic manner by the Galgenberg tunnel collapse (Schubert & Riedmüller, 1995), the occurrence of large displacements and strains in the ground can cause stress concentrations in more competent portions of the rock mass. For the same reason, considerable slip is induced between rock bolts and the grout, thus severely compromising the capacity of the rock bolts. The combination of these two effects can have catastrophic consequences: the system has low residual bearing capacity and the rock mass has a brittle response to the stress concentrations, leading to a sudden collapse (Schubert & Riedmüller, 1995; Blümel, 1996).

- *Segmented shotcrete lining with installed yielding elements*, applied as a consequence of the Galgenberg tunnel collapse, a revised support strategy with increased emphasis on support resistance and safety was devised. It

features yielding elements inserted in the shotcrete gaps (Figure 17), thus allowing deformations to occur, while granting a considerable amount of support pressure.

Figure 17. Top heading with four rows of installed yielding elements, Galgenbergtunnel, Haberlstörung (courtesy of Prof. Wulf Schubert)

The basic combination of shotcrete, rock bolts and yielding elements can be applied in conjecture with both top heading advance with or without temporary invert and in full face excavation with immediate ring closure. As proven at the Gotthard tunnel, the concept can be applied in combination with a hard rock TBM advance as well. However, the limited amount of overexcavation as provided by the TBM represents an additional design requirement which conflicts with the concept of a yielding support to a certain degree. Due to the presence of yielding elements, the structural integrity of the lining is usually not endangered, but even relatively low fluctuations in the ground quality can lead to too high displacements and a violation of the clearance profile. The application of elements with higher capacity inevitably calls for thicker shotcrete shells, thus decreasing the valuable space for deformations as well. This renders the design of ductile linings for a TBM advance a very sensitive and unforgiving task (Ramoni & Anagnostou, 2010).

- *TH sets with sliding joints*, as proposed by Kovari et al. (2005). The system has inherited the same drawbacks from its initial application in mining, featuring low support capacity and high sensitivity to the occurrence of bending moments due to an asymmetric displacement field.

Additional modifications to the pre-cast concrete segments used in shield TBM tunnelling have been proposed as well. However, the TBM advance (disregarding whether a hard – rock TBM, allowing relatively early installation of the support, or a shield TBM, is used) through a faulted ground is always associated with more difficulties than a conventional excavation. The limited amount of over-excavation and poor performance in severely fractured ground (frequently leading to the occurrence of an "advance face",

with loose material being removed without making any advance) pose practical limitations which cannot be easily circumvented. The length of the shield and the associated late activation of the support only increase the difficulties inherent to this construction method. As presented in chapter 2.2.1, the displacement development is strongly dependent on the face advance, thus a shield TBM can become stuck disregarding the advance speed (Amberg, 2009). This fact leads to two most likely scenarios: if the ground is so weak that the capacity of the pre-cast concrete segments is exceeded, then the machine would probably get stuck in the first place. On the other hand, if the ground features such a displacement development behaviour that the TBM does not get blocked, then the capacity of the support is probably not threatened in the first place. Thus, the application of ductile supports based on pre-cast concrete segments is limited to conditions featuring high degree of time dependency.

- *HPC (High Performance Concrete) pre-cast segments*, intended to replace the regular pre-cast concrete segments used in a shield TBM advance in portions where large displacements are expected (Wagner et al., 2009). The concept is based on merely increasing the support capacity of the pre-cast concrete segments to such level that the excessive displacements can be held at bay. The issues of significantly lower bearing capacity under asymmetric loading, irregular bedding by the pea gravel in the initial stages of loading and late support activation due to the length of the TBM shield are currently not answered in a satisfactory manner.

- *Ribbed pre-cast concrete segments*, as proposed by Vigl et al. (2007). It features specially shaped pre-cast concrete segments with outward ribs and spaces between them, thus allowing the ground to deform into these spaces without excessive build-up of support loading (Figure 18). The system has not been tested in practice yet.
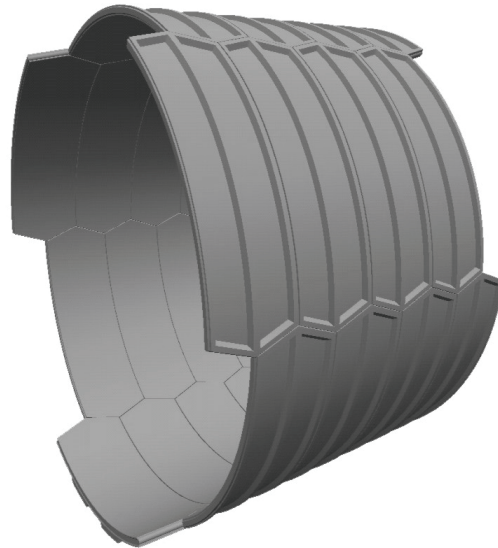
Figure 18. "Ribbed" pre-cast concrete segments (Vigl et al., 2007)

- *Pre-cast concrete segments with yielding elements* have been recently proposed by Eisenhütte Bochum and utilise yielding elements installed between pre-cast concrete segments. The flexible connection between segment rings in longitudinal direction is solved by steel dowels with ball joints, allowing for a certain difference in convergence. The issue of possible clearance violation associated with ductile support characteristic and limited TBM overexcavation ability has yet to be resolved.

- *Highly compressible mortar between ground and pre-cast segments* is intended to replace the pea gravel while tunnelling through weak ground (Schneider et al., 2005). The mortar is mixed with a significant content of Styrofoam material, thus granting high porosity and deformability of the mortar. The system has been successfully tested in the Jenbach tunnel, however only with logistical and construction aspects such as mortar pumpability and buoyancy of concrete segments in mind, and not in true squeezing conditions (Gamper et al., 2009).

2.3.3 Yielding element types

As already stated in the introduction, various yielding elements have been developed in the past 15 years. A rough differentiation is possible along the material used for the construction: porous elements based on cement materials and steel elements. Both groups feature a high amount of variation with regard to capacity and general load – displacement behaviour. An overview of the elements' basic functioning principle and their mechanical properties is given.

2.3.3.1 Lining Stress Controllers

The lining stress controllers have been developed at the Institute for Rock Mechanics and Tunnelling, Graz University of Technology (Moritz, 1999). The

system is being distributed by the ALWAG Company. It features groups of axially loaded steel pipes (Figure 20). The required space for deformation is granted through the appropriate choice of the length of the main tube, and no limitations are present with regard to the magnitude of shortening. The load displacement behaviour of a single element is characterised by a rather soft load mobilisation, requiring 40 – 100 mm of deformation until the yield load is reached (Figure 19).
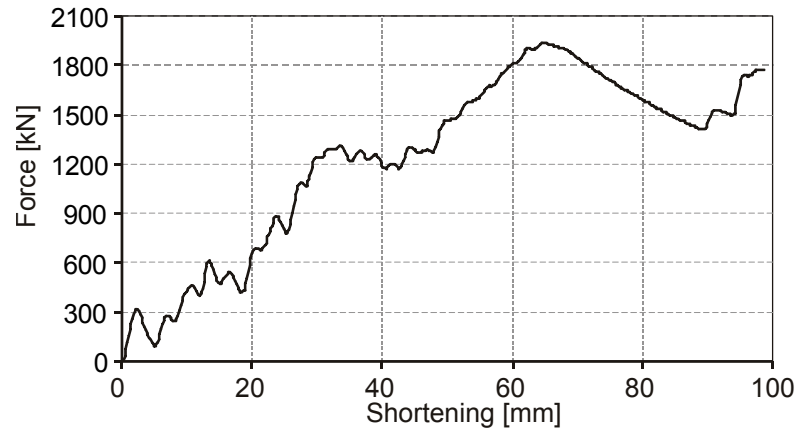
Figure 19. Load – displacement of a LSC element, Type B IIIb

The initially soft behaviour has been deliberately ensured by the taper of the central (load-bearing) tube, in order to prevent damage to the young shotcrete. The taper geometry can be varied in a broad range (in addition to the fact that either one side of the load-bearing tube or both sides can be tapered), thus granting great flexibility with regarding to the load mobilisation characteristic.

After the yield is reached, the elements feature small oscillations around the ideally plastic line, with the load level being kept stable by the two enclosing tubes and their interaction with the buckling behaviour of the central tube. The overall load-displacement behaviour of a group of lining stress controllers is steered both by the number of the used elements and by the appropriate length difference of the installed elements thus ensuring their staged activation (Figure 20).
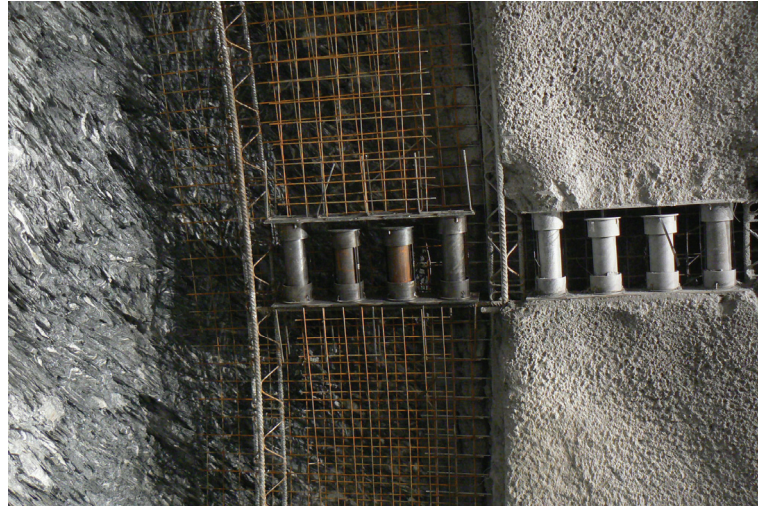
Figure 20. Built – in lining stress controllers (note the shorter inner pair of steel tubes, allowing staged activation of the elements and low initial stiffness. Photo by R. Vergeiner)

In the course of the research and development work conducted by Moritz (1999), various combinations of tube diameters and wall thicknesses have been examined, and seven distinct "models" of lining stress controllers have been developed. Their weight, basic dimensions and basic data with regard to the load – displacement behaviour are presented in Table 2. By using better steel quality (all experiments have been conducted on regular St 360) and changing other geometric parameters (pipe distance and wall thickness, taper), further combinations are possible, basically allowing the load-displacement behaviour to be custom-tailored to the project specific requirements.

Table 2. Summary of the LSC elements' properties.

Type	Shortening at yield [mm]	Force at yield [kN]	Av. yield force [kN]	Initial stiffness [kN/mm]
A I	40	225	200	5,6
A II	48	720	550	15,0
A III	44	850	750	19,3
B I	44	1050	900	23,9
B II	28	1300	1250	46,4
B IIIa	21	1850	1500	88,1
B IIIb	64	1950	1600	30,5
B IV	28	3200	3200	114,3

Type	D [mm]	t [mm]	H [mm]	m [kg]**
A I	88,9	2,9		4,36
A II	114,3	6,3		5,69
A III	139,7	6,3		6,82
B I	244,5	6,3		11,72
B II	355,6	8,0	400*	17,32
B IIIa	244,5	11,0		12,25
B IIIb	244,5	11,0		11,22
B IV	355,6	12,5		17,14

D – outer diameter of the central (load-bearing) tube
t – tube wall thickness
H – common element height
m – Weight
* - as already stated, the height of the element and the available shortening capacity can be modified depending on project – specific requirements.
** - The element weight has been calculated from the assumption of an overall element height of 400 mm, and confinement tubes having 300 mm.

2.3.3.2 WABE system

The WABE system has been developed and is being distributed by Eisenhütte Bochum. The elements are made of a group of steel tubes held in place by two steel plates and loaded transversely to their main axis. The ductile behaviour is achieved by the generation of plastic hinges at the sides and at the connection points of the tubes. An increase of the resistance can be achieved by subsequent insertion of additional steel tubes (Figure 21).

Figure 21. installed WABE elements
(please note the inserted additional tubes)

The required shortening can only be steered by adding further tube rows, thus being modifiable only stepwise, with the tube diameter as common divisor. As a positive effect, the initially stiff response becomes gradually softer with the installation of additional rows, in an analogy to a serial installation of springs.
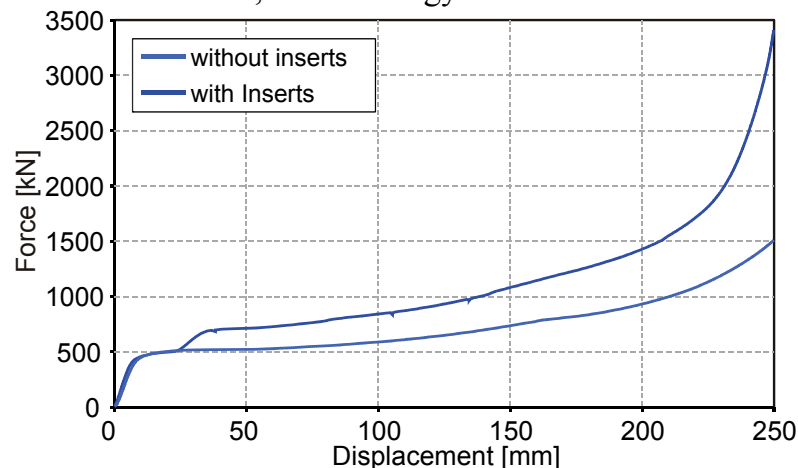
Figure 22. The load-displacement characteristic of the WABE element composed of three layers containing five tubes each (Schubert, 2008b)

Surprisingly, the initial response of WABE elements is very stiff. For the usual range of pipe dimensions, yield is reached after approximately 5 mm (single row), after which the load stays relatively constant until the ductile plateau of the steel is exhausted and final hardening takes place. In the laboratory testing on 5 tubes with 114.3 mm external diameter, 200 mm length and 7.1 mm wall thickness, yield load equalled 500 kN. Additional resistance is slowly, yet continuously mobilised by the decrease of the internal cantilever arm, since the plastic moment of the pipe wall cross section is basically constant. Numerical studies utilising steels with higher yield stresses show that higher yield loads are attainable as well. However the required mass of steel in order to obtain load levels comparable to LSC elements is much higher, and the issue of high initial stiffness remains.

2.3.3.3 hiDCon

The highly deformable concrete elements have been developed by Solexperts. The material used for the construction of hiDCon elements is based on high strength concrete matrix with porous additives (Figure 23).

Figure 23. Installed hiDCon element (taken from Barla et al., 2007)

Since the elements can be produced in all sizes, a stress-strain relationship instead of a load – displacement relationship is depicted in Figure 23. The relationship has been obtained from tests conducted on Politecnico di Torino in the course of the preliminary design of the Lyon – Turin access adit (Barla, 2009).
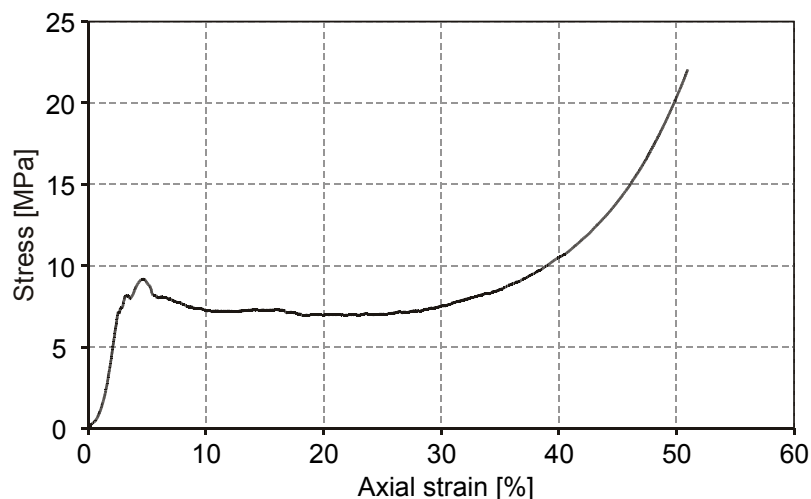
Figure 24. The stress – strain relationship of hiDCon elements, courtesy of Prof. Giovanni Barla

The material (and analogously the elements as well) features a relatively stiff initial response and yields at approximately 9 MPa. After the yield, the material behaves almost perfectly plastic up to an axial strain of 35% and keeps the stress level at approximately 7.5 MPa. The overall load-displacement behaviour of the hiDCon elements can be modified by insertion of Styrofoam sheets and/or appropriate choice of the element length (Barla, 2009). The density of the hiDCon material lies between 900 and 1300 kg/m³. Based on the load-

displacement relationship presented above (yield stress at approx. 10 MPa and yield strain of 4,5 %) and the mean density of 1000 kg/m³, the overview of the element weight depending on the initial stiffness and required yield load is presented in Figure 25. As it can be seen, the required height and the weight of the elements increase drastically with the required low initial stiffness.
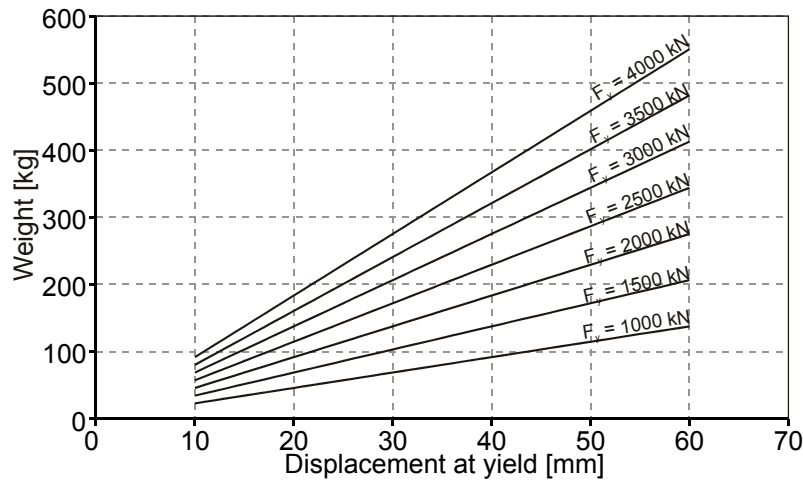
Figure 25. Dependency of element weight on the required initial deformability and yield load

2.4 Prediction of system behaviour in weak ground

The system behaviour is the result of the interaction between the excavation method, excavation sequence, support measures, ground properties and influencing factors (primary stress state, ground water conditions et cetera). Due to the uncertainties in the ground properties, the process of tunnel design has to result in a prediction of *measurable and observable* aspects of system behaviour, allowing timely identification of abnormalities and application (if any) of mitigation measures (Peck, 1969; Austrian Society for Geomechanics, 2008). Hence, the analysis of the interaction between the ground, excavation and support measures must not limit itself to providing evidence that the chosen support has the required capacity and fulfils the project specific requirements; it has to make predictions with regard to the expected final displacements, displacement development and/or other relevant quantities (in case of TBM tunnelling: pre-cast segment loading, machine operation parameters).

Currently, there are various approaches for assessing the system behaviour and a short overview is given in this chapter. The empirical rock mass classification systems are completely omitted, since they merely propose appropriate support concepts and no prediction of the respective system behaviour is possible.

2.4.1 Convergence confinement method

The convergence-confinement method is probably the oldest and most transparent technique for representing the basic interrelationships between the

ground properties, the primary stress state, the amount of pre-displacements and the support stiffness and support capacity when tunnelling through weak ground. In its simplest form, it requires two characteristic curves.

The "ground reaction curve" is obtained by gradually decreasing the support pressure applied at the circular excavation boundary of a two dimensional ground "slice". The gradually developing radial displacements of the ground are applied on the support, and the thus activated support pressure plotted against the displacements yields the "support characteristic curve". The intersection of the both is the point of equilibrium between the deforming ground and the installed support, while obeying the imperative of displacement compatibility of both system components. In the German – speaking region, this methodology is called "Fenner – Pacher Curve", named after the pioneering work of the two engineers (Fenner, 1938; Pacher, 1964) who were the first to propose the concept.

The most important extension to this concept has been published by Panet & Guenot (1982) and Sulem et al. (1987), allowing a construction of a "longitudinal deformation profile" (LDP), defining the dependency between radial displacement and the face position (Figure 26).
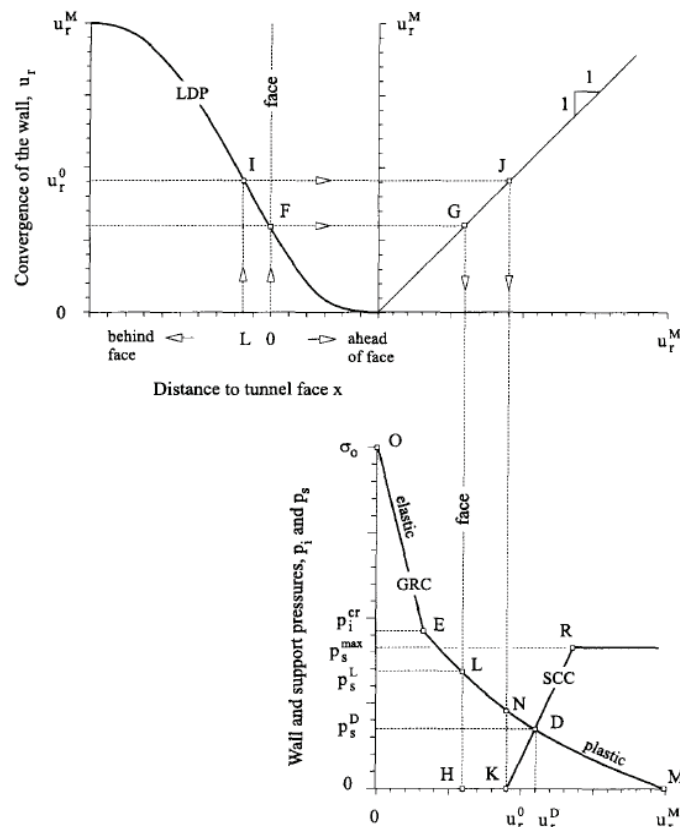
Figure 26. Schematic representation of the Longitudinal Deformation Profile (LDP), Ground Reaction Curve (GRC) and Support Characteristic Curve (SCC) (taken from Carranza – Torres & Fairhurst, 2000)

Additional empirical relationships describing the longitudinal displacement profile have been compared and summarized in Diederichs & Hoek (2008),

where the influence of the round length on the displacement development has been examined as well.

Based on results of a three-dimensional numerical analysis in elasto-plastic ground obeying the Hoek-Brown failure criterion, Hoek et al. (2008) published an empirical relationship assessing the pre-displacements in relation to the radius of the failure zone. In an independent and simultaneous research effort, Pilgerstorfer (2008) performed almost the same study in Mohr-Coulomb material and verified the aforementioned relationship.

When combined with the information gained from the longitudinal displacement profile, these recent additions allow incorporating the influence of the distance between face and support installation. They form a closed set of relationships with a limited space for speculation.

The drawbacks of the convergence confinement method are also easily identifiable:

- It is rigorously applicable only for isotropic, homogenous ground conditions and hydrostatic primary stress situation.

- It is rigorously applicable only in case of circular excavation shape and uniform radial displacement field (thus featuring no tangential displacements). Hence, only full-face excavation can be analysed.

- The determination of the influence of the "active" support measures (such as grouted rock bolts) can be conducted only by indirect means. Either the ground properties are changed in order to account for the presence of rock bolts or the ground is divided into annular zones and the force equilibrium equations (assuming displacement compatibility between bolt and ground) are solved numerically (Oreste, 2008). The latter approach yields reasonable results, however it is associated with considerable implementation effort.

- In reality, the excavation causes the surrounding ground to experience vastly different stress paths as the ones determined by the pre-relaxation analogy of a two-dimensional analysis (Barla, 2001; Anagnoustou, 2009). If more sophisticated constitutive laws are used, the results of a two-dimensional analysis can differ strongly when compared to three-dimensional analyses.

- The influence of pre-support measures (face bolting, spiles) can be assessed only by changing the assumed amount of pre-displacements. No true interaction between the installed support, ground and pre-support is assessable.

- The installed support influences the amount of pre-displacements (Barlow, 1986, Anagnostou, 2010). Especially in case of a massive support, the

convergence confinement analysis underestimates the support loading, since the stiff support reduces the pre-displacements and actively "attracts" the loads.

- The time-dependent behaviour of the ground and the shotcrete lining can be assessed only for the simplest assumptions of rheological behaviour. The shotcrete shows strong dependency on time, strain and stress history, thus causing a causal loop which is not solvable. In order to determine the final displacements while paying attention to the rheological behaviour of the shotcrete, the entire displacement/strain path up to that point has to be known. However, the longitudinal deformation profile can only be determined after the final displacements are known.

2.4.2 Numerical analysis

The numerical methods for solving the partial differential equations describing the mechanical behaviour of a (dis)continuum represent the state of the art since the middle of the past century. The discussion on the appropriateness of different *calculation methods* (discontinuum vs. continuum modelling) for dealing with prediction of ground or system behaviour is deliberately omitted, since this is an unresolved issue of rock mechanics and should be treated in a separate study. Currently, the commercially available numerical solvers can model almost all of the mechanical peculiarities from the field of rock mechanics in a relatively satisfactory manner. The practical application of the more sophisticated models is usually handicapped by the difficulties posed by the issue of finding appropriate calculation parameters, especially in the light of the natural scatter of the rock mass parameters in the first place.

The two-dimensional numerical analysis represents the state of the art in tunnel analysis for over four decades (Zienkiewicz & Taylor, 2006). The major drawbacks associated with the purely two-dimensional treatise of tunnel construction are basically identical (apart from the first three points) with the ones referring to the convergence confinement method, listed above. In addition, the ability to model more complex ground conditions renders the empirical relationships describing the amount of pre-displacements and the displacement development highly questionable. Hence, apart from simplest geotechnical models, the amount of pre-relaxation (in order to account for the effect of pre-displacements) has to be assessed by engineering judgment.

The three-dimensional numerical analysis accounts for most of the relevant mechanisms and interactions between the support and the ground. The pre-displacements, the displacement path and the support loading solely depend on the assumed ground properties and support characteristics. The effects of tunnelling through a heterogeneous ground and tunnel advance through rock mass with contrasting quality on the system behaviour are a priori captured and

in good agreement with the observed behaviour (Rupnik, 2008; Golser, Steindorfer, 1996; Mösslacher, 2007). Thus, a three-dimensional analysis predicts the system behaviour with the lowest amount of assumptions and outside interventions, with the displacement paths and associated support loading being "solely" the consequence of the assumed ground properties, constitutive law, calculation method and modelled support measures. The disadvantages are the long calculation times and the increased complexity of the numerical model, rendering parameter studies addressing the uncertainties in the ground conditions, still unfeasible in engineering practice.

3 Definition of objectives

After reviewing the state-of-the-art, the following issues requiring additional research and clarification associated with tunnelling in weak ground have been identified:

1. **Geomechanical characterisation of tectonic faults.**
   Having the presented mechanical behaviour of fault material in mind, the following issues have to be clarified:

   a) What are the appropriate laboratory testing procedures for the fault materials, and how the tests should be conducted?

   b) Derivation of rock mass properties on the scale of excavation, in the light of the anisotropy and general heterogeneity.

2. **Appropriate constitutive modelling.**
   After the rock mass characterisation has been performed, the determination of the ground and system behaviour has to be performed with an appropriate constitutive law. Hence:

   a) What are the appropriate constitutive laws for a realistic and comprehensive depiction of the mechanical behaviour of rocks?

   b) How can the heterogeneity and the internal structure be depicted? Are reasonable results always attainable with "smeared" continuum models, or is there a "threshold", after which only discontinuum models produce meaningful results?

3. **Derivation of additional semi-empirical relationships predicting the amount of pre-relaxation and longitudinal displacement profiles.**
   Since the two-dimensional analysis is indisputably the most meaningful calculation approach in the initial stages of design, the issue of pre-relaxation should be clarified in order to reduce the amount of speculation. The empirical relationships similar to the ones presented by Panet & Guenot (1984), Hoek et al. (2008) and Pilgerstorfer (2008) and should be derived for the more complex constitutive laws as well.

4. **Analytical and numerical modelling of support measures.**
   Regardless of the calculation method, there is still considerable room for improvement when referring to the modelling of the two most common support measures in tunnelling: rock bolts and shotcrete. Especially under intensive loading, shotcrete exhibits strong time-, load-, strain- and temperature-dependent behaviour. It creeps, shrinks and develops its strength simultaneously with its loading due to the tunnel excavation and associated deformations (Schubert, 1988; Aldrian, 1991; Hellmich, 1999). The assumptions of linear elastic and ideally plastic behaviour are rudimentary (at best) under such circumstances. In addition, the models

describing the mechanical behaviour of rock bolts in highly deformable ground, involving a plethora of interactions between the rock bolt, young grout and weak rock mass, are still very rough and simplified.

5. **Comparison of yielding elements and their influence on the system behaviour**. There is still no objective decision making criterion regarding the application of one or another yielding system. The reason lies in the lack of simple design methods due to the multitude of influential factors. Schubert (2008b) examined the influence of the various yielding elements' load-displacement relationships on the shotcrete utilisation, however assumed the same displacement development in all cases. The paper by Radoncic et al. (2009) contains a more comprehensive examination, taking the influence of the load-displacement behaviour on the support mobilisation (and thus, on the final displacements) as well. However, the calculation model used in that study is also based on two-dimensional analysis and empirical relationships assessing the longitudinal displacement profile.

Based on these conclusions, the goals of this thesis have been defined:

1. Derivation of new relationships for the calculation of the support characteristic curve and incorporating the kinematics of the ductile support measures in conventional tunnelling. In addition, the time-dependent strength development has to be incorporated as well, in order to enable sound reasoning with regard to the applicable yielding elements' load-displacement characteristics and the overall support layout.

2. Designing and conducting in-situ shear tests in order to determine the bond characteristics between shotcrete and cataclastic rock mass.

3. Extending the convergence-confinement method, making treatment of non-circular geometries possible as well. The main goal is not the replacement of the two-dimensional numerical calculations, but the development of means for fast and reliable system behaviour assessment. Such a method would make the probabilistic treatise of the system behaviour in the initial stages of design possible, thus allowing execution of sensitivity analyses and determination of lower and upper boundaries for the dominant aspects of the system behaviour.

4. A comparison of the different yielding element types and their influence on the system behaviour using a three-dimensional numerical model. The constitutive law used for modelling of the ground has to be able to depict most of the mechanical characteristics listed in chapter 2.2.1. In addition, a comparison of system behaviour featuring top heading excavation, temporary invert and full-face excavation is conducted as well. Finally, the influence of uncertainties in the ground properties on the system

behaviour is analysed, with particular focus on the respective displacement development and shotcrete utilisation.

The issues of geomechanical characterisation of faults, appropriate numerical modelling and derivation of additional pre-relaxation relationships are treated only marginally in the further course of this thesis, since they are the main topics of separate research efforts at the institute (Pilgerstorfer, 2010; Leber, 2010). The issue of modelling of rock bolts in weak ground is left at status quo. The improvement of both, the insight regarding this particular ground-support interaction mechanism and the associated analytical or numerical model development is left to future researchers.

4 Pre-Design

The developed extensions to the convergence confinement method and its application to ductile lining design are regarded as support pre-design utilities, due to the unavoidable simplifications in the assessment of the system behaviour. The focus lies on correct treatise of the kinematical behaviour of a lining shell with integrated yielding elements and the determination of its influence on the overall support response. In addition, a novel method based on work balance considerations and allowing application of the convergence confinement method to both non-circular geometries and anisotropic ground conditions is presented as well. Finally, the work balance is also used for defining the novel boundaries of "squeezing".

4.1 System behaviour with yielding elements

Since the system is subject to loading from the moment of its installation, the design of a ductile lining has to consider the time and face position dependent displacement development, rheological behaviour of shotcrete, rock bolt action, yielding element load-displacement relationship and the kinematics of the entire support concept in order to come up with a safe and economical solution.

The application of yielding elements results in certain kinematical peculiarities which have to be accounted for. Since the deformations are mainly being "absorbed" by the yield elements, this inevitably results in relative displacements (slip) developing between the shotcrete and the ground, and additional shear loading of the installed rock bolts (Pöttler, 1996; Mattle & John, 2007; Radoncic et al., 2009). The occurring slip and its consequences have a significant influence on the axial forces in shotcrete segments and the overall support mobilisation. In addition, if only the top heading is excavated, the axial loading of the shotcrete is usually unsustainable by the ground beneath the lining feet, and they considerably penetrate into the ground. This leads to the generation of two additional "yielding elements" and translational movement of the entire support (Figure 27).
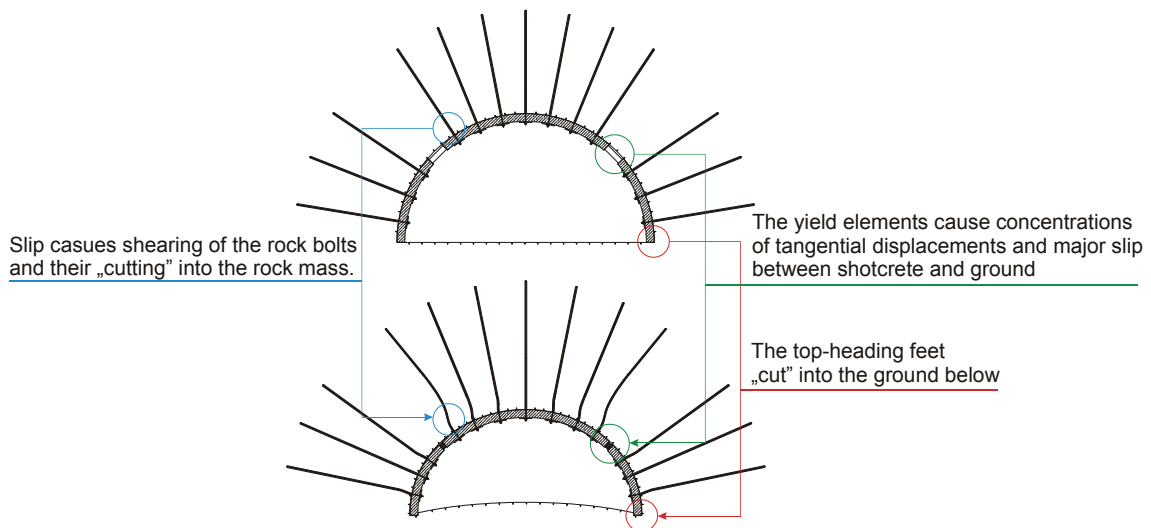
Figure 27. Large deformations and their influence on the lining incorporating yielding elements (top: undeformed system state. bottom: deformed system state).

The ductile systems based on radial "buffer zones" such as "Compex" and ribbed pre-cast concrete segments behave in a completely different manner. The excessive deformations are accounted for by providing additional radial deformation space, thus leading to no concentrations of tangential displacements and relatively low slip between the rock mass and the pre-cast segments. As already stated in chapter 3, these ductile systems are not treated within the scope of this thesis.

4.1.1 Time-dependent shotcrete properties

There are numerous research works concerning the influence of ongoing hydration under simultaneous loading on the mechanical behaviour of shotcrete (Schubert, 1988; Aldrian, 1991; Hellmich, 1999; Macht, 2002; Pichler, 2009; Schütz, 2010). They unanimously state that the globally perceived deformation behaviour is a consequence of the entire strain, temperature and loading history, with the majority of deformations being caused by non-reversible time – dependent strains. The secant Young's moduli determined under such circumstances are an order of the magnitude lower then the moduli of completely hydrated concrete applied in normal civil construction. Neglecting this fact leads to an exaggerated support stiffness and an unrealistic prediction of system behaviour.

4.1.1.1 Overview of the available constitutive models

The empirical relationships presented by Schubert (1988) and Aldrian (1991) are applicable only to uniaxial stress states. In addition, the estimation of the associated material parameters is very tedious and has to be performed for every new shotcrete mix (Figure 28).
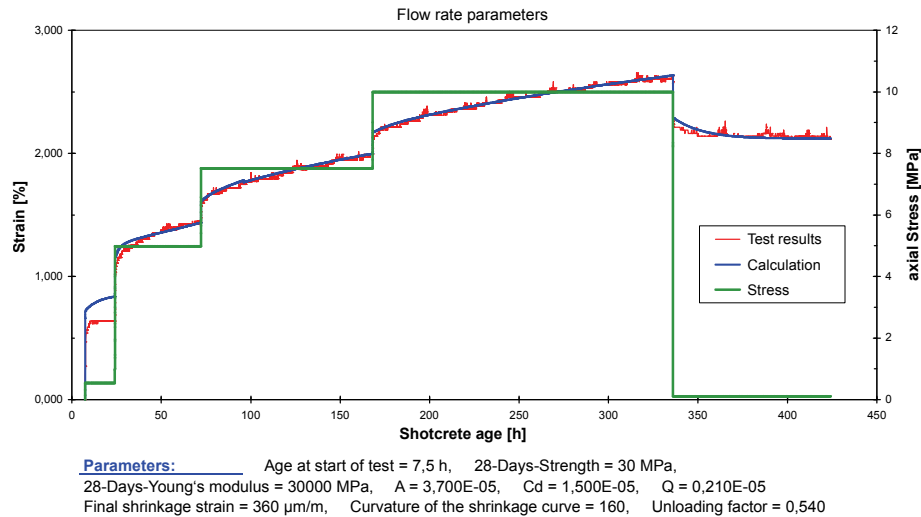
Figure 28. Least squares fit between the empirical relationship by Aldrian and long-term creep test on young shotcrete (Müller, 2001).

The thermo-chemo-mechanical model, as presented by Hellmich (1999) and Macht (2002), takes a different approach and tries to predict the mechanical shotcrete behaviour on the basis of the mesoscopic mechanisms (thermal and chemical) associated with the hydration and loading. This model has been successfully incorporated in a commercial monitoring software application TunnelMonitor (Brandtner et al., 2007), allowing the back-analysis of shotcrete stresses from the displacement monitoring data. The required input parameters are associated with the thermodynamical aspects of hydration, and scatter much less than the ones required for the empirical relationships mentioned above. Unfortunately, currently there are no commercial numerical solvers incorporating this kind of material behaviour.

Pichler et al. (2009) are developing a completely new constitutive law for shotcrete, based on the assumption that the only "true" variable in the shotcrete rheology is the water/cement ratio of the hydrate paste. The amount of aggregates in the final shotcrete is accounted for by complex up-scaling relationships. The approach is very promising, with both time – dependent elastic response and the strength development being in good agreement with laboratory testing. Current development is devoted to incorporating the time-dependent irreversible deformations. The advantages of this approach are great: the costly parameter estimation tests could be completely circumvented, since the model would be able to correctly predict the rheological behaviour of the shotcrete based only on its "recipe".

Schütz (2010) has developed a new viscoplastic constitutive law capturing the macroscopic behaviour of shotcrete, thus being somewhat of an extension to the empirical relationships presented above. It is able to capture the shotcrete behaviour under multi-axial loading; however it also relies on an extensive testing program in order to determine the required model parameters.

4.1.1.2 Realistic shotcrete stiffness assessment

In order to obtain more realistic initial values for shotcrete deformability, a parametric study was conducted with the relationship proposed by Aldrian (1991), while the respective parameters have been taken from the in-situ testing results presented by Müller (2001). The utilisation ratio (defined as ratio between the current stress and the available shotcrete strength) was kept constant, and the stress-strain curves were calculated for the first ten days (Figure 29).
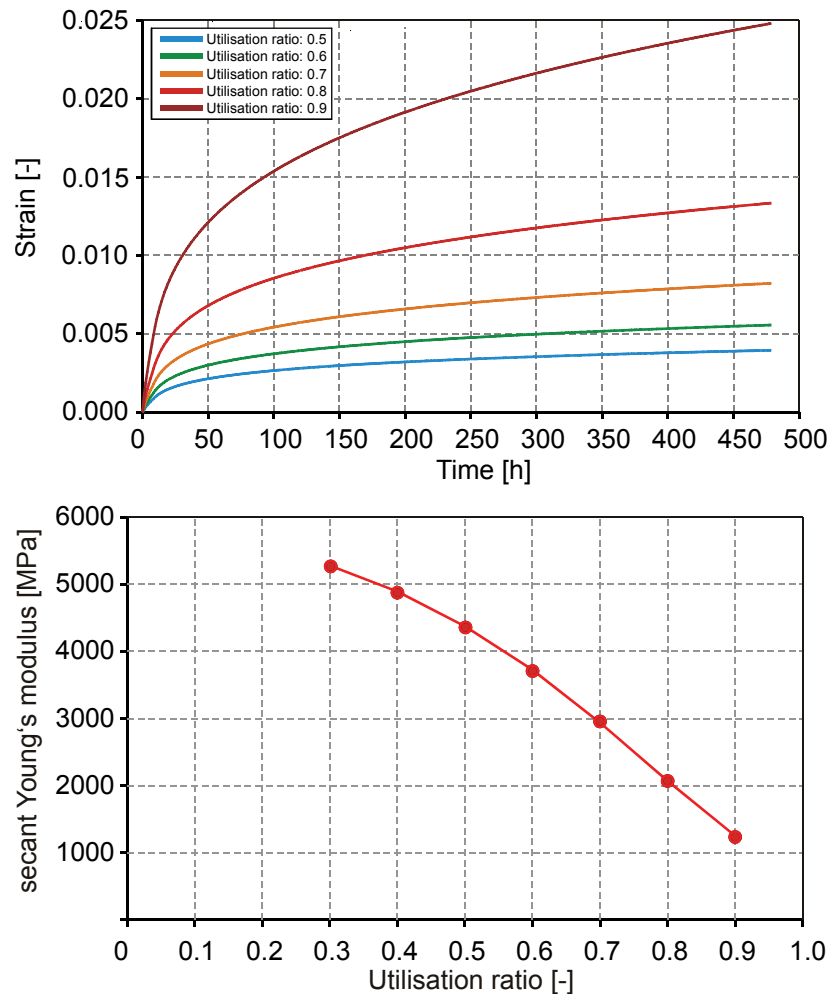
Figure 29. Top: the time-strain relationships of shotcrete for the first ten days in dependence from the utilisation ratio. Bottom: the associated secant Young's moduli (Radoncic et al., 2009).

An assumed secant Young's modulus is correct (in strict manner) only if the final displacements, the mobilised support resistance and the strain evolution are identical to the initial assumptions. Hence, the only possibility to take these interactions into account during the calculation is by applying a correct rheological model and implicitly solving the interaction between the ground and the lining. This renders the rigorous estimation of the shotcrete stress path a very challenging task and limits it only to three-dimensional analyses.

4.1.2 Mechanical behaviour of rock bolts

In stark contrast to their frequent application as a support measure, the mechanical behaviour of grouted rock bolts can be only qualitatively described. Due to the intricate displacement field caused by the rock mass structure, the rock bolts are loaded in a highly complex manner. The main effects of the systematic rock bolting are the increase of "ductility" in the system behaviour, caused by the homogenisation of the ground and "smoothing" of the shear movement along the discontinuities (Hoek, 2007; personal discussion with Prof. Schubert; Oreste, 2008).

4.1.2.1 Behaviour under axial loading

The rock bolts (and thus, the grout as well) are subjected to extreme displacements from the moment of their installation. Disregarding the structural and all other influences, the displacement rate is always highest after the face passage (Sulem et al., 1987). In the Inntal tunnel, the first –day measurements of up to 20 cm have been recorded, with final displacements in the order of the magnitude up to one meter regularly occurring (Schubert, 1996). This implies that in case of rigid bond between the rock bolts and the ground, the rock bolts almost immediately have to yield and that the failure strain of steel is regularly reached in further stages of loading. The experience clearly contradicts these conclusions.

In reality, the rock bolt mobilisation is considerably lower and the distribution of the axial forces is much more complex than assumed by most models. Considerable slip occurs both between the rock bolt and the grout, and the grout and the surrounding rock mass. As shown by Blümel (1996) and more recently Kilic et al. (2002), the grout is very young at the onset of loading, rendering the mobilisation and final capacity of rock bolts strongly dependent on the rate of deformation and the rib geometry (Figure 30).

In presence of discontinuities or planes of favoured movement (such as shear bands formed by tectonic faulting) the mobilisation of rock bolts becomes even more intricate. The bending of the rock bolts generates areas where slip of the rock bolt is hindered, and the subsequent strains are concentrated on the portions between such points.
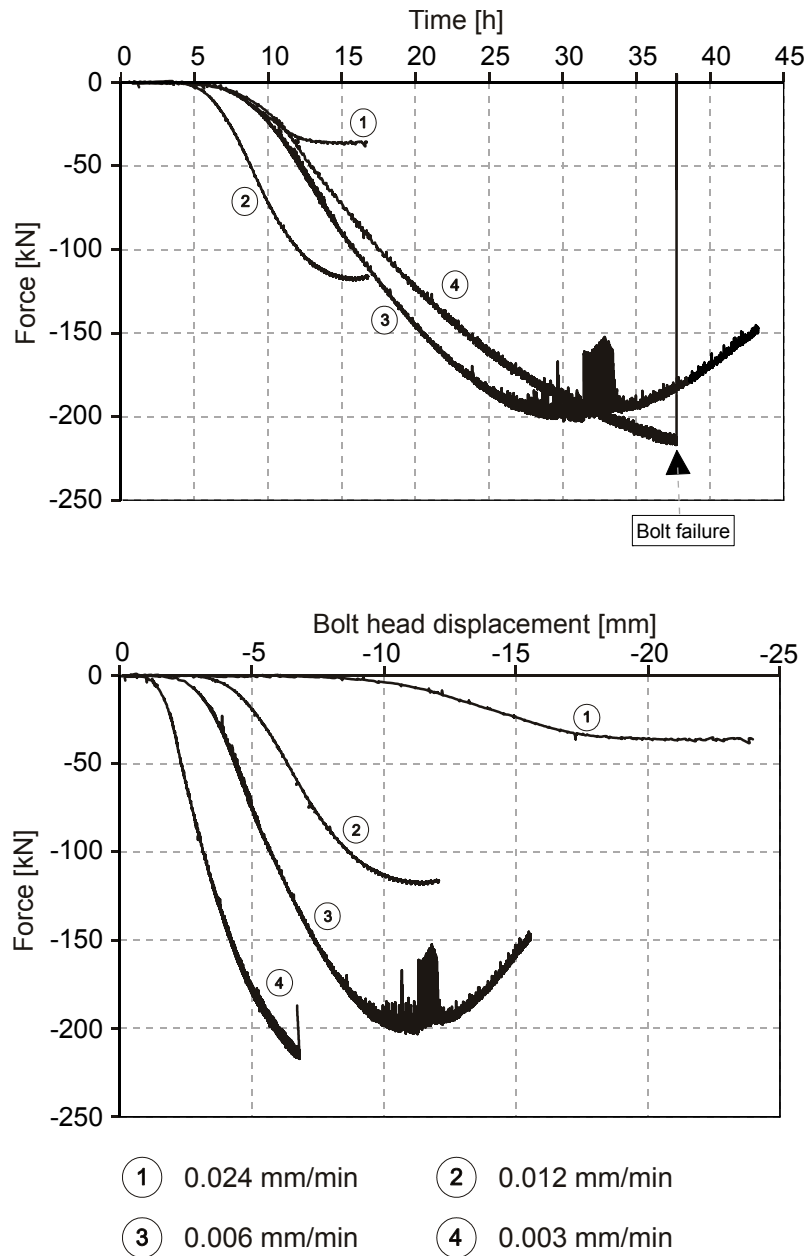
Figure 30. Results of a rock bolt pull out test conducted with the same rib geometry, but different displacement rates (Blümel, 1996).

4.1.2.2 Behaviour under transverse loading

A rock bolt crossing a discontinuity under shear loading features an entirely different kind of resistance mobilisation than described above. In competent, high strength rocks, the rock bolts act as dowels and mobilise considerable resistance at very low relative displacements (Schubert, 1984; Spang, 1988). On the other hand, rock bolts in weak ground penetrate into the surrounding rock mass and the load transfer is governed by formation of two plastic hinges at the ends of the penetration area (Figure 31).
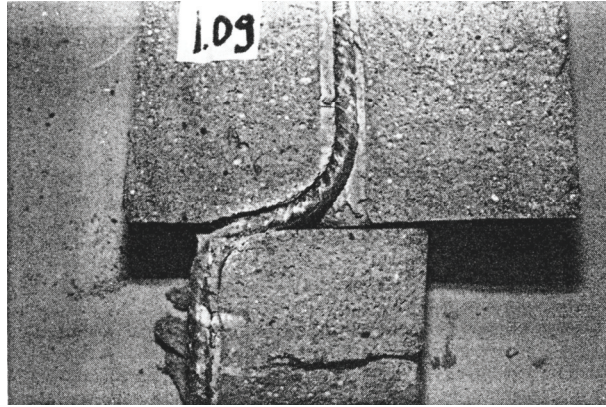
Figure 31. Test specimen after the shear test Spang (1988)

The basic resistance in such deformation regime is utilised by the "tilting" of the rock bolt and the section between the hinges acting like a truss member. On the contrary to the usual engineering intuition, the increase of shear resistance is not caused by the elastic response to the elongation of this section and simultaneous linear increase of the axial force. The section between the hinges is constantly yielding, and the dominant portion of the resistance is mobilised by the change of geometry (Pellet & Egger, 1996). Simply put, the growing "tilt" of the rock bolt causes more force to act in the direction parallel to the shear direction. Since the geometry of the bent/tilted portion of the rock bolt is predominantly influenced by the rock mass strength, the ground properties have a major influence on the load – displacement behaviour. The stronger the surrounding rock is, the lower is the distance between the plastic hinges and the rock bolt reacts in a stiffer manner. In order to illustrate this, the closed-form solution presented by Pellet & Egger (1996) was used to conduct a parametric study (Figure 32).
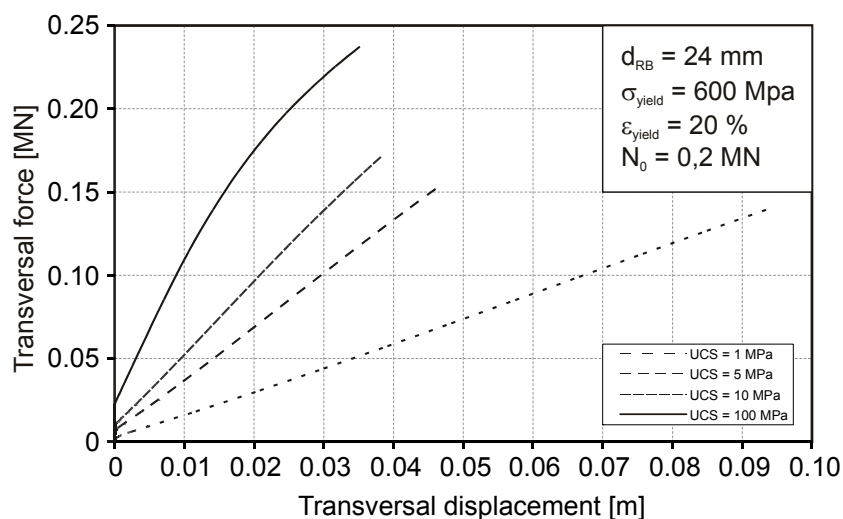
Figure 32. Influence of the rock mass strength on the load – displacement behaviour of rock bolts under transversal loading

Due to its simplicity and reasonable prediction ability (its predictions regarding the load displacement relationship of bolted joints have been successfully tested against a series of tests), the solution presented by Pellet & Egger (1996) is used for the assessment of the influence of rock bolts on the axial force distribution in

the lining. Its mathematical treatise is excellently presented in the original paper and will not be reproduced here. The mobilisation of transversal forces due to shear at the shotcrete– rock mass boundary is treated as if happening along a joint between two identical rock blocks. In reality, the ongoing hydration of the grout and the shotcrete causes constantly changing boundary conditions of the problem, and the applied relationship should be merely treated as a plausible assessment.

4.1.3 Bond strength between shotcrete and rock mass

Due to the high shear strength contrast between the rock mass and shotcrete, it is assumable that the strength properties of the contact surface are nearly identical to the strength properties of the ground. However, several issues with regard to the mechanical properties of the contact surface have been identified, leading to the design and execution of in-situ shear tests in the instrumentation and testing adit of the exploratory tunnel Paierdorf (Koralm):

- Identification of the "location" of the shear band. Where does the shear failure occur?

- Determination of the shear strength envelope of the contact surface.

- Examining the influence of shotcreting on the ground properties in the nearest vicinity of the excavation.

4.1.3.1 Geological conditions

The instrumentation adit was excavated at chainage 1248.66 of the exploratory tunnel Paierdorf. The main goal of the adit construction has been the execution of an extensive in-situ testing program and subsequent determination of reliable ground properties (3G Gruppe Geotechnik Graz, 2010) in the core zone of the Lavanttal fault zone.

Strongly tectonised, low strength and intensely fractured shale gneiss and coarsely grained cataclastic rocks composed the majority of the rock mass encountered during construction, accompanied by erratically occurring lenticular insertions of moderately competent rocks. The entire region is intersected by thin shear bands composed of finely grained cataclastic material. The intact rock strength varies between less than 1 MPa to 50 MPa, depending on the degree of tectonisation.

Due to tectonic processes, the material has been frequently sheared along the foliation and slickenslides are usually parallel to the foliation orientation. The dominant discontinuity set (foliation and the associated slickenslides) dips steeply towards south-east / south-west.

4.1.3.2 Specimen preparation and setup

No support measures, apart from the lattice girders, have been installed in the invert of the last two excavation rounds. To allow for realistic conditions in the contact surface, the debris and rebound shotcrete material have been removed from the invert with compressed air. The cast forms (rectangular frames) have been aligned with the rock mass excavation boundary, fixed and filled with shotcret (Figure 33). In order to prevent bonding between the specimens, the cast frames have been removed and the void has been immediately cleared of the excess shotcrete.

Figure 33. Cast forms aligned in the invert of the first round – ready to shotcrete

The initial idea was to conduct the tests at different and low shotcrete ages, in order to have a good contrast between the respective shotcrete strength and thus capture its influence. Unfortunately, due to water inflow from the face and parallel extensometer borings, it was not possible to conduct the shear tests until 26 days after casting.

4.1.3.3 Test setup

The force normal to the contact surface was applied with a "loading arm", composed of a load cell, hydraulic cylinder and associated assembly, holding the measurement and load parts in place. An eye bar was used as the joint between the cross beam and the loading arm, thus allowing the normal loading to follow the horizontal movement of the specimen during shearing (Figure 34).
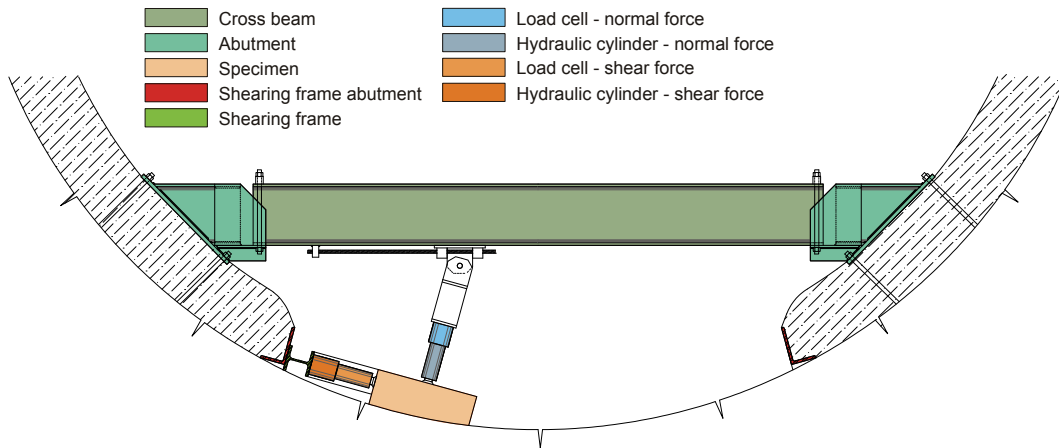
Figure 34. Schematic representation of the test setup

The proper alignment of the test specimen was ensured by the frame with side rollers allowing unhindered movement in the direction parallel to the shear loading, but preventing rotation or side movement (Figure 35). The shear displacements have been measured by two LVDTs, mounted on both sides of the shear loading assembly (Figure 36). The measurement of the displacements perpendicular to the shear plane (dilatancy) has been deliberately omitted, since it was envisioned to conduct the test in a finely grained cataclastic material featuring rather low dilatancy.

Figure 35. Test assembly before the test

Figure 36. Detail of the alignment frame with the loading arm and LVDTs

The initial normal stresses have been envisioned to vary between 0.20 and 0.40 MPa, thus being in the usual magnitude of the support pressure mobilised with a ductile support.

However, the first test indicated that the rock mass was better than anticipated and featured strong dilatancy caused by shearing along the foliation. This resulted in strong increase of the normal force during the test, and the subsequent tests were conducted with lower initial normal stresses, in order to avoid damage to the test set-up. The shear surface of two specimen was strongly contaminated by the rebounded shotcrete (logically, always the last specimen in each shotcreting round) and the specimen failed prematurely. In the end, three successful tests have been conducted with an initial normal stress of 0.06 MPa, two tests feature 0.12 MPa and one test was conducted with the initial normal stress of 0.18 MPa.

4.1.3.4 Test result post-processing

Due to the high stiffness of the hydraulics assembly used for the application of the normal loading, it can be assumed that the test was conducted under constant normal stiffness conditions. The high degree of fracturing of the rock mass and the relatively low initial normal stresses lead to the dominant failure mechanism of sliding along already existent discontinuities (Figure 37). This corresponds to the mechanical behaviour of discontinuities under low normal loading, described in Pattons' Law (1960), where the frictional resistance and dilatancy are mobilised together.

Figure 37. Failure surface formed by the structure

In order to determine the dilatancy, the normal displacements have been calculated from the change in the normal forces during the test. The assembly stiffness has been calculated from the partial stiffness of the involved assembly parts (Figure 38 / Equation 2).
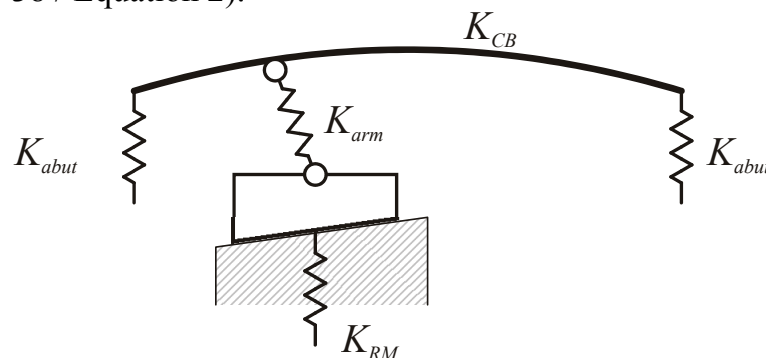
Figure 38. Partial stiffness accounted for in the calculation of the overall assembly stiffness

$$\frac{1}{K_{ass}} = \frac{1}{K_{CB}} + \frac{1}{K_{abut}} + \frac{1}{K_{arm}} + \frac{1}{K_{RM}}$$

Equation 2

The rock mass stiffness has been calculated from the equations describing the stress-settlement behaviour of a square foundation. Since the rock mass modulus of elasticity was determined by a series of in-situ load plate tests, its value has been directly used in the determination of the load-settlement relationship (3G Gruppe Geotechnik Graz, 2010). A certain amount of vertical displacement occurs gradually with the shearing of the specimen, due to the rotation of the normal force arm (Figure 39).
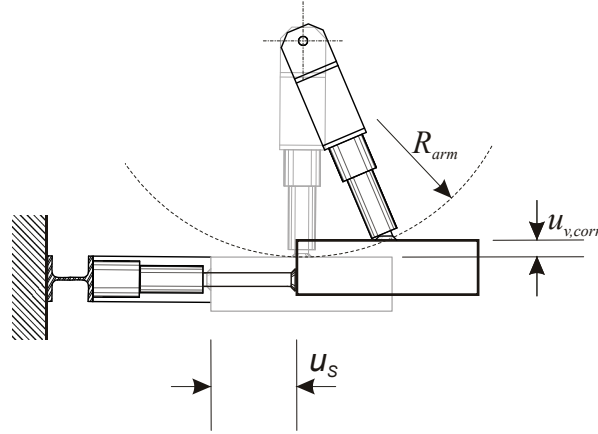
Figure 39. Vertical movement kinematics of the load arm

This displacement is calculated from the measured shear displacements (Equation 3), since the kinematical relationships of the test assembly are known and constant in all tests. The thus obtained normal displacements have to be added to the displacements calculated from the normal force change and the system stiffness, in order to obtain total normal displacements (Equation 4).

$$u_{n,corr}(u_S) = \frac{2R_{arm}^2 - \sqrt{4R_{arm}^2 - 4u_S^2}}{2}$$ **Equation 3**

$$u_{n,tot}(u_S) = \frac{F_N(u_S) - F_{N0}}{K_{ass}} + u_{n,corr}(u_S)$$ **Equation 4**

Wherein:
$u_{n,tot}$ – Total normal displacement
u_S – Shear displacement
K_{ass} – Total assembly stiffness
F_N – Normal force at the horizontal displacement u_H
F_{N0} – Initial normal force (begin of shearing)
R_{arm} – Radius of the loading arm
$u_{n,corr}$ – Normal displacement correction due to test kinematics

After the normal displacements have been determined, both the dilatancy and the friction angle can be easily determined from the normal and shear force measurement logs.

4.1.4 Results

The assessment of the dilatancy yields reasonable results, especially when the failure mechanism, the low normal stresses and the shape of the contact surfaces are considered (Figure 37). The summary of test results is shown in Figure 40 and Table 3.
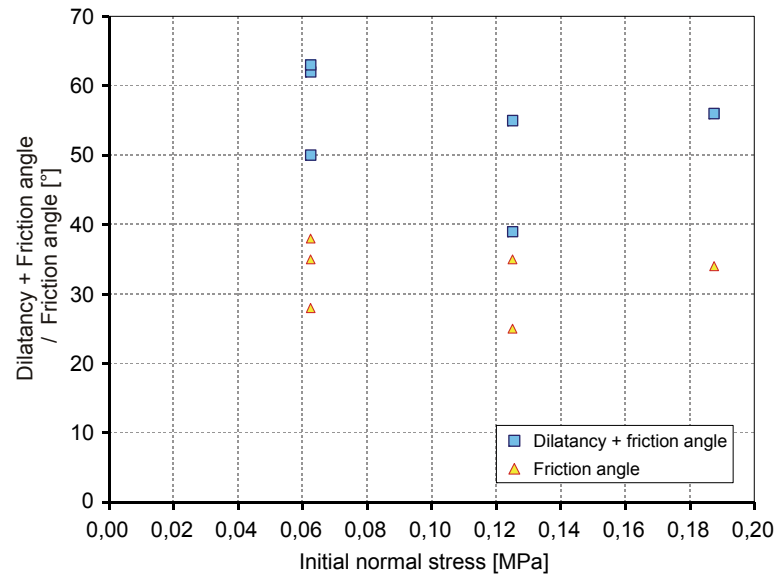
Figure 40. Summary of test results

Table 3. Summary of test results

	Initial normal stress [MPa]	Norm. stress at peak [MPa]	Peak shear stress [MPa]	Friction angle [°]	Dilatancy [°]
Test 1	0,06	0,08	0,17	24,2	34,5
Test 2	0,13	0,24	0,27	31,3	23,0
Test 3	0,06	0,20	0,21	26,8	30,0
Test 4	0,07	0,19	0,24	31,6	27,9
Test 5	0,13	0,14	0,12	21,0	15,0
Test 6	0,19	0,22	0,33	30,4	22,2

A clear decrease of dilatancy with growing initial normal stresses is observable, while the friction angle is rather constant. The mean value of the friction angle is 32°, and in very good agreement with laboratory direct shear tests on the same material (3G Gruppe Geotechnik Graz, 2010). The test results suggest that no cohesion is present, while the laboratory test results and the experiences gathered during excavation back the contrary. The reason for this apparent contradiction lies in the failure mechanism, causing strong concentrations of shear strain and almost immediate contact separation (tensile failure) of all surfaces averted from the general direction of movement. Since the cohesion and friction angle are usually being mobilised separately, the cohesion is lost almost immediately after non-reversible shear displacements occur, while the friction angle is mobilised in a rather ductile and long-stretched manner (Barton & Bandis, 1990; Martin, 1997). The following conclusions are drawn from the tests:

- The bond strength between the rock mass and the shotcrete also in relatively good ground conditions is higher than the shear strength of the ground. In heavily tectonised ground, the strength contrast is even higher and the relative slip between the shotcrete and the ground is governed by the shear properties of the ground.

- The enhancement of the ground properties in the area nearest to the excavation boundary and due to the shotcreting could not be observed. While the rebound material (underneath the two failed specimen) was strongly cemented by the shotcreting, forming porous, up to 10 cm thick structures underneath the actual specimen, the strongly compacted cataclasite is unlikely to behave in the same manner.

- Disregarding the applied calculation approach (convergence confinement method, numerical methods), the effect of the installation of yielding elements can be correctly estimated only if the slip between shotcrete and rock mass is accounted for. If a rigid bond between the ground and the shotcrete lining is assumed, the system response becomes too stiff and the yielding elements become basically meaningless – since the strain of the liner is forced to equal the strain of the ground. Analogously, the omitting of the bond strength and shear resistance of the rock bolts considerably underestimates the overall support resistance. In numerical calculations, the modelling of slip can be achieved either by the application of contact elements (Gradsack, 2010) or by using a very fine mesh and a strain – softening constitutive law, allowing the formation of localised shear bands. In the latter case, particular attention has to be paid to the separate mobilisation of cohesion, friction angle and dilatancy with the increase of plastic deviatoric strains.

4.1.5 Design requirements

The design requirements on a ductile support system are straightforward:

- The mobilised support resistance and the chosen overexcavation have to ensure that the clearance profile is not violated.

- The yielding elements load-displacement behaviour has to be compatible with the time- and excavation dependent displacement development and the time-dependent shotcrete strength. Simply put, the stresses in the lining have to be kept below the available capacity.

- The shotcrete utilisation and the overall support resistance have to be as high as possible, in order to arrive at an economical design and prevent excessive rock mass disintegration in the vicinity of the cavity.

- The support resistance of the applied support system has to be above the dead weight of the assumed loosened portion of the rock mass.

4.2 Extensions to the convergence confinement method

4.2.1 Ground reaction curve

Basically every closed – form solution for an elasto-plastic material can be used for the calculation of the ground reaction curve. In the further course of this thesis, the ground reaction curve is calculated by the relationship proposed by Feder & Arwanitakis (1976). It allows treatment of linear elastic – brittle plastic material behaviour (ideal plastic conditions being obtainable by setting the post-failure ground parameters equal to the peak parameters). The effects of dilatancy and the intermediate principal stress on the displacement field are accounted for, the latter being ignored in the earlier solution proposed by Kastner (1968).

The amount of pre-displacement is assessed by the relationship proposed by Hoek et al. (2008), writing as

$$\frac{u_0}{u_{max}} = \frac{1}{3} e^{-0,15\frac{R_{pl}}{R}} \, , \qquad \textbf{Equation 5}$$

with u_0 – representing the radial displacement at face passage,
       u_{max} – final displacement in unsupported case,
       R_{pl} – plastic radius,
       R – tunnel radius, respectively.

The research performed by Pilgerstorfer (2008) verified this relationship, underlining that it fully applies for all constitutive laws assuming ideal plasticity. In case of determining the ground reaction curve by more sophisticated constitutive laws, an axial-symmetric analysis is advisable in order to correctly determine the amount of pre-relaxation.

4.2.2 Support characteristic curve

Due to the nonlinear behaviour caused by the interaction between the different support types described above, the support characteristic curve for the described kinematical behaviour has to be calculated iteratively. Due to the imperative of radial displacement compatibility between the rock mass and the support, the overall tangential shortening of both excavated cross section (its change of circumference) and the installed support has to be the same. However, while the strain field of the rock mass at the excavation boundary is constant, the strain field in the installed support has to vary according to the occurring relative stiffness of the lining components (yielding element and shotcrete). Assuming a symmetrical layout of the deformation gaps (Figure 41), then the shortening $u_{\varphi,tot}$ of one half-segment (caused by the radial displacement u_{rad} forced onto the entire system) can be easily calculated from the change of the system circumference and the number of installed deformation gaps n_{gaps} (Equation 6).

$$u_{\varphi,tot} = \frac{\pi \cdot u_{rad}}{n_{gaps}}$$

Equation 6

The reason for considering only one half-segment lies in the symmetry of the problem: the middle point of every shotcrete segment does not experience any relative tangential movement with regard to the surrounding rock mass. Needless to say, if the origin of the coordinate system is set at the middle point, then both the rock mass and the shotcrete feature zero tangential displacement at this point, and both have to experience the total tangential shortening of $u_{\varphi,tot}$, simply being the change of the arch length L_{seg} between the middle point and the symmetry plane (middle point of the yielding element).
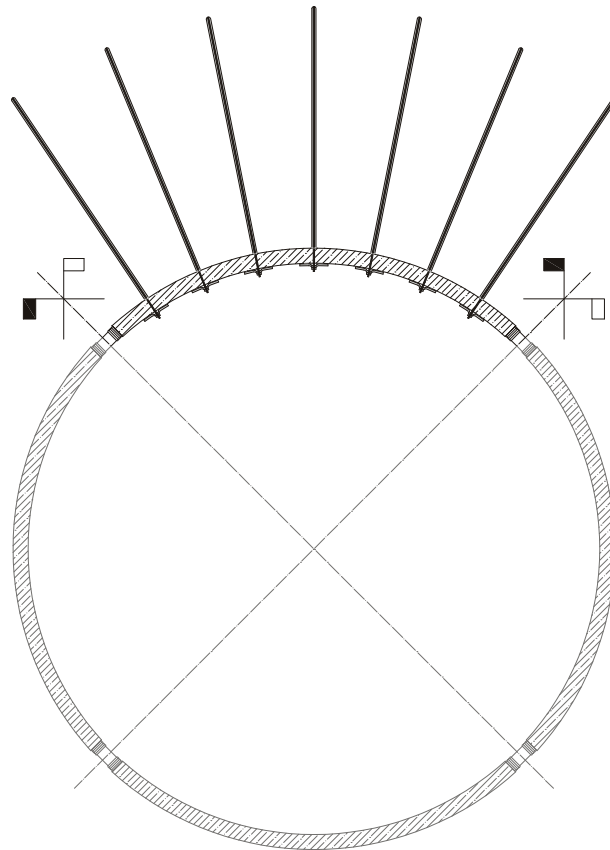
Figure 41. Idealised support model and the shotcrete – yielding element segment under consideration

In order to calculate their internal tangential displacement field, the shotcrete segments are discretised into truss elements[2] (Figure 42). The shear resistance of rock bolts and the frictional bond between shotcrete and rock mass are accounted for by applying external forces at the respective nodes.

---

[2] In all further equations, nodal quantities are noted with an subscript, for instance $F_{shear,i}$ denoting the external shear force acting at the node i. Analogously, all quantities associated with the truss elements are denoted with a superscript, thus K^i being the axial stiffness of the i-th element.
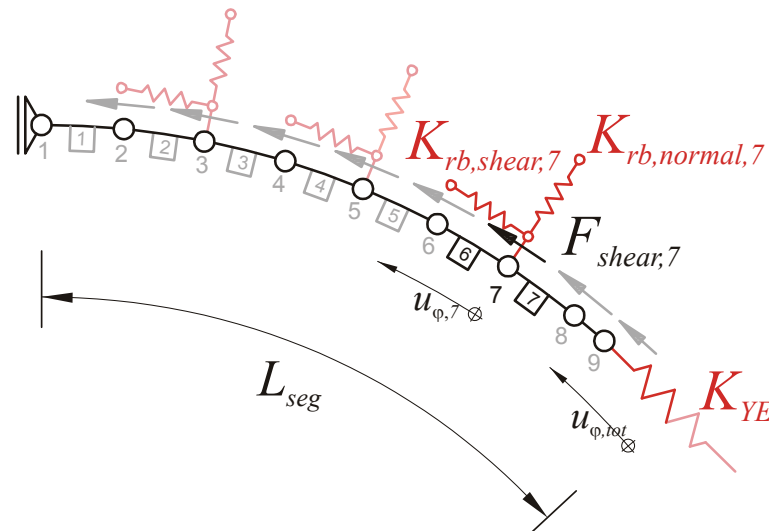
Figure 42. Applied discretisation and the calculation model

The thrust mobilised from deforming the yielding element is calculated by taking into account the tangential displacement of the final shotcrete node n (in Figure 42: node 9) and subtracting it from the overall segment shortening $u_{\varphi,tot}$. Since only one half-segment is considered, the entire yielding element (for which the non-linear load-displacement relationship K_{YE} is known) experiences the double shortening (Equation 7).

$$F_{YE} = K_{YE}\left(2 \cdot \left(u_{\varphi,tot} - u_{\varphi,n}\right)\right)$$

Equation 7

The radial stress σ_{rad} acting between the lining and rock mass is assessed by dividing the thrust F_{YE} mobilised at the yielding element with the tunnel radius R (Equation 8).

$$\sigma_{rad} = \frac{F_{YE}}{R}$$

Equation 8

Hence, the nodal shear forces can be easily calculated by weighted element-wise linear integration of the radial stress (Equation 9).

$$F_{shear,i} = \tan\varphi_{con}\sigma_{rad}\left(L^{i-1} + L^i\right)$$

Equation 9

The contribution of fully grouted rock bolts to the contact normal stresses between the ground and the rock mass is deliberately neglected, because the mobilisation of shear resistance causes a considerable and non-linear decrease of normal loading (Pellet & Egger, 1996). The development of a rigorous solution was deemed as too complex for the pre-design stage. The shear stiffness of the rock bolts $K_{rb,shear}$ is calculated by determining the secant stiffness from the load-displacement relationship proposed by Pellet & Egger (1996) and discussed in chapter 4.1.2.2. Hence, the forces resulting from the rock bolt resistance to shear deformation are calculated by multiplying the rock bolt shear stiffness $K_{rb,shear}$ with the respective relative tangential displacement (Equation 10).

$$F_{rb,i} = K_{rb,shear,i} \cdot (u_{\varphi,i} - u_{\varphi,i,RM})$$ **Equation 10**

The term $u_{\varphi,i,RM}$ is included since the rock bolt resistance is mobilised only by the relative tangential displacement between the rock mass and the shotcrete. $u_{\varphi,i,RM}$ can be simply calculated as the change of the arch length (Equation 10) associated with the respective node.

$$u_{\varphi,i,RM} = \frac{L_i}{L_{seg}} u_{\varphi,tot}$$ **Equation 11**

The respective truss element stiffness calculation is straightforward:

$$K^i = \frac{E_{shot} A_{shot}}{L^i}$$ **Equation 12**

wherein L^i represents the length of every respective element. After all the quantities have been determined as presented above, the global stiffness matrix **K** and the global tangential load vector **q** can be assembled (Equation 13, Equation 14). The relationships proposed by Pellet & Egger (1996) also yield the maximum shear displacement of a rock bolt (based on the rock mass strength, rock bolt diameter and the failure strain of the steel). Hence, the slip at every rock bolt is being monitored and, in case of exceeding the maximum allowable shear displacement, the rock bolt shear contribution is removed from the loading vector **q**.

$$\mathbf{K} = \begin{matrix} K_{11}^1 & K_{12}^1 & 0 & 0 & 0 \\ K_{21}^1 & K_{22}^1 + K_{22}^2 & K_{23}^2 & 0 & 0 \\ 0 & K_{23}^2 & K_{33}^2 + K_{33}^3 & ... & 0 \\ 0 & 0 & ... & ... & ... \\ 0 & 0 & 0 & .... & K + K \end{matrix}$$ **Equation 13**

$$\mathbf{q} = \begin{matrix} 0 \\ F_{shear,2} \\ F_{shear,2} + F_{rb,shear,3} \\ ... \\ F_{shear,n} + F_{YE} \end{matrix}$$ **Equation 14**

The relationships above are coupled by the standard equation of the deformation method / FE analysis (Equation 15):

$$\mathbf{K}\mathbf{u}_\varphi = \mathbf{q}$$ **Equation 15**

Needless to say, this poses an implicit non-linear problem, since all of the quantities defined in load vector **q** depend on the assumed nodal displacement vector $\mathbf{u}_\varphi$. Luckily, the solution is quite simple: either any of the established non-linear finite-element solution techniques is applied (Zienkiewicz & Taylor, 2006) or the system is solved by defining an error-loading vector (representing

unbalanced forces) $\mathbf{q}_{err}$ (Equation 16) and using it as an objective vector function for the built-in MatLab solver (Equation 17).

$$\mathbf{q}_{err}(\mathbf{u}_\varphi) = \mathbf{K} \cdot \mathbf{u}_\varphi - \mathbf{q}$$

Equation 16

$$solve(\mathbf{q}_{err}(\mathbf{u}_\varphi)) \to \mathbf{0}$$

Equation 17

The applied reformulation in conjecture with the Levenberg-Marquart algorithm (Mathworks, 2007) has shown to be very stable and convergent. The solution for each assumed radial displacement increment (imposed on the support) yields the thrust and slip distribution for the shotcrete segments (Figure 43).
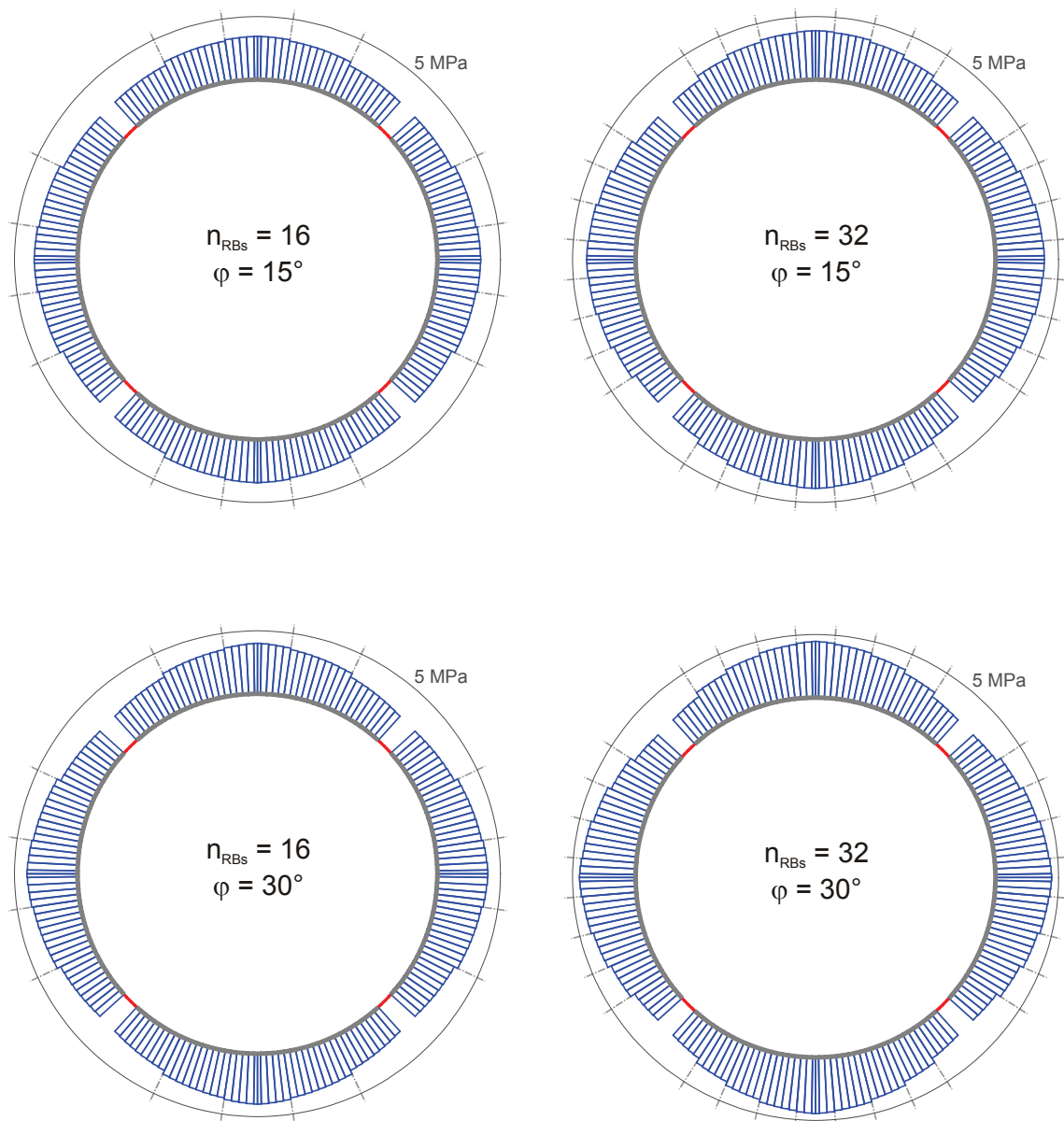

Figure 43. Influence of rock bolting density and friction angle at the rock mass – lining contact surface on the thrust distribution in shotcrete ($UCS = 1$ MPa, $F_{YE} = 900$ kN, $R = 5$ m)

As it can be seen, the friction angle, the shear resistance of rock bolting, the shotcrete stiffness and the yield element load-displacement characteristic stand in an intricate relationship.

The overall support resistance contribution of the shotcrete lining with installed yielding elements is calculated by weighted averaging of the thrust forces in the lining segment (Equation 18).

$$p_{Lining}(u_{rad}) = \frac{1}{R}\left(\sum_{i=1}^{n} \frac{F^i(u_{rad}) \cdot L^i}{L_{seg}} + \frac{F_{YE}(u_{rad})L_{YE}}{2L_{seg}} \right) \qquad \textbf{Equation 18}$$

The axial support action of the rock bolts is calculated by taking the elongation between the excavation boundary and their outermost points (Figure 44) into account.
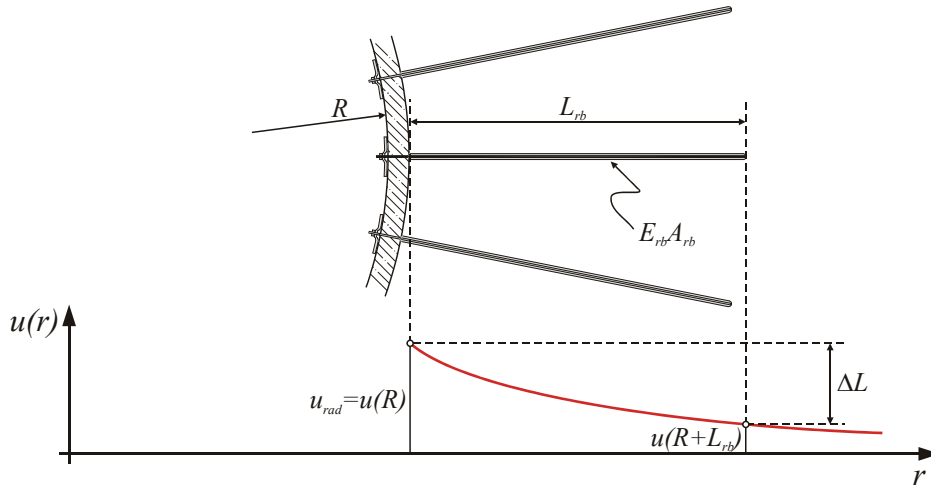

Figure 44. Calculation model used for determining the axial force mobilisation

Hence, the calculation of the axial forces in the rock bolts and the associated support resistance depend merely on the load displacement characteristics of the rock bolt material and the deformation behaviour of the ground (Equation 19 and Equation 20).

$$F_{rb}(u_{rad}) = \begin{cases} E_{rb}A_{rb}\big/L_{rb} \ \Delta l(u_{rad}) & \Delta l(u_{rad}) < \varepsilon_{yield} \cdot L_{rb} \\ A_{rb}\sigma_{yield} & \text{for} \ \Delta l(u_{rad}) \geq \varepsilon_{yield} \cdot L_{rb} \\ 0 & \Delta l(u_{rad}) \geq \varepsilon_{u} \cdot L_{rb} \end{cases} \qquad \textbf{Equation 19}$$

$$p_{Bolts}(u_{rad}) = \frac{n_{bolts}F_{rb}(u_{rad})}{2\pi R} \qquad \textbf{Equation 20}$$

This approach to describing the rock bolt behaviour was chosen because of the simplicity of its implementation. The relationships allowing more accurate rock bolt modelling (accounting for the interaction between the rock mass, grout and rock bolt along the entire bond length), such as presented by Oreste (2008), require numerical solving of the displacement compatibility and force equilibrium equations. Hence, they were considered beyond the scope of the

efforts undertaken in the course of this thesis, which is focusing on principal method development. A more accurate modelling of the rock bolt behaviour can be easily added in later development stages.

The total support resistance of the installed support measures is given by combining the support pressure resulting from rock bolts and lining (Equation 21).

$$p_{tot}(u_{rad}) = p_{Bolts}(u_{rad}) + p_{Lining}(u_{rad})$$ **Equation 21**

This allows finding the equilibrium between the deforming rock mass and the support (Figure 45).
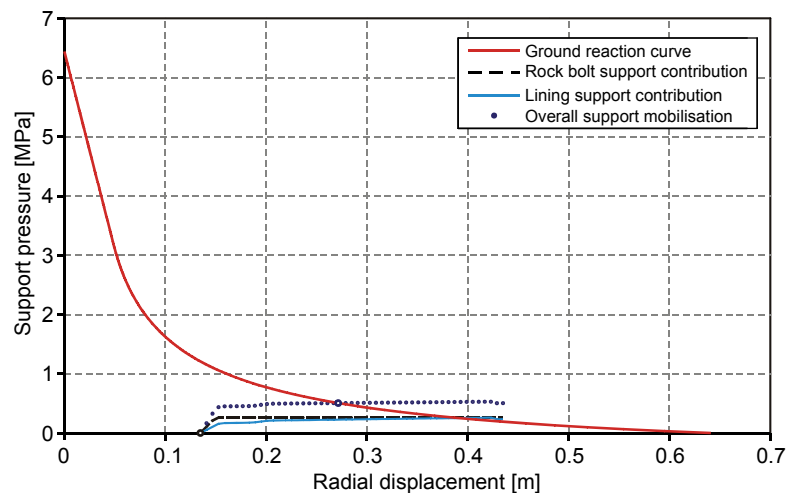

Figure 45. The support characteristic curve for dense rock bolting and ductile lining support (please note the downward step in the final deformation stages due to rock bolt shear failure)

4.2.3 Assessment of the shotcrete capacity

As presented above, the friction angle, rock bolting density and the load-displacement behaviour of yielding elements strongly influence the shotcrete stresses. Needless to say, a sound design has to account for the time dependent shotcrete strength development.

High capacity of yielding elements lowers both the final displacements (due to the higher system resistance) and thus also the slip between the rock mass and the shotcrete. This also results in lower shear loading of rock bolts, but also in high *a priori* loading of shotcrete (disregarding other influences). On the other hand, relatively high support pressures can be mobilised as well, if dense bolting and a relatively low number of yielding elements are implemented. However, the shotcrete utilisation becomes poorly balanced (low at the lining stress controllers and dangerously high in the segment middle points), accompanied by high slip and rock bolts subjected to strains exceeding the ultimate capacity. Both damage to the shotcrete lining (due to the thrust accumulation) and rock bolt failure (usually highly dangerous for the tunnelling personnel) would be the

consequence. Needless to say, the tendency of increasing the number of yielding elements is countered by economical reasons: their installation is associated with increased material costs and personnel effort.

In order to examine these dependencies while focusing on shotcrete capacity, additional information about the anticipated system behaviour is required. Following steps have to be performed:

1. *Determination of the support characteristic and equilibrium*
    The relationships described above are used to determine the support resistance and the distribution of the axial forces for every radial displacement increment. As already presented, the highest thrust in the shotcrete lining occurs in the middle-point of the shotcrete segment enclosed by the yielding elements (hence, in truss member 1 - as designated by the discretization scheme shown in Figure 42). By dividing it by the tunnel radius, we obtain the maximum support pressure mobilised in the shotcrete lining (Equation 22).

    $$p_{L,\max} = \frac{F^1}{R}$$ **Equation 22**

    The depiction of the maximum shotcrete thrust is of utmost importance, since it allows adjustment of the rock bolt density and yielding element characteristic to the time-dependent shotcrete strength.

2. *Construction of the longitudinal displacement profile*
    The equation proposed by Panet & Guenot (1982) has been found to be exceptionally well suited for describing the displacement development due to excavation in ideally plastic materials (Pilgerstorfer, 2008):

    $$u(x) = u_0 + (u_{\max} - u_0) \cdot \left[1 - \left(\frac{0.84 \cdot R_{Pl}}{x + 0.84 \cdot R_{Pl}} \right)^2 \right]$$ **Equation 23**

    With u_0 – representing the radial displacement at face passage,
    u_{max} – final displacement of unsupported tunnel,
    R_{pl} – plastic radius,
    x – distance between the cross section under consideration and the tunnel face.

    However, in order to describe the displacement development characteristic wit supported, the plastic radius associated with the equilibrium between the support measures and the rock mass $R_{pl,eq}$ has to be used instead of the plastic radius R_{pl} occurring in unsupported conditions. This accounts for the rapid stabilisation of the displacement development due to support installation (Figure 46).
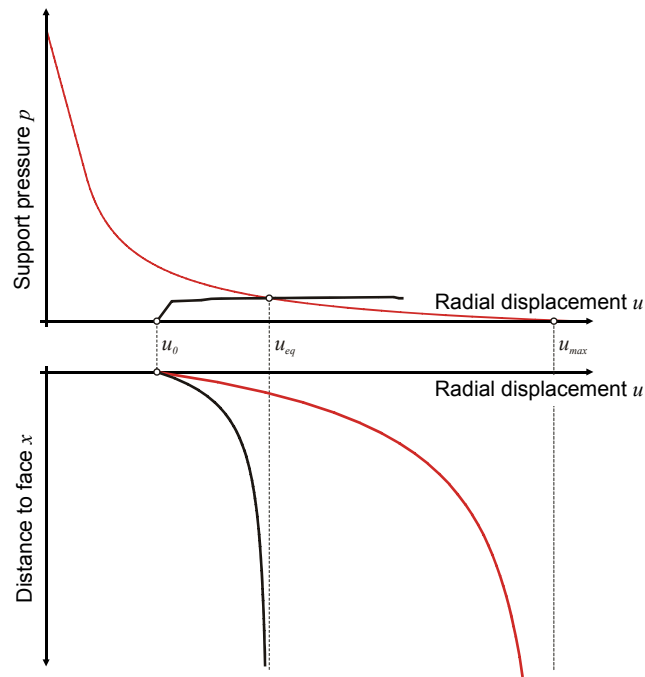
Figure 46. Determination of the longitudinal displacement profile accounting for support installation

Analogously, the final displacement in an unsupported case u_{max} has to be replaced by the radial displacement at the equilibrium point u_{eq} (Equation 24).

$$u(x) = u_0 + (u_{eq} - u_0) \cdot \left[1 - \left(\frac{0.84 \cdot R_{Pl,eq}}{x + 0.84 \cdot R_{Pl,eq}} \right)^2 \right]$$ **Equation 24**

The thus obtained longitudinal displacement profile is still an approximation of the true displacement development, since neither the effect of the support installation on the predisplacement magnitude nor the effect of changing support stiffness (due to the presence of yielding elements) are properly incorporated (Gschwandtner, 2009). More correct assessment of the displacement development can be obtained only by using a numerical model, and adjusting the support mobilisation characteristic to the findings presented above.

3. *Plotting the face position against the time*
   The face advance rate a has to be assumed, allowing plotting of the face distance x against the time t (Equation 24).

$$x = a \cdot t$$ **Equation 25**

4. *Determination of the maximum shotcrete thrust capacity*
   The time-dependent shotcrete strength $\beta(t)$ is given by the relationships proposed by Müller (2001), based on the 28-days shotcrete strength β_{28}:

$$\beta(t) = \beta_{28} \sqrt{\frac{(t + t_{init}) - 0.212}{116 + 0.841(t + t_{init})}}$$
   Equation 26

   The additional time interval t_{init} (in this equation, in hours) accounts for the effect of sequential excavation. Since a considerable amount of time (in the light of rapidly developing early shotcrete strength) passes between the shotcreting and the subsequent round excavation, the thus "available" curing time has to be accounted for. A reasonable guess is obtained by analysing the assumed advance rate and excavation size, allowing a rough estimate of the time required for mucking, rock bolt and spile installation and preparation work for the next round. In the further course of this thesis, t_{init} is assumed to equal one half of the total time required for one round. The assumed shotcrete lining thickness t_{shot} allows the conversion of the maximum available thrust into the maximum available support resistance p_{max} (Equation 27).

$$p_{max}(t) = \frac{\beta(t) \cdot t_{shot}}{R}$$
   Equation 27

5. *Assigning the shotcrete capacity to the respective support displacements*
   By the virtue of knowing both the displacement development and the face advance rate, it is possible to construct a line of maximum shotcrete thrust capacity depending on the radial displacements (Figure 47).
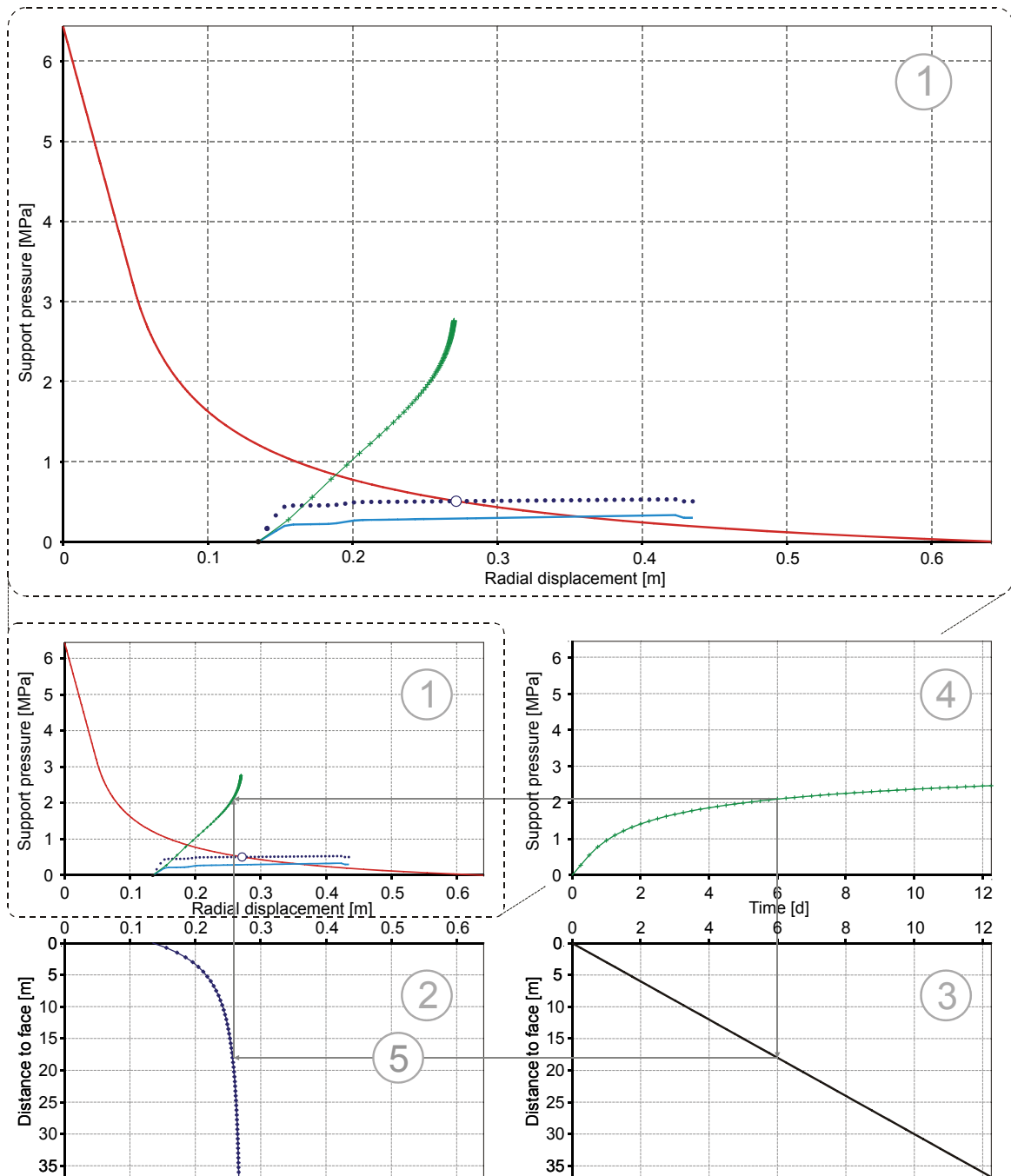
Figure 47. Determination of the shotcrete thrust capacity (blue line: maximal mobilised shotcrete thrust $p_{L,max}$, dotted line: total support resistance p_{tot}, green line: shotcrete thrust capacity p_{max})

6. *Modifying the support parameters until all requirements are met*
   The execution of the five steps documented above yields a sound prediction of the system behaviour in all its aspects. The cross-dependencies between the ground conditions, rock bolting density, shotcrete lining capacity and the yielding element characteristic are captured, thus allowing initial estimates about the displacement development and the shotcrete utilisation. The latter is easily assessed by inspecting the development of the shotcrete capacity against the displacements, since the line of maximum lining mobilisation has

always to lie *below* it. The practical meaning of this imperative is obvious: the shotcrete stresses induced in the lining have to be below the shotcrete strength, associated with the respective time and hence with the respective radial displacement. Besides the influences of yielding element characteristic and shear load transfer between shotcrete and ground, the advance rate has also a strong influence on the shotcrete utilisation (Figure 48).
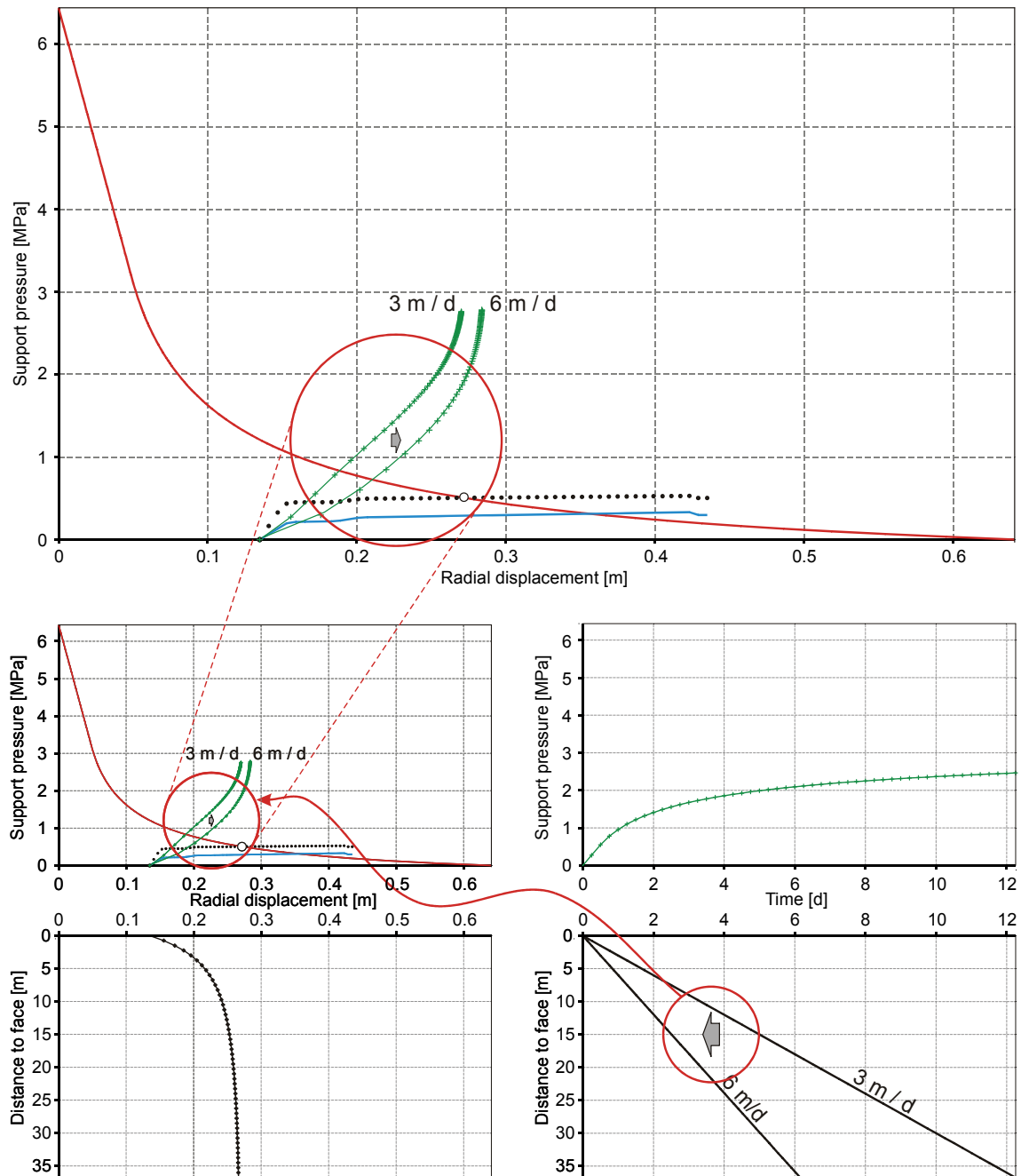
Figure 48. The influence of the advance rate on the shotcrete utilisation

The inner workings are intuitive: since the ground deformations are assumed to develop only due to the face advance, a more rapid excavation causes the same displacements (and thus: thrust forces) to be forced upon the lining in an earlier moment. The shotcrete strength, on the other hand, is solely time-dependent, thus resulting in higher utilisation (up to the point of failure). As presented in Figure

48, the applied support concept is appropriate in case of an advance rate of 3 m/d, however it results in shotcrete overloading if an advance rate of 6 m/d is applied. The determined utilisation deviates somewhat from the one determined by applying a more sophisticated rheological model, since the presented method relies on an a priori assumption of a secant Young's modulus. If this assumption is plausible (see chapter 4.1.1), the resulting discrepancy is marginal (Gradsack, 2010), rendering the obtained accuracy sufficient (given the fact that this is a calculation method to be used in early design stages).

Possible mitigation measures leading to an acceptable utilisation are:

- Lower overall support resistance (accompanied by over-excavation). However, even the complete omitting of yielding elements can lead to shotcrete damage, provided that dense rock bolting, reasonable shotcrete-rock mass bond strength and too long shotcrete segments are present.

- Adjustment of the initial stiffness of the applied yielding elements (if possible), in order to comply with the early shotcrete capacity.

- Installation of more yielding elements, thus both lowering the initial system stiffness (since more "springs" are installed in the system in a serial manner) and minimising the thrust peaks resulting from the slip between the shotcrete and the rock mass.

- Slowing the advance rate, granting more time for shotcrete hydration.

4.2.4 Application example

In order to illustrate the application of the presented methodology, it is applied to realistic rock mass conditions, derived from the monitoring data gained during the advance of the exploratory tunnel Paierdorf (Schubert et al., 2009). The rock mass conditions and design requirements are listed in Table 4.

Table 4. Ground conditions and requirements on system behaviour

Ground conditions	
Young's modulus E [MPa]	300
Poisson ratio v [-]	0.30
Friction angle φ [°]	28
Cohesion c [MPa]	0.30
Overburden H [m]	270
Unit weight γ [MN/m³]	0.023
Requirements	
Tunnel radius R	4.5
Desired final displacement u_{eq} [mm]	$100 - 200^3$
Peak shotcrete utilisation [-]	0.80

---

[3] Measured since face passage (omitting the predisplacements).

Utilising the closed form solution by Feder & Arwanitakis (1976) and the relationship proposed by Hoek (2008) determining the pre-displacements, we obtain the final radial displacement in an unsupported case u_{max} of 690 mm and displacements ahead of the face u_0 of 147 mm. After that, the initial guess regarding the support concept is made (Table 5).

Table 5. Support concept

Rock bolts	
Yield stress σ_{yield} [MPa]	600
Diameter d_{rb} [mm]	32
Length L_{rb} [m]	4
Number of bolts n_{bolts} [-]	24
Shotcrete	
Secant modulus E_{shot} [MPa]	3000
Lining thickness t [cm]	25
28 days-strength β [MPa]	35
Yielding elements	
Number of gaps [-]	4
Yield load (Set 1) [kN]	500
Shortening to yield (Set 1) [mm]	15
Length difference between sets [mm]	0
Yield load (Set 2) [kN]	500
Shortening to yield (Set 2) [mm]	15
Boundary conditions	
Advance rate a [m/d]	4

The application of the calculation method described above yields the following results (Figure 49).
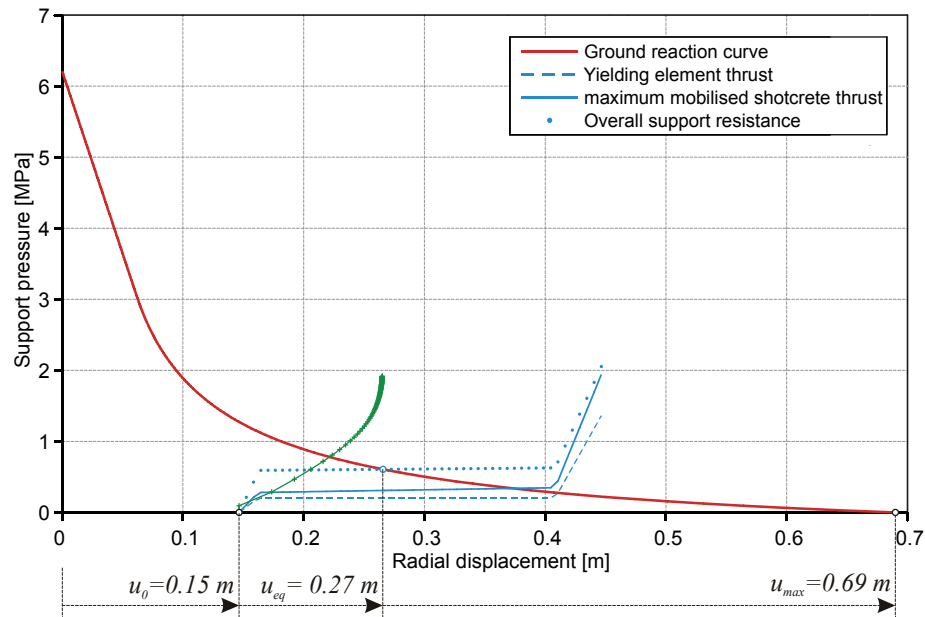
Figure 49. Mobilisation of the support and the expected final displacement under the assumed conditions

As it can be seen, the stiff initial characteristic of the assumed ductile elements (Strengen – Type) leads to shotcrete overstressing. The simplest way to change the support characteristic would be to modify the load-displacement behaviour of the yielding elements by shortening the 2nd set. In addition, the final displacements comply with the requirements (120 mm of final deformation), so the number of the installed rock bolts is reduced from 24 to 20. These changes result in a 20 mm increase of final displacements, and lower the early shotcrete utilisation to reasonable levels (Figure 50). However, the requirement of a peak shotcrete utilisation of 80% is still not met. If the decision is taken that the yielding elements are not to be changed, the problem can only be solved either by additional changes in the rock bolting density, or by a slight increase in the shotcrete thickness, thus raising the thrust capacity. Since an additional decrease in the number of rock bolts would also lead to a decrease of the overall support resistance, the latter solution is applied: the shotcrete thickness is increased to 30 cm.
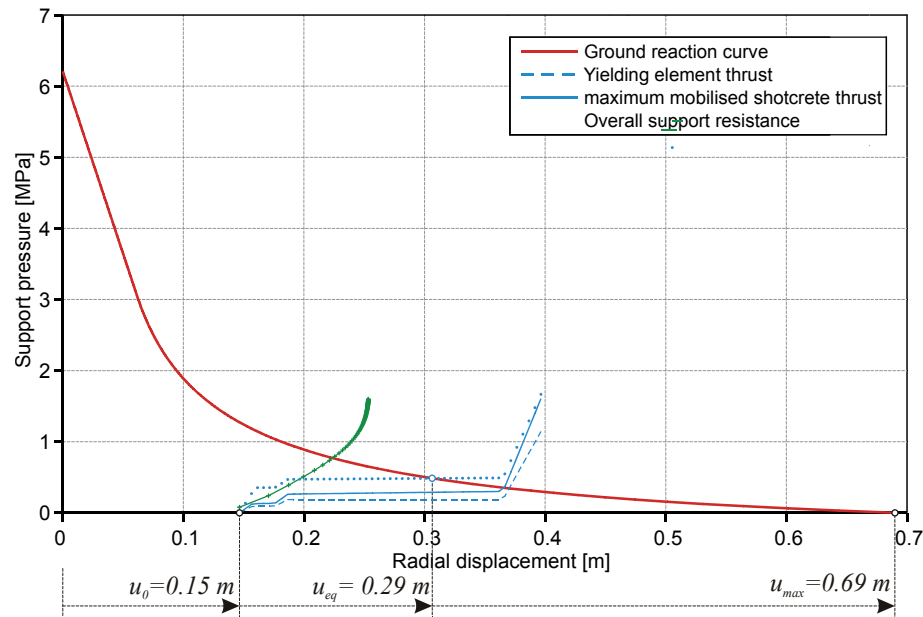
Figure 50. System behaviour in the second iteration step

This results in slightly lower final displacements (285 mm /. 145 mm - if the pre-displacements are omitted) and peak shotcrete utilisation of approx. 80%, making the design acceptable. A priori complications are posed by the application of too stiff Strengen-type elements. They render the finding of a design fulfilling both the imperative of acceptable safety against failure of young shotcrete and the imperative of a well balanced mobilisation of the shotcrete in later stages an almost impossible task (Schubert, 2008; Radoncic et al., 2009). In this particular case, the final utilisation drops to approx. 20%. The application of more sophisticated LSC – elements would raise the utilisation to approx. 50% while still leaving the young shotcrete "unharmed" (Radoncic et al, 2009).

Needless to say, the decision making process in the course of the design has to be oriented on costs and site availability of the envisioned support measures. There is always more than one way to obtain an acceptable design, even when such rudimentary design methods are used. The final design has to pay respect to the relative orientation of the rock mass structure and all other aspects of ground behaviour (as presented in chapter 2.2.2) as well.

4.2.5 Concluding remarks

The presented extensions to the convergence – confinement method capture the most relevant aspects of system behaviour, emerging when utilising yielding elements. Certain drawbacks are inherent to the method itself (assumptions of the radial symmetric displacement field and circular excavation), while others may be circumvented by additional research:

- Determination of additional relationships describing the longitudinal displacement profile in case of support installation;

- Interactions between the support stiffness and the amount of pre-displacements;
- Derivation of additional closed-form solutions for more sophisticated constitutive laws (if possible).

In the light of the widespread use of staged excavation in tunnelling, the major drawback lies in the inability to correctly predict the system behaviour associated with a top heading – bench advance. Especially in case of omitting the installation of a temporary invert, the assessment of system behaviour obtained from the convergence confinement method always exaggerates the mobilisation of the support resistance.

4.3 Support design of a top heading advance

The fields of the mechanical quantities (e.g. stresses, strains et cetera) for most of the non-radial-symmetric problems can be determined only by conducting a numerical analysis. As numerical analysis is always associated with the drawback of increased calculation time, thus parameter studies or probabilistic analysis of the system behaviour still are very rare and usually bound to academic application examples (Schweiger, 2010). In order to retain the advantages of the convergence confinement method (fast analysis and transparent depiction of all relevant relationships), but to broaden its field of application to non-symmetric problems, a novel approach has been developed.

The basic idea is founded on the fact that the calculation of the ground response to the excavation causes the highest amount of calculation time (the support measures can be usually modelled by very simple means). On the other hand, the closed-from solutions describing the strain, stress and displacement fields in case of the simple and most widely used constitutive laws (Mohr-Coulomb, Hoek-Brown) are already known, and capture the basic relationships between the ground properties, excavation size and primary stresses. Hence, an "adjustment" relationship for the closed-form solution should be derived, describing the displacement field for other excavation geometries with reasonable accuracy. In order to obtain the "adjustment relationships", a numerical parameter study with widely scattering ground parameters has been conducted, leading to determination of the displacement development associated with every particular case. The results are compared to the respective results of a closed – form solution, yielding a set of correction factors. If an appropriate interpolation relationship is used and the sampling range is wide enough, then the ground response for arbitrary parameter combinations can be predicted reasonably well. For a realistic assessment of the system behaviour with arbitrary geometric boundary conditions, following issues have to be solved:

- *Reference model*. Since the displacement field is unknown, a set of numerical simulations has to be conducted with well – chosen and widely ranging ground properties. In this case, a FLAC^{3D} model with a very fine grid was used for this purpose.
- *Interpolation relationship*. The determined correction factors have to be interpolated for arbitrary ground parameters, assuming that their values are between the ones used in the sampling run. The used interpolation technique has to be robust, transparent and not prone to over-fitting.
- *Assessment of pre-relaxation*. Since the excavation shape is not circular, the empirical relationship describing the magnitude of predisplacements for a full face excavation has to be reevaluated.

- *Equilibrium conditions.* The resulting displacement field is not radial symmetric, and thus does not mobilise a homogenous, constant pressure distribution at the boundary between the lining and the rock mass. A new equilibrium criterion has to be applied in order to obtain rigorous analysis results.
- *Longitudinal displacement profile.* All of the currently published relationships have been derived from models assuming circular excavation. Hence, a new set of relationships has to be developed in case of top-heading advance.

In the following chapters, the theoretical framework of the interpolation technique and the equilibrium finding process will be presented and discussed first. Subsequently, the developed solutions for the issues presented above will be discussed in detail, followed by the application of the developed methodology to realistic ground conditions and results verification.

4.3.1 Work balance as equilibrium criterion

The equilibrium between two deforming bodies in contact can be reformulated by using Castiglianos second theorem. Instead of seeking and finding the tractions equilibrium in the contact area, the equilibrium equations can be assembled by analysing the external work performed by the deforming entities.

The internal energy change of the ground ΔU is governed by various processes triggered by the stress change due to excavation. In general, it is composed of elastic deformation and associated change of potential $\Delta \Pi$, intact rock cracking and ductile shearing processes converting the mechanical work into heat and damped wave emissions (both representing dissipative work) $W_{diss,int}$, shearing of discontinuities $W_{diss,joint}$ and movement of mass in the gravity field of the Earth, hence resulting in a potential change $\Delta \Pi_{grav}$ (Equation 28). A well documented summary of the complex internal energy balance terms has been published by Salomon (1984)[4] and is being used since then in the distinct element code UDEC (Itasca, 2009).

$$\Delta U + \Delta \Pi + \Delta \Pi_{grav} + W_{diss,int} + W_{diss,joint} = 0 \qquad \textbf{Equation 28}$$

Since the calculations presented in the scope of this work assume the ground to behave as a continuum, the energy balance terms associated with the shearing, cracking and discontinuity movement mechanisms are "smeared" into the overall dissipative work term W_{pl}, representing the strength properties of the ground and their relation to the stress state. Hence, the internal change of energy is always governed by the assumed constitutive law, dictating the relationship between stresses and strains. If the potential change associated with mass movement is

---

[4] The balance terms and the sign convention have been taken over from Salomon (1984), however the variable nomenclature has been changed for the sake of better understanding of the equations.

neglected, the external work of the ground (treated as continuum) can be easily determined, simply being the volume integral of the product of stress change $\Delta\boldsymbol{\sigma}$ and strain history $d\boldsymbol{\varepsilon}$ (Equation 29).

$$W = \Delta U = \int_V \int_\varepsilon \Delta\boldsymbol{\sigma} d\varepsilon dV \qquad \textbf{Equation 29}$$

The external work of the ground W equals the total internal energy change in the ground, composed of the elastic potential change ΔU and dissipative work W_{diss}, as mentioned above. The simplest example of the external ground work calculation is the integration of the ground reaction curve obtained from the closed form solution by Feder & Arwanitakis (1976). Since the ground reaction curve is defined by the internal support pressure p_{sup} and corresponding radial displacements u_{rad}, the integral equation is straightforward (Equation 30).

$$W(u_{rad}) = 2R\pi \int_0^{u_{rad}} p_{sup}(u_{rad}) du_{rad} \qquad \textbf{Equation 30}$$

If the sign convention has been obeyed rigorously, one comes to the conclusion that the work performed by the ground is always *negative*. This is, after a brief inspection of internal workings of excavation induced stress redistribution, utterly logical: after the excavation, the new equilibrium state has to be at a lower energy level (being one of the basic principles of physics), hence leading to an energy release. Due to the stored energy (gravity potential and primary stresses / strains), the deforming ground "wants" to perform work on whatever support measures are installed (Salamon, 1984; Brady & Brown, 1985).

On the other hand, the work performed on the support W_{sup} is always positive, since work has to be performed on the support in order to deform it. This raises its internal energy level and/or dissipates the external work. The equilibrium point of the system ground + support is given when the sum of both works W_{tot} is at its extremum, with the one-dimensional formulation of this requirement given in Equation 31.

$$\frac{d(W_{sup} + W)}{du} = 0 \qquad \textbf{Equation 31}$$

If the deforming ground "wishes" to perform the same amount of work on the support as would be activated by the given deformation, then the system is at the equilibrium and no further displacements occur. In case of a one – dimensional problem as posed by the boundary conditions assumed when applying the convergence confinement method, it can be easily shown that both approaches to equilibrium finding are interchangeable and yield identical results.
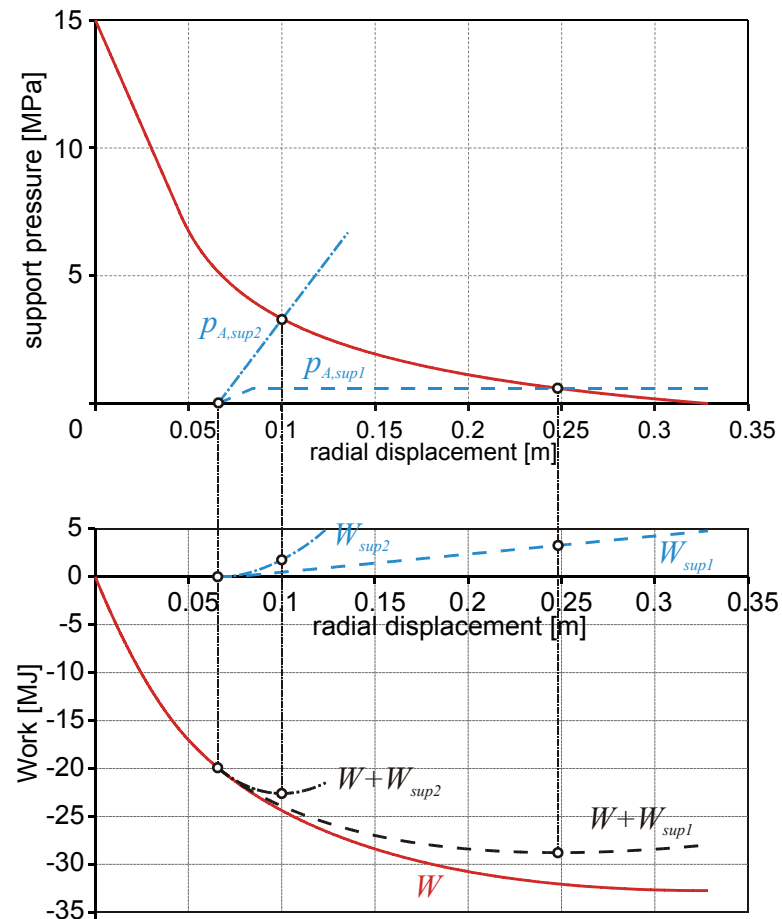
Figure 51. The equivalence between convergence confinement method and work balance equations. Above: equilibrium finding in case of a stiff ($p_{A,sup2}$) and ductile ($p_{A,sup1}$) support characteristic. Below: the same problem expressed by the balances of the external work.

In Figure 51, two different support reaction curves have been considered, demonstrating that more work is performed on a stiff support (assuming equal displacements), thus obtaining an earlier equilibrium. For excavation geometries other than circular and/or anisotropic material behaviour, the scalar derivative of the work balance has to be replaced by the gradient along the displacements $\mathbf{u}_{CP}$ of the points describing the displacement field (Equation 32).

$$\nabla W(\mathbf{u}_{CP}) + \nabla W_{sup}(\mathbf{u}_{CP}) = \mathbf{0}$$

Equation 32

Equation 32 yields the equation system as obtained by every implicit numerical method (finite and boundary elements), required to solve the ground-support interaction at the contact boundary. Every partial derivative of the work balance yields the associated force (stiffness).

In the course of this work, the finding of equilibrium (as presented in Equation 32) is approximated by the assumption that the displacement field of a top heading is reasonably well described by three control points and their respective radial and tangential displacements (see also next chapter). It is assumed that each step of stress removal from the excavation boundary is uniquely associated

with one energy level and one associated displacement field of the crown, shoulder and sidewall point, and does not change by the support installation. This is an incorrect assumption, since same energy states can be attained either by high crown displacements and low sidewall displacements or vice versa (possessing an infinite number of combinations), depending on the local stiffness of the installed support and its resistance to the ground deformation. However, if the above simplification is used, then the equilibrium can be easily found by a stepwise removal of the internal stresses and applying the resulting displacement field on the lining shell and analysing the balance of work. As already mentioned, no local modification of the displacement field of the ground is performed. Thus, the installation of a support results in a ground displacement field associated with a lower relaxation ratio. The stiffer the support is - the less relaxation occurs.

This solution represents only a local minimum of the energy level in the ground – support system, since no variational calculus (as shown in Equation 32) is performed. The local force equilibrium is slightly harmed, since merely the work balance is considered and rough discretization of the ground (three control points) is used. However, if no concentrations of support measures (for example dense rock bolting in the sidewall, and no rock bolts in the crown area) or sudden stiffness jumps in the lining shell are present, the discrepancy between the results of rigorous analysis and the presented approximation method is reasonably low.

4.3.2 Moving Least Squares approximation

In contrast to the fixed set of correction functions proposed by Gonzales-Nicieza et al. (2008), the issue of finding the appropriate correctional relationships in order to describe the displacement field of an arbitrary excavation geometry (and/or ground structure) is solved by applying the Moving Least Squares (MLS) approximation technique (Levin, 1998). The main advantage lies in the flexibility, since almost every continuous displacement field can be described reasonably well if the sampling density (the amount of considered reference cases) is sufficient. In addition, the approach is fairly transparent, since it relies on simple mathematical relationships and allows direct scrutiny of the interpolation quality. Although a full mathematical treatise of the topic would be beyond the scope of this work and is basically irrelevant for the issues treated within the thesis, a brief description of the used technique is given nevertheless. Basic understanding of the concept and the flexibility it offers has high relevance for the discussion of the results and argumentation regarding further development. For in-depth information, two publications offering excellent treatise are recommended: Levin (1998) and Nealen (2010). The following short explanation is based on the research work on numerical back analysis by Grešovnik (2006).

The least squares fitting of simple polynomials to series of sampling points (for example containing measurement data) is a very old and ubiquitous technique. For instance, the reference function $r(x)$ is known at m points:

$$r(x_i) = \bar{y}_i, i = 1,...,m.$$

Equation 33

The coefficients of a linear combination of n functions $f_1(x),...,f_n(x)$ are sought for

$$y(x) = a_1 f_1(x) + a_2 f_2(x) + ... + a_n f_n(x),$$

Equation 34

such that

$$y(x) \approx r(x).$$

Equation 35

Hence, we want the approximation function $y(x)$, composed of a combination of primitive (usually polynomial) functions $f_i(x)$ to fit the measurement data given by the points $[x_i, r(x_i)]$ in a best possible way. The least – squares fitting means that the square of the difference is minimized with respect to the fitting parameters a_i:

$$\phi(\mathbf{a}) = \sum_{k=1}^{m} w_k^2 (y(x_k) - \bar{y}_k)^2.$$

Equation 36

The weighting parameters w_k represent the focus "put" on the point $[x_k, r(x_k)]$, allowing "steering" of the respective points relevance. The optimal parameters a_i are given, when the gradient of the function $\phi(\mathbf{a})$ equals zero:

$$\frac{d\phi(\mathbf{a})}{da_k} = 0 \text{ with } k = 1,...,n.$$

Equation 37

The partial derivatives of the Equation 36 are given as:

$$\frac{d\phi(\mathbf{a})}{da_i} = 2\sum_{k=1}^{m} \left(w_k^2 \left(\sum_{j=1}^{n} a_j f_j(x_k) - \bar{y}_k \right) f_i(x_k) \right),$$

Equation 38

leading, after the multiplication and using the Equation 37 (each derivative has to be zero), to the following system of equations for the unknown coefficients a_j:

$$\sum_{j=1}^{n} a_j \sum_{k=1}^{m} \left(w_k^2 f_j(x_k) f_i(x_k) \right) = \sum_{k=1}^{m} \left(w_k^2 y_k f_i(x_k) \right), \ i = 1,...,n.$$

Equation 39

The coefficients **a** can be obtained by solving the linear system of equations

$$\mathbf{Ca} = \mathbf{d}$$

Equation 40

where

$$C_{ij} = \sum_{k=1}^{m} w_k^2 f_i(x_k) f_j(x_k)$$

Equation 41

and

$$d_i = \sum_{k=1}^{m} w_k^2 f_i(x_k) y_k.$$

Equation 42

Hence, for a linear combination of fitting functions, no optimisation algorithm is required and the parameters can be obtained directly from the assumed fitting function and the sampling point data. The basic idea of Moving Least Squares is

that, since a primitive fitting function $y(x)$ cannot fit large sets of arbitrary data, a *local* weighting function $w(x_k)$ is introduced. By an appropriate choice of this function (usually a Gaussian), the points in the vicinity of the sampling point x_k gain high importance, and the fitting function $y(x)$ is easily able to fit the data in this narrow range x. For every sampled point, the weighting function $w(x)$ "slides" to the new sampling point and a new fitting local function $y_k(x)$ is calculated (Figure 52).
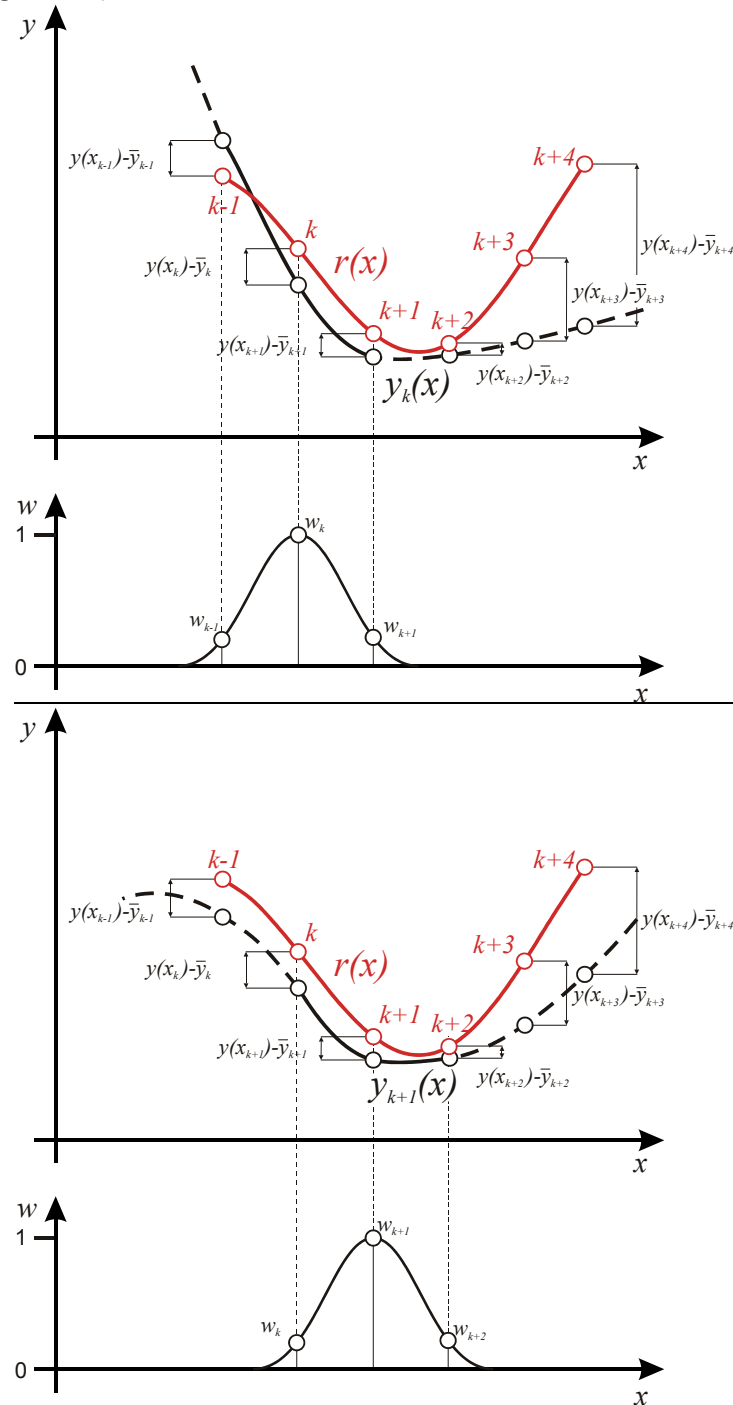

Figure 52. The principle of the moving weighting function $w_k(x)$. Above: local fit and weighting for the sampling point x_k. Below: local fit and weighting for the sampling point x_{k+1}.

The global fitting function, composed of the sum of the local fitting functions, is obtained by adding the weighted average of all weighting functions:

$$y(x) = \sum_{k=1}^{m} \frac{w_k(x)}{\sum_{i=1}^{m} w_i(x)} y_k(x).$$

Equation 43

The great advantage of Moving Least Squares over other approaches used for fitting a complex function response is given by their transparency and the ability to switch between mere interpolation (if the weighting function w is set to a narrow shape) and approximation of complex function shapes (if the weighting function is wide). Hence, the amount of "over-fitting", usually present with other interpolation/approximation techniques (such as Lagrangian polynomials or neuronal networks) can be easily controlled by fine-tuning the weighting function parameters. In order to demonstrate the approximation abilities and noise robustness of the MLS algorithm, the test function

$$r(x) = \sin(4x) + 0.5 \cdot e^{x/2} + \begin{Bmatrix} 0; x < 4.7 \\ -4; x \geq 4.7 \end{Bmatrix}$$

Equation 44

has been sampled in the interval (0,6). The local fitting function $y_k(x)$ is quadratic:

$$y_k(x) = \frac{1}{2} a_{k1} x^2 + a_{k2} x + a_{k3}$$

Equation 45

with the function shape parameters a_{k1}, a_{k2} and a_{k3}. The weighting function $w_k(x)$ is Gaussian:

$$w_k(x) = e^{-\left((x-x_k)^2 / d \right)^2},$$

Equation 46

and its area of influence is steered by the choice of the parameter d. With an increasing value of the parameter d, the algorithm tends more to *approximation* and away from interpolation. The results with no noise added to the sampling and MLS fitting with the shape parameter d set to 0.35 are shown in Figure 53. As expected, the basic shape of the function is excellently fitted, and only the discontinuity at $x = 4.7$ causes problems. If the shape parameter is set to 0.70, the fit becomes worse, and the global fit function tends more to describing the general shape of the reference function (Figure 54). Finally, if a slightly denser sampling is applied, the basic shape of the function can be found even if the response of the reference function is noisy (Figure 55). Especially this feature is important for the capturing of the displacement field, since the numerical model used as reference model features intrinsic noise associated with discretization and floating point round-off errors.

The approach can be easily extended to *n*-dimensional functions, allowing robust fitting of surfaces. The main field of application of the MLS approximation is laser scanning and general image acquisition, since it represents an elegant way for shape recognition in case of a point cloud (usually obtained from laser scanning). More recently, it is also becoming used as means for initial

approximation the objective function in numerical analysis (Grešovnik, 2006) and in upcoming meshless methods (Pan et al., 2004).
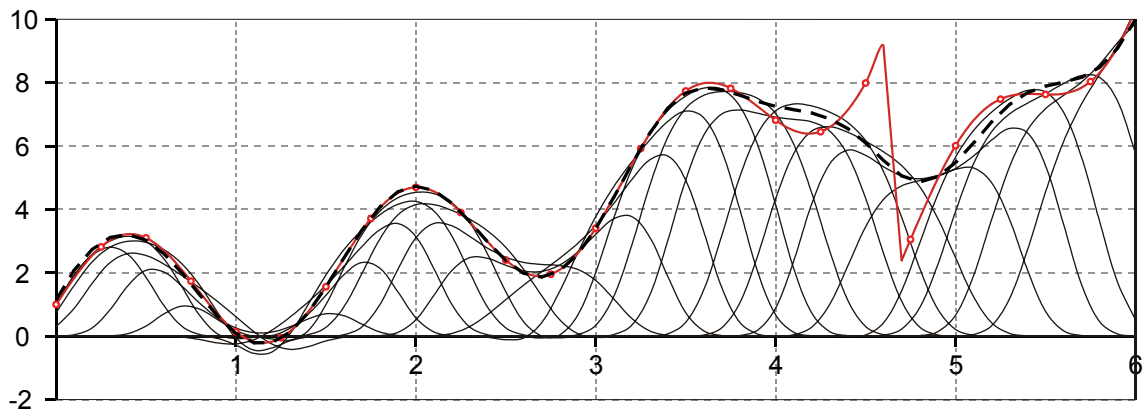

Figure 53. Results of MLS fitting with the reference function featuring no noise and range parameter set to 0.35. Red line: reference function with the sampling values (red dots). Black line: global fitting by MLS. Thin black lines: local approximations
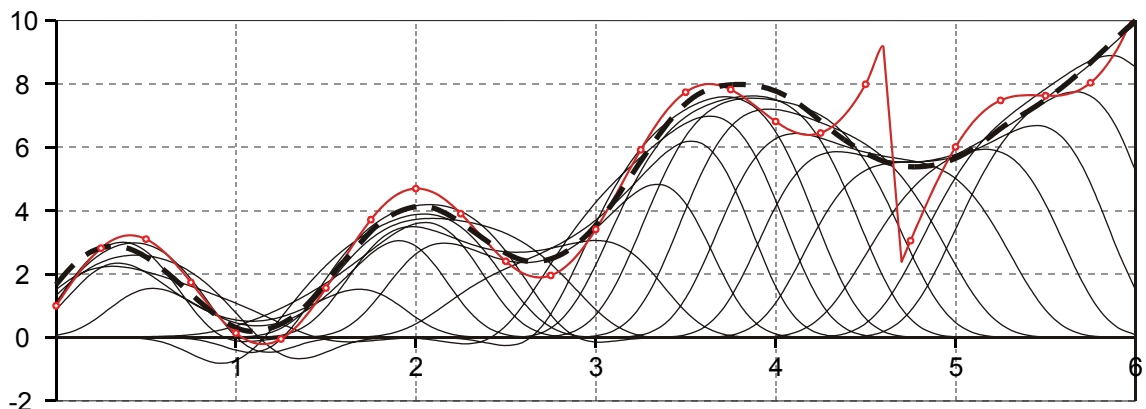

Figure 54. Results of MLS fitting with the reference function featuring no noise and range parameter set to 0.70.
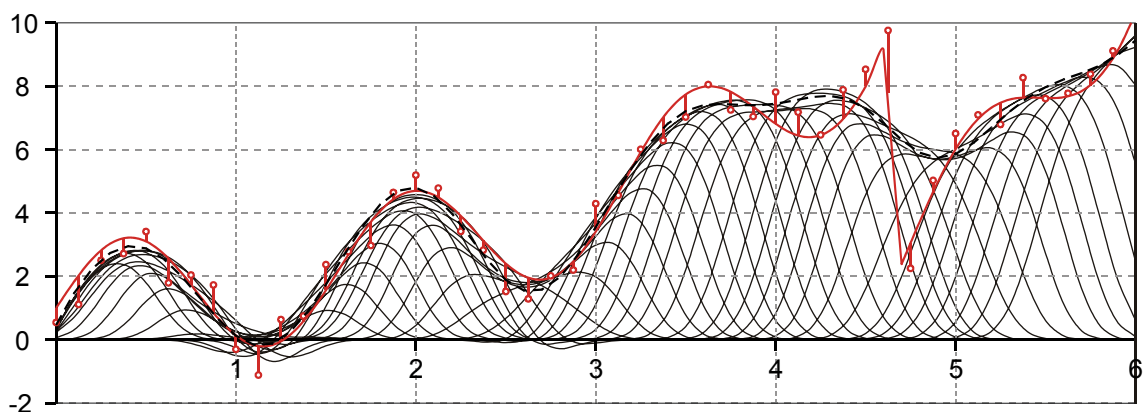

Figure 55. Results of MLS fitting with the reference function featuring strong noise, range parameter set to 0.35 and increased sampling density.

4.3.3 Determination of the displacement field

In order to obtain the correction factors describing the displacement field of a top heading in Mohr-Coulomb medium, a series of FLAC3D calculations with a very fine discretization and large model (in order to keep the boundary truncation errors as low as possible) have been conducted. In the first step, the numerical model has been verified by modelling full-face excavation (the top heading has been modelled as a half-circle, thus making the model symmetrical) and comparing the calculated stresses, strains and displacements with those presented in the closed form solution by Feder & Arwanitakis (1976). The behaviour of the model was deemed highly satisfactory, with errors less than 1%. The ground parameters have been chosen in such way that the friction angle and the plastic radius R_{pl} (calculated from the closed-from solution) form a regular grid, similar to the work conducted by Pilgerstorfer (2008). The cohesion values associated with each plasticity ratio (defied as plastic radius R_{pl} divided by the tunnel radius R) and the respective friction angles are presented in Table 6, along with the elastic parameters.

Table 6. Overview of the sampling parameters

	Friction angle φ [°]			
R_{pl}/R	15	20	25	30
1,0	11.5	10.48	9.55	8.63
1,5	5.08	4.15	3.28	2.47
2,0	3.38	2.57	1.85	1.24
2,5	2.58	1.86	1.24	0.75
3,0	2.11	1.45	0.91	0.51
3,5	1.80	1.19	0.71	0.31

Bulk modulus K [MPa]	555.56
Shear modulus G [Mpa]	416.67
Primary stress p_1 [Mpa]	15.0

Both in the numerical model depicting the top-heading response and in the closed-form solution, a hydrostatic primary stress state ($K_0 = 1.0$) is assumed.

In the numerical model, the internal support pressure p_{sup} is removed stepwise from the excavation boundary, with the relaxation parameter λ ranging between 0 (primary stress state) and 1 (full relaxation):

$$p_{\text{sup}} = p_1(1-\lambda).$$ **Equation 47**

Analogously to the convergence confinement method, this yields the "ground reaction curves" for every point at the excavation boundary. The occurring displacements of the control points representing sidewall, shoulder and crown position have been recorded in each numerical run. Their positions have been set at 5°, 45° and 90° in the polar coordinate system, counted clockwise from the global x – axis (Figure 56). In order to obtain direct comparison with the radial displacements obtained from the closed form solution assuming equal ground

conditions, the displacements are decomposed into their radial and tangential components (Figure 56).
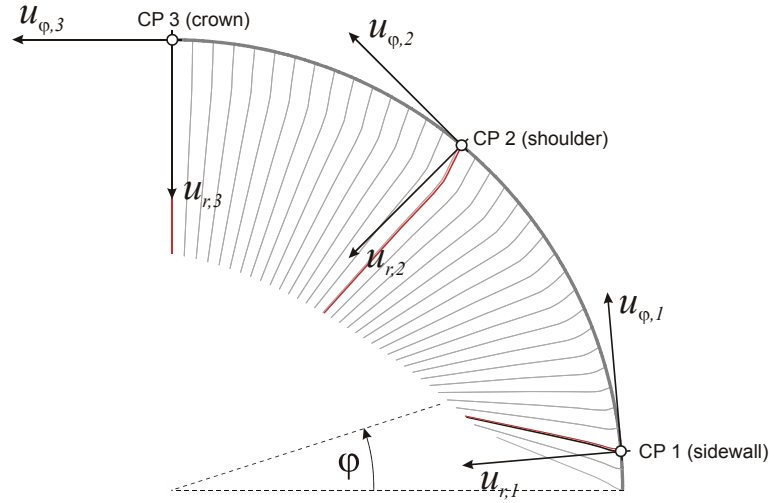

Figure 56. Control points definition and the applied local coordinate systems (grey lines: displacement paths of all grid points, red lines: displacement paths of the control points)

In all further calculation steps, the displacement field of the top heading is assumed to be fully described by the spline interpolation of the radial and tangential portions of the three control points. As presented in Radoncic & Schubert (2009), the deviations from the true response are reasonably low even if more sophisticated, anisotropic constitutive laws are applied.

The correction ratios $k_{r,i}$ and $k_{\varphi,i}$ are obtained by dividing the radial and tangential displacements $u_{r,i}$ and $u_{\varphi,i}$ of each control point i, at each relaxation step and for each set of ground parameters by the final radial displacement obtained from the closed-form solution u_{rad}, (Equation 48 and Equation 49).

$$k_{r,i} = \frac{u_{r,i}(\lambda,c,\varphi,K,G)}{u_{rad}(\lambda=0,c,\varphi,K,G)}. \qquad \textbf{Equation 48}$$

$$k_{\varphi,i} = \frac{u_{\varphi,i}(\lambda,c,\varphi,K,G)}{u_{rad}(\lambda=0,c,\varphi,K,G)}. \qquad \textbf{Equation 49}$$

Hence, for the 24 parameter sets and 11 relaxation sets, three radial correction factors and two tangential correction factors (since the crown point features zero tangential displacement in the assumed conditions) are obtained, respectively. The decision to normalise the displacements with the final displacements from the closed form solution has been made upon inspecting the data – all other relationships yielded highly oscillating interpolation surfaces. Analysis of the data yielded negligible dependency of the correction ratios on the friction angle, with the depth of the plastic zone being the dominant parameter influencing the displacement field of the top heading. As the depth of failure increases, the displacements tend to become more and more radial.

In the next and final step, approximation surfaces for the five correction factors are established by the MLS algorithm. The co-ordinate system is spanned by the ratio between the plastic radius R_{pl} and the tunnel radius R (x-axis) and the respective relaxation ratio λ (y-axis), rendering the found relationship independent from the excavation size (since all used variables are unit less). The MLS fitting is easily extended to three-dimensional problems by introducing a quadratic surface as the local fit function

$$z(x,y) = a_1 \frac{1}{2}x^2 + a_2 \frac{1}{2}y^2 + a_3 xy + a_4 x + a_5 y + a_6 , \qquad \textbf{Equation 50}$$

and an anisotropic Gaussian weighting function:

$$w_k(x,y) = e^{-\left((x-x_k)^2/d_1 + (y-y_k)^2/d_2\right)^2} . \qquad \textbf{Equation 51}$$

The definition of an anisotropic function is required due to the different distance of the sampling point along the respective axes: while the ratio R_{pl}/R ranges from 1 to 3.5, the relaxation factor λ spans only values between 0 and 1. The resulting global interpolation function for the correction values (regarding radial displacements) of the crown point in shown in Figure 57.
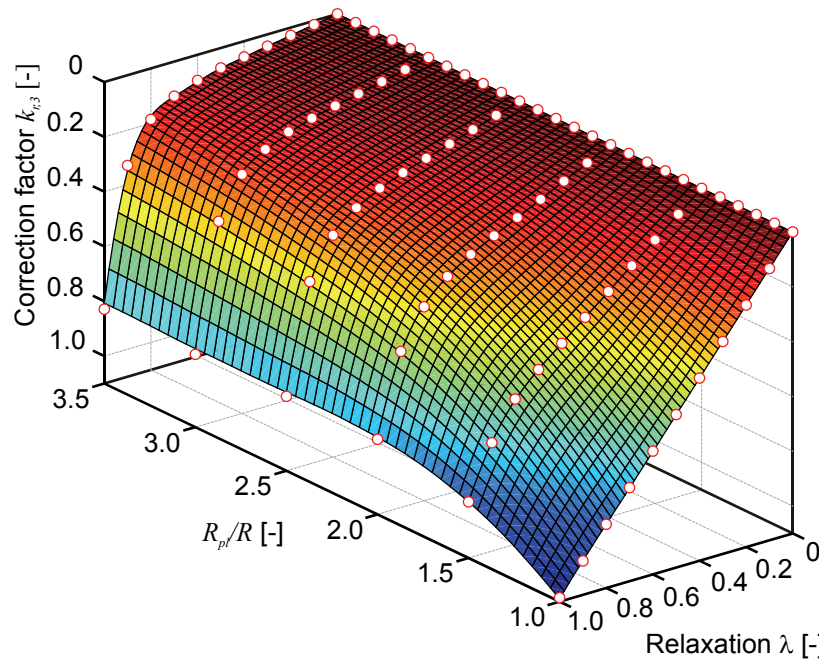

Figure 57. Global interpolation function for the radial displacement correction coefficients $k_{r,3}$ of the crown point (white dots mark the results of the numerical analysis, e.g. the used sampling points)

As is can be seen, in elastic conditions ($R_{pl}/R = 1$) the crown point of a top heading features higher radial displacements than in the case of circular excavation. This is logical, since the top – heading excavation causes additional disturbance in the stress field and hinders the development of a smooth stress distribution around the tunnel. With growing depth of the failure zone, the correction coefficient value quickly converges towards 0.82 (in case of full relaxation). The low variation of the function values above a certain value of

R_{pl}/R has been observed in all interpolation surfaces, and is being used for predicting the displacement fields in conditions where the coefficient R_{pl}/R is higher then 3.5. Since the variation of the function value in the direction of increasing failure zone depth is minimal, the values associated with the $R_{pl}/R = 3.5$ should be applied, if the ratio R_{pl}/R is above 3.5.

Concluding the above explanations, in case of Mohr-Coulomb material and top heading, five distinct interpolation surfaces have been generated (see Appendix 1). The correction relationships have been verified by utilising a new numerical model with differing discretization, randomly generated ground parameters and other excavation size. The differences between the displacement field obtained from a two-dimensional numerical analysis and from applying the correction surfaces to the closed-form solution are minimal and highly satisfactory in all considered cases (Figure 58).
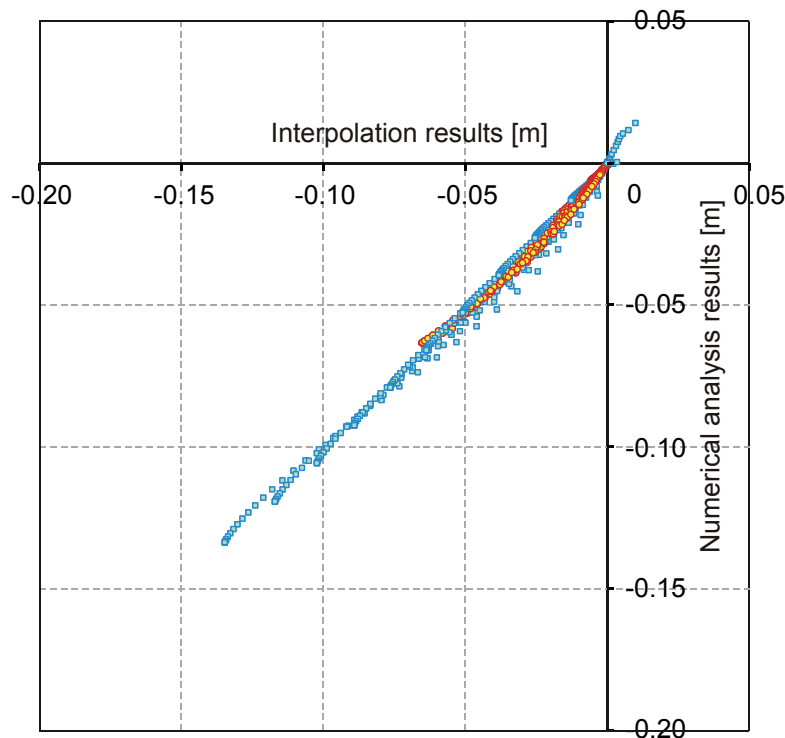

Figure 58. Comparison of the displacement field obtained from numerical analysis and the presented interpolation approach. All grid point displacements of the model have been exported and compared to the interpolation results (For the same position in the cross-section). Dots: horizontal displacements, squares: settlements.

4.3.4 Determination of the external work of the ground

Analogous to the issue of the displacement field associated with a top heading excavation in Mohr-Coulomb material, the external work of the ground has also to be determined on the basis of a numerical reference model. Since FLAC^{3D} doesn't calculate and log the model energy quantities, a short FISH routine was written in order to calculate both the internal energy change and the external

work of the model. The calculation of the internal energy change is straightforward, simply performing element-wise summation of the work densities:

$$\Delta U = \sum_k \boldsymbol{\sigma}_k \dot{\boldsymbol{\varepsilon}}_k \Delta t V_k \quad \text{with } k = 1,...,\text{number of elements.}$$

Equation 52

Since FLAC^{3D} incrementally updates the stress and strain field (explicit time-stepping), the most accurate way of performing the calculation is using the strain rate tensor $\dot{\boldsymbol{\varepsilon}}$ and multiplying it with the internal timestep Δt. Hence, the internal energy change ΔU continuously changes with the ongoing calculation, and only the values obtained upon reaching model equilibrium are logged. However, it captures both the work performed on the arch of the top heading (where the liner is installed) and the work performed by invert heave (which, in case no temporary invert is installed, performs no work on the support). If the equilibrium between the liner installed in the arch and the deforming ground is sought for, then only the fraction of the energy change, associated with the liner deformation, has to be taken into account. Needless to say, this applies only in case of the simplified (equilibrium approximation) analysis - see chapter 4.3.1.

In order to determine the external work of the upper part, the summation of the work performed by boundary forces acting at the respective grid points has to be performed, since it is impossible to know exactly which elements contribute to the deformation of the arch (Figure 59).


$W = \Delta U$ \qquad\qquad $W_{TH} = ?$
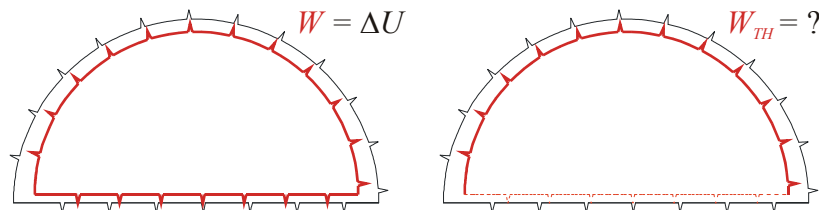
Figure 59. The problem of the external work balance, if only the arch of the top heading is considered.

The calculation is analogous to the one presented above, using the grid point velocities, forces and the model time step:

$$W_{TH} = \sum_k \mathbf{F}_k \mathbf{v}_k \Delta t \quad \text{with } k = 1,...,\text{number of gridpoints.}$$

Equation 53

Both calculation strategies (internal energy change and external work determination) have been verified by performing full-face circular excavation and checking the results against the integral of the respective ground reaction curve obtained from a closed form solution. The occurring discrepancy was found to be negligible.

After the verification, the same set of parameters as used for determining the displacement correction surfaces has been used to examine the relationship between the energy release due to top heading excavation and the one caused by

full face excavation. Luckily, the results follow a very clear trend, thus eliminating the need for complex interpolation relationships (Figure 60).
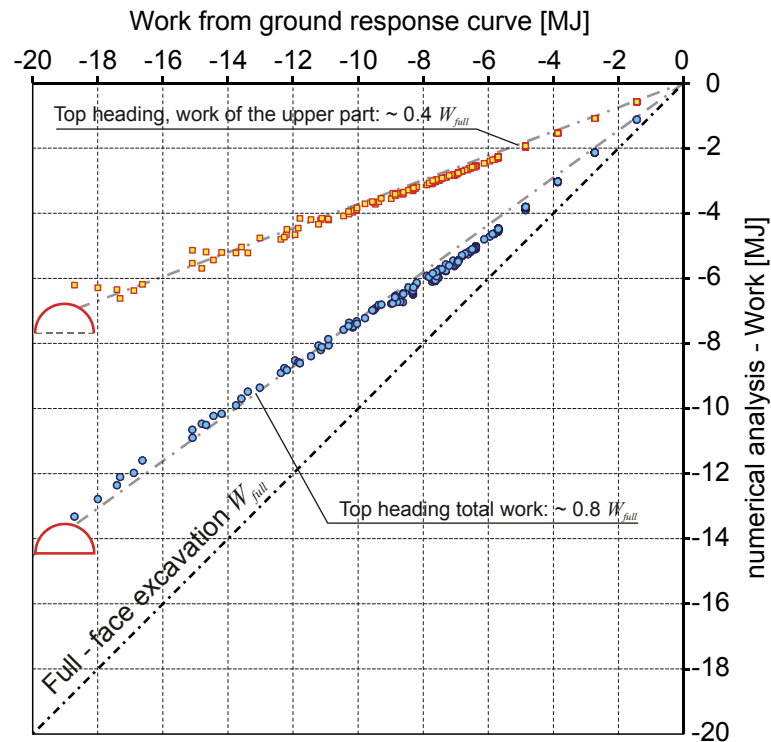

Figure 60. Energy release of the top heading compared to the circular full - face excavation (all relaxation stages)

As it can be seen, the top heading arch performs 40% of the work which would be performed by a full face excavation, while the overall energy release equals 80% of the reference case. This underlines the already common and proven practice of NATM in weak ground and under high overburden: the construction of a top heading without invert support and application of a flexible support concept lead to a considerable relaxation of the rock mass. If the top heading has been constructed successfully, then usually no problems and no "squeezing" can be expected while constructing the bench and the invert. This means that after the construction of the top heading with a flexible support, a major part of the energy stored in the ground has been released.

4.3.5 Determination of pre-relaxation

The determination of the pre-relaxation has been performed by conducting a parameter study with a three-dimensional model and the parameters shown in Table 6, already used for the determination of the interpolation relationships described before. Since a fast and accurate prediction of the displacement field in case of two-dimensional analysis is possible by applying the interpolation relationships, determining of an equivalent relaxation at the moment of face passage is straightforward. The relaxation in the two dimensional model with ground parameters equalling the ones used in the reference model (3D calculation) has to be varied until best fit is achieved. This approach is very similar to the one applied by Pilgerstorfer (2008), however it extends to non-circular excavation geometries. The sketch of the applied principle is shown in Figure 61.
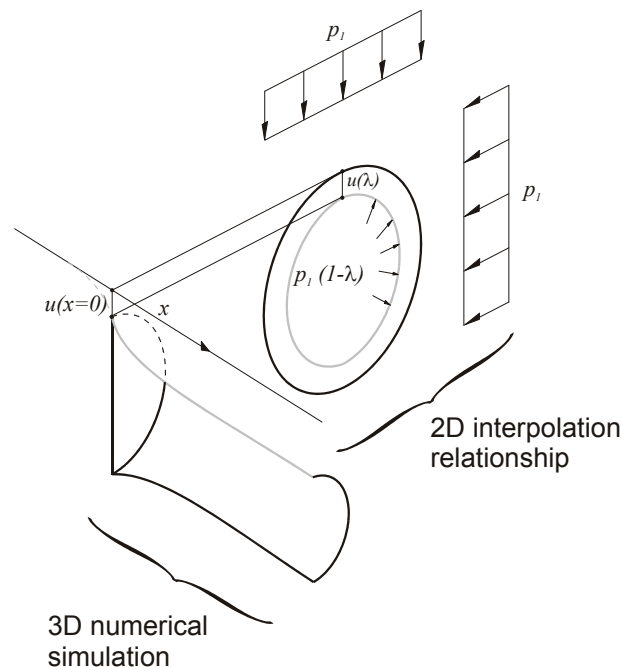

Figure 61. Displacement development due to face advance and the equivalent support pressure (at the face)

However, the displacement path described by the points at the excavation boundary is not entirely the same in both models, since the three dimensional model also accounts for spatial stress re-distribution and results in entirely different stress paths. In order to circumvent this, an objective function $o(\lambda)$, defining the discrepancy between the reference model $u_{3D,r,i}$ and the radial displacements predicted by the "2D model", has been introduced (Equation 54). Only the displacements at the predefined three control points have been taken into account, and the differences in the tangential displacements have been deliberately neglected. Due to the fact that greatest differences are observable in the tangential domain, the optimisation algorithm has shown somewhat adverse convergence behaviour after the tangential displacements have been included.

$$o(\lambda) = \sum_{i=1}^{3} \left(u_{r,i} - u_{3D,r,i} \right)^2 \qquad \textbf{Equation 54}$$

For each parameter set, the optimisation algorithm has been applied to the objective function, determining the respective best-fitting relaxation factor λ. The determined results are coherent and plausible, as depicted in Figure 62.
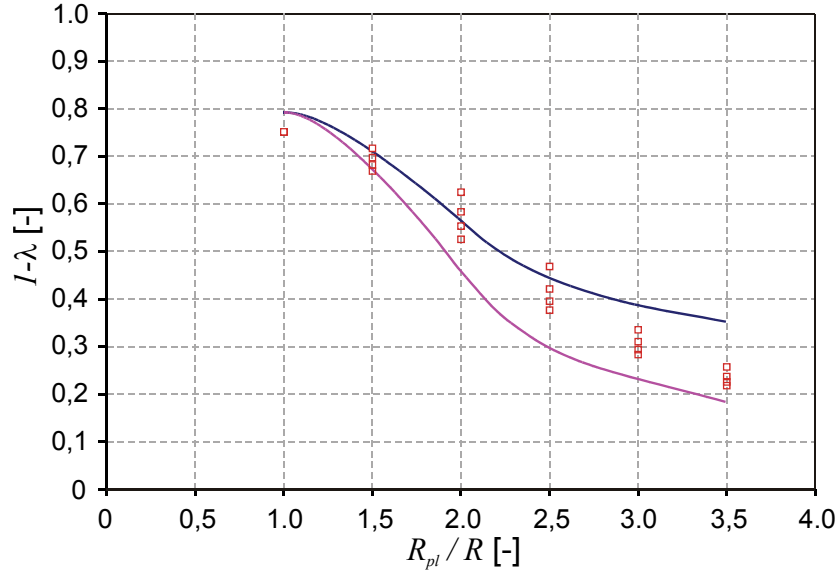

Figure 62. Comparison between the new empirical relationship and the results from the numerical analysis (red squares). The empirical relationship is defined by the red line, marking a friction angle of 30° and the blue line, marking 15°.

The empirical relationship proposed by Hoek et al. (2008) was modified in order to account for the different excavation geometry (Equation 55).

$$u_0 = \frac{1}{4} \cdot 1.5^{\left(-0.30 \frac{R_{pl}}{R} - 0.15 \right)} u_{max} \qquad \textbf{Equation 55}$$

The pre-relaxation ratio is thus defined indirectly by the ratio between the final displacement u_{max} and pre-displacement u_0 obtained from a closed form solution for the same ground conditions. Such a definition was chosen because the direct mathematical description of the pre-relaxation relationship would require a three-dimensional function. While the ratio between pre-displacements and the final displacements primarily depends on the depth of the failure zone, the equivalent pre-relaxation ratio spans a surface defined by the friction angle and the extent of the plastic zone, as shown by Pilgerstorfer (2008) and Hoek et al. (2008). Due to the fact that the results are subject to discretization errors (strongly varying distance from the points, depending on the respective friction angle), the proposed relationship was deemed accurate enough. The discrepancy occurring in the elastic state is basically irrelevant, since squeezing behaviour in ground behaving purely elastic represents only a theoretical possibility. In the code implementation for the calculation method presented here, the equivalent pre-

relaxation is determined each time by utilising Equation 55 and the respective ground reaction curve.

In general, it can be said that the top heading advance behaves "stiffer" (featuring lower pre-displacements) than the equivalent full-face excavation, however this behaviour rapidly disappears with growing depth of failure. Above a certain extent of the plastic zone, the amount of pre-relaxation virtually equals the full face excavation, since the stress peak at the boundary between the plastic and elastic area is far from the excavation.

4.3.6 Determination of longitudinal displacement profiles

The longitudinal displacement profiles have been obtained from the results of the parameter study used for the determination of the pre-relaxation ratios. For all three control points, the radial displacements have been calculated and the function proposed by Panet & Guenot (1982) has been modified until best fit was obtained. The top-heading advance results in slightly more acute displacement development then the full-face excavation, resulting in the lower value of the R_{pl} multiplier:

$$u_i(x) = u_{0,i} + (u_{\max,i} - u_{0,i}) \cdot \left[1 - \left(\frac{0.58 \cdot R_{Pl}}{x + 0.58 \cdot R_{Pl}} \right)^2 \right],$$ **Equation 56**

with $u_i(x)$ – control point displacement at the face distance x,
       $u_{0,i}$ – control point displacement at face passage,
       $u_{\max,i}$ – final control point displacement and
       R_{pl} – plastic radius obtained from the closed-form solution assuming equal ground conditions.

The relationship is valid both for radial and tangential displacements of the control points. As depicted in Figure 63, it allows very good prediction of the displacement development due to face advance for all three control points.

As a final validation step, all displacements (radial and tangential, for each excavation round) have been plotted against their respective predictions according to Equation 56. The results lie on an almost straight line (which denotes perfect congruence), thus verifying the findings above.
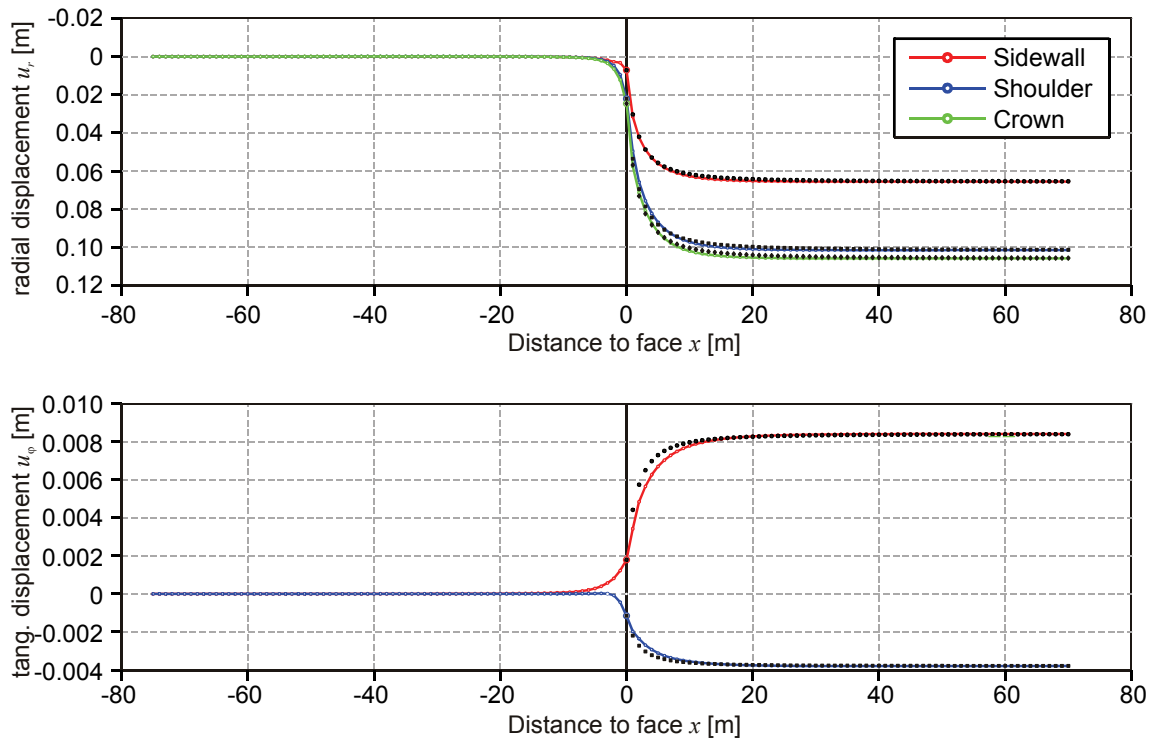
Figure 63. Comparison between the displacement development obtained from the numerical model (lines) with the modified relationship after Panet & Guenot (1982).
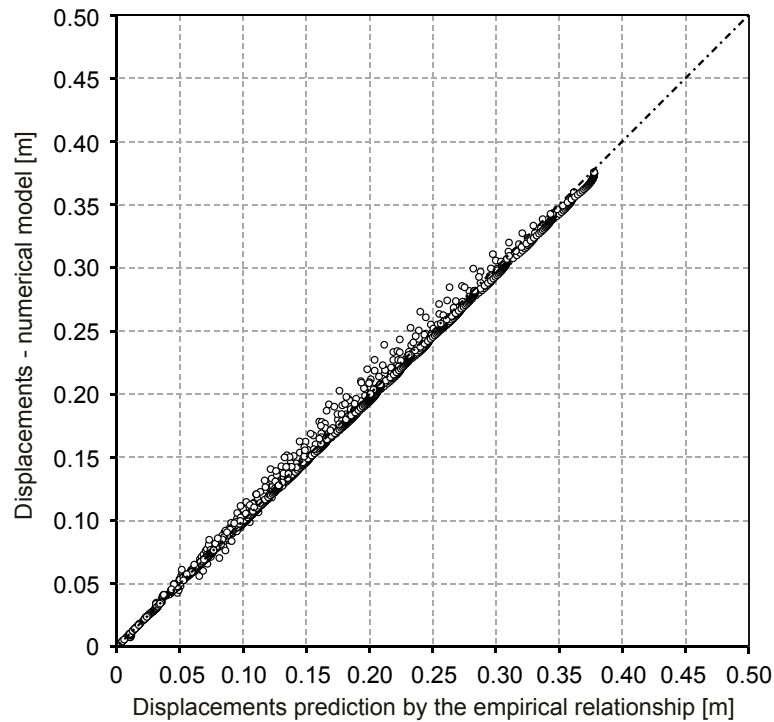

Figure 64. Displacements after face passage, all parameter sets, control points and face positions.

4.3.7 Determination of the support mobilisation

The determination of the system behaviour is conducted analogously to the approach presented in chapter 4.2.2. After the displacement development in the cross section has been determined for all relaxation steps, it is imposed on a discretized model of the top-heading lining (Figure 65). It is assumed that the radial displacements of the lining are equal to the radial displacements of the rock mass, however the tangential portions have to be found, due to the occurrence of slip. Hence, for each relaxation step and the associated rock mass displacement field, the internal force equilibrium of the lining is first attained by solving the associated equation system, and then the external work performed on it is calculated.
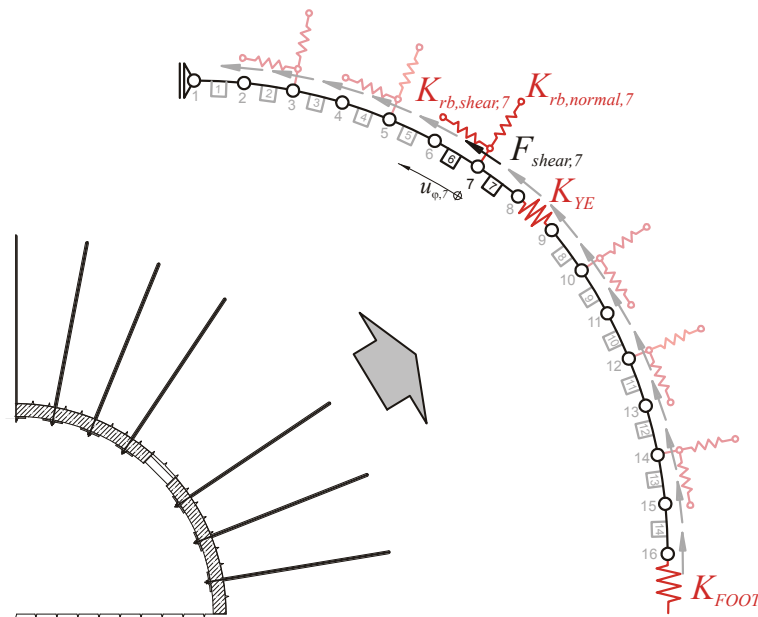
Figure 65. Discretized model of the top heading lining with integrated yielding elements

The equilibrium determination of the lining is performed by assembling a system of node-wise equilibrium equations, representing the unbalanced forces at every node (an example for node 7 is presented in Equation 57[5]). The assembling of a stiffness matrix is omitted completely, and the solution is obtained by varying the tangential displacements until the nodal out-of-balance force vector equals zero.

$$F_{unbal,7} = F^6 + F^7 + F_{shear,7} + F_{rb,7}$$ **Equation 57**

The normal contact forces acting between the lining nodes and the rock mass are calculated by local equilibrium considerations, e.g. by analysing the thrust forces in the lining and calculating the pressure $\sigma_{cont,i}$ acting normal to it:

---

[5] The notation convention presented on page 50 is still valid: subscript index indicates nodal quantities, while superscript denotes truss element quantities. Hence, F^6 denotes the thrust force mobilised in the truss member 6, and dependent on the tangential displacements of nodes 6 and 7.

$$\sigma_{cont,i} = \frac{F^{i-1} + F^i}{2R} .$$

Equation 58

The associated shear force mobilisation is obtained by node-wise integration of the respective contact pressures (simply being multiplied with the associated contact surface associated with the node) and accounting for the friction angle at the contact surface:

$$F_{shear,i} = \sigma_{cont,i} \frac{L^{i-1} + L^i}{2} \tan\varphi .$$

Equation 59

The contribution of rock bolts to the thrust development in the lining is calculated in the same manner as presented in chapter 4.2.2. The slip (shear displacement) between the lining and the rock mass is determined at the respective point, and the secant rock bolt shear stiffness is used to calculate the resulting shear force:

$$F_{shear,i} = \sigma_{cont,i} \frac{L^{i-1} + L^i}{2} \tan\varphi .$$

Equation 60

The relaxation is performed for a series of relaxation factors λ_k, with λ_1 denoting the pre-relaxation at the moment of face passage (see chapter 4.3.5), and λ_n being the final value considered, with λ equalling 1 (full relaxation). Theoretically, only two values are mandatory (λ_2=1), however the series are usually composed of 100 – 200 intermediate steps, ensuring numerical stability and precise determination of the support mobilisation. The calculation of the external work increment of the support measures $\Delta W(\lambda_k)$, associated with the displacement field occurring at the relaxation factor λ_k, is straightforward:

$$\Delta W_{\sup}(\lambda_k) = 2\sum_{i=1}^{n_{TE}} \Delta U_{lin}^i + 2\sum_{i=1}^{n_{rb}} \Delta U_{RB}^i + 2\sum_{i=1}^{n_{YE}} \Delta U_{YE}^i + ...$$

$$... + 2\Delta U_{FOOT} + 2\sum_{i=1}^{m} \Delta W_{shear,i}$$

Equation 61

With ΔU_{lin}^i – work performed by deforming the truss element i of the lining,

ΔU_{RB}^i – work performed on the rock bolt at node i (axial elongation and shear),

ΔU_{YE}^i – work performed by deforming the yielding elements,

ΔU_{FOOT} – work performed by "translation" of the top heading and settlement of the top heading feet

$\Delta W_{shear,i}$ – dissipative work performed by frictional sliding between the lining and the rock mass, calculated nodewise,

n_{TE} – number of truss elements (representing the lining),

n_{rb} – number of installed rock bolts,

n_{YE} – number of yielding elements,

m – number of nodes associated with the lining discretization.

The total external work on the support associated with each relaxation factor λ_k is simply the sum of the work increments:

$$W_{\text{sup}}(\lambda_k) = \sum_{i=1}^{k} \Delta W_{\text{sup}}(\lambda_i).$$ **Equation 62**

After the external work performed on the support has been determined in this manner, it is added to the external work of the ground (associated with the same relaxation factor and the respective field), leading to the determination of the extremum and final displacements associated with the examined support installation.

4.3.8 Application example and verification

In order to verify the new calculation method, the back-analysed ground properties of the Lavanttal fault zone have been used and the results of the calculation method are compared to the measurement data. The back analysis has been conducted by using the convergence-confinement method for the initial parameter guess, while FLAC has been used for fine tuning (Schubert et al., 2009). Since the ground conditions have already been presented in Table 4, only the support configuration is presented in Table 7.

Table 7. Support measures used in the Lavanttal fault system and calculation parameters

Rock bolts	
Yield stress σ_{yield} [MPa]	600
Diameter d_{rb} [mm]	32
Length L_{rb} [m]	4
Number of bolts n_{bolts} (sidewall) [-]	4
Number of bolts n_{bolts} (crown) [-]	8
Shotcrete	
Secant modulus E_{shot} [MPa]	3000
Lining thickness t [cm]	35
28 days-strength β [MPa]	35
Yielding elements	
Number of gaps n_{YE} [-]	2
Gap position φ_{YE} [°]	40/140
Yield load (Set 1) [kN]	500
Shortening to yield (Set 1) [kN]	15
Length difference between sets [mm]	0
Yield load (Set 2) [kN]	500
Shortening to yield (Set 2) [kN]	15
Boundary conditions	
Advance rate a [m/d]	4
TH feet stiffness K_{FOOT} [MN/m]	0.50

In addition, a relatively early construction of a temporary invert (5-10 m behind the face) has been performed. The excavation geometry and the sketch of the support measures listed above are shown in Figure 66.
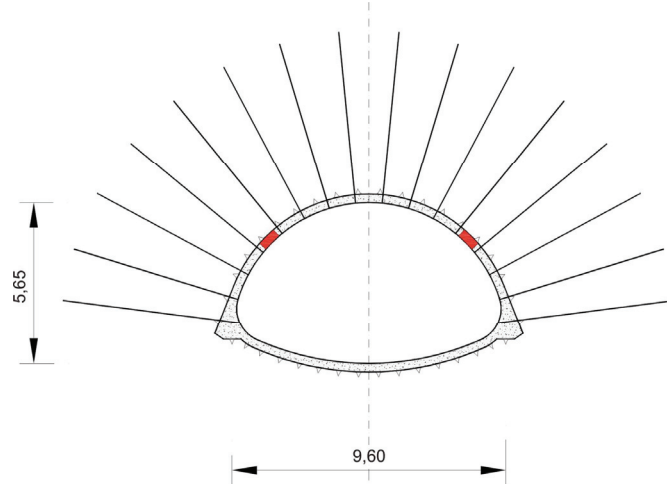
Figure 66. The applied support concept (taken from Schubert et al., 2009)

The comparison between the displacement monitoring data of the measurement cross sections MCS 1136.2, MCS 1194.3, MCS 1238.4, MCS 1268.6, MCS 1304.7 and the calculated displacements is presented in Figure 67.
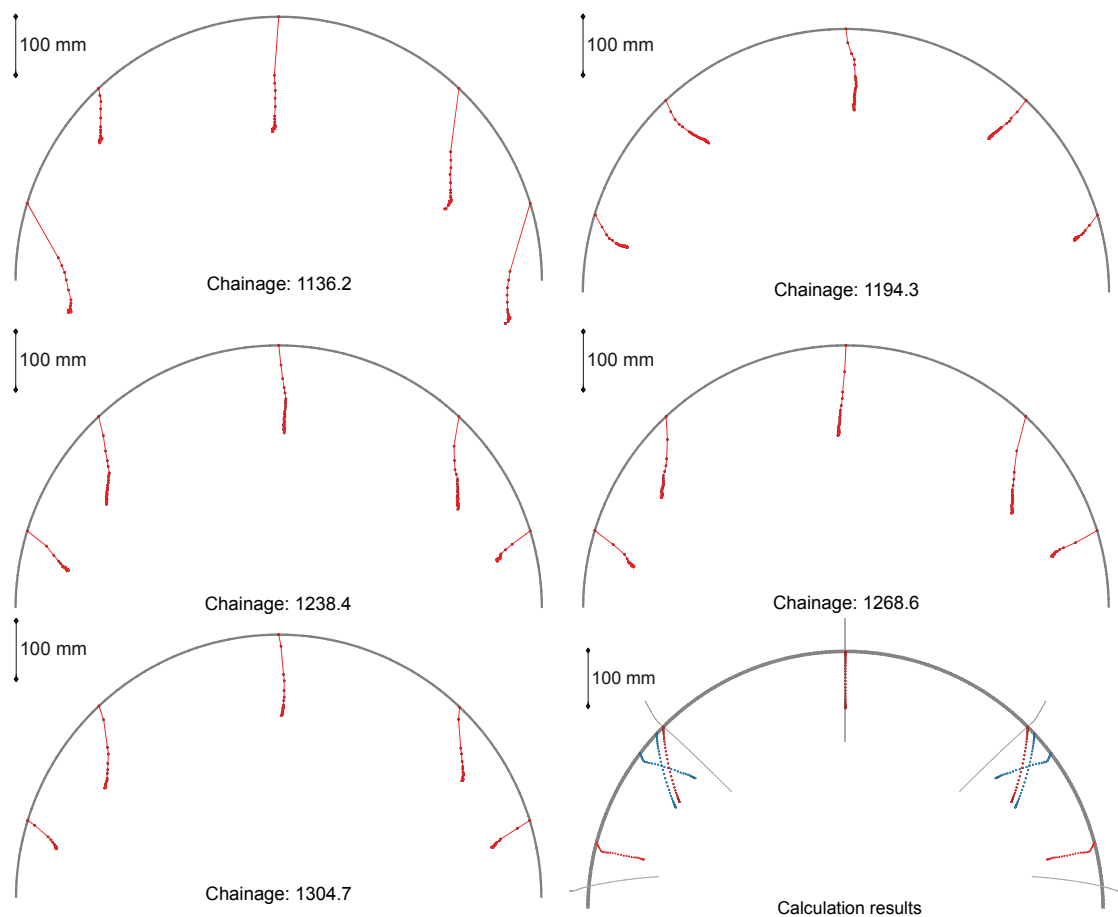
Figure 67. Comparison between displacements measured in the Lavanttal fault and the displacement field predicted by the presented calculation method (grey lines denote the rock mass displacement).

As can be seen, the rock mass anisotropy and heterogeneity make a perfect fit between the monitoring data and calculated displacement field almost impossible. In addition, the chosen stiffness of the top heading feet abutment is too high. In reality, the sidewall segments slide in an almost unhindered manner until the temporary invert is installed, resulting in strong downward components of both sidewall and shoulder measurement points. However, the measured shortening of the yielding elements and the overall displacement magnitude are very similar, thus underlining the validity of the relationships presented above.

By the virtue of relationships proposing the longitudinal displacement profiles, the forces in the lining can be calculated for all intermediate steps between support installation and final equilibrium. Analogously to chapter 4.2.3, assuming an advance rate allows direct association between time, respective shotcrete strength and mobilised thrust (Figure 68).
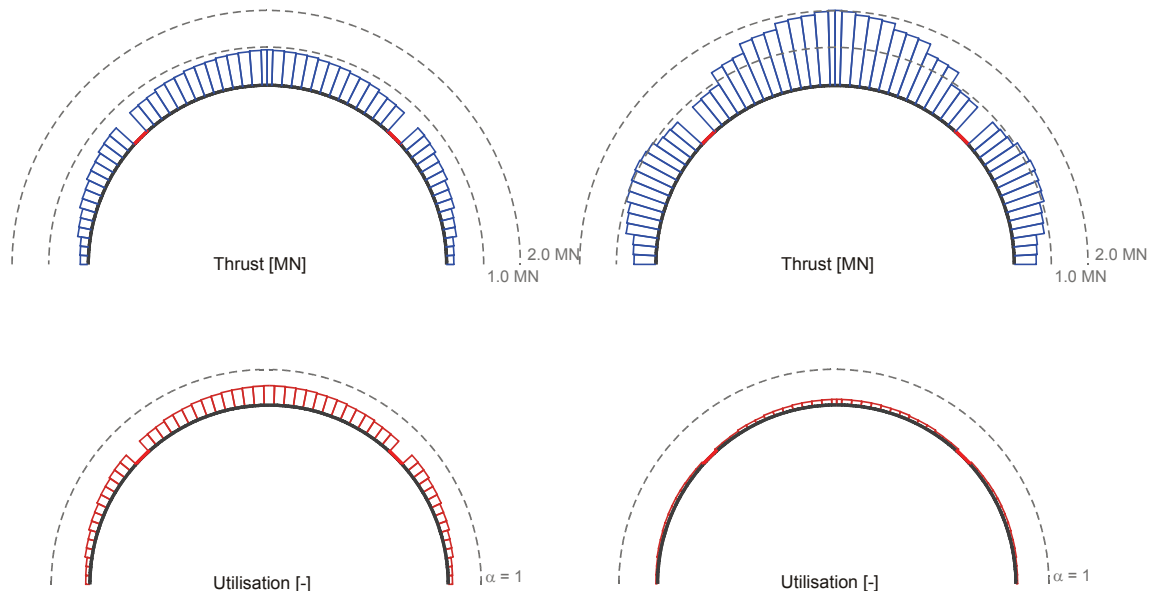
Figure 68. Left: mobilised thrust forces one day after support installation. Low absolute magnitude of thrust, but high utilisation due to young shotcrete can be observed. Right: mobilised thrust at the equilibrium. Note the change of the thrust distribution in the sidewall segments, due to element yield and associated reversal of slip direction.

4.3.9 Probabilistic prediction of system behaviour

Since the calculation time is very short, a probabilistic analysis of the system behaviour is possible as well. The exemplary calculation is also based on the advance through the Lavanttal fault zone, and the support measures have been taken from the previous chapter (Table 7). Assuming a constant probability density distribution, the strength parameters have been varied in a certain range (Table 8), while the Young's modulus of the rock mass has been assumed to be correlated to the rock mass strength, as relatively high rock mass strength being accompanied with a low Young's modulus is rather unlikely.

Table 8. Range of the sampling parameters for the Monte-Carlo simulation

	Min.	Max.
Friction angle φ [°]	25	35
Cohesion c [MPa]	0.20	0.40
Young's modulus E [MPa]	445 * *UCS*	
Poisson's ratio v [-]	0.20	

100 calculations have been performed, with all aspects of system behaviour being logged. The resulting density distribution of the crown displacements is shown in Figure 69.
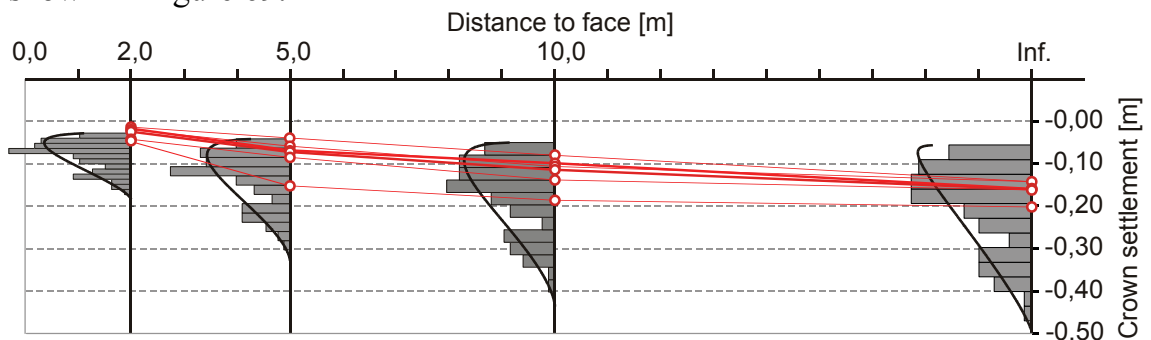
Figure 69. Empirical and fitted theoretical density distributions compared to the displacement monitoring data (red lines).

Apart from the initial displacements (measured at the face distance of 2 m), the results bracket the displacement monitoring data very well. The majority of the measurement values are positioned in the vicinity of the median value of the respective density distributions, indicating that the assumed rock mass property range is plausible and realistically captures the rock mass properties' scatter. The associated density distribution of the peak shotcrete utilisation has been recorded at the same face positions. The influence of the advance rate is clearly depicted, shifting the peak utilisation (observed at approx. 2 m from the face) towards higher values if the excavation is performed rapidly (Figure 70).
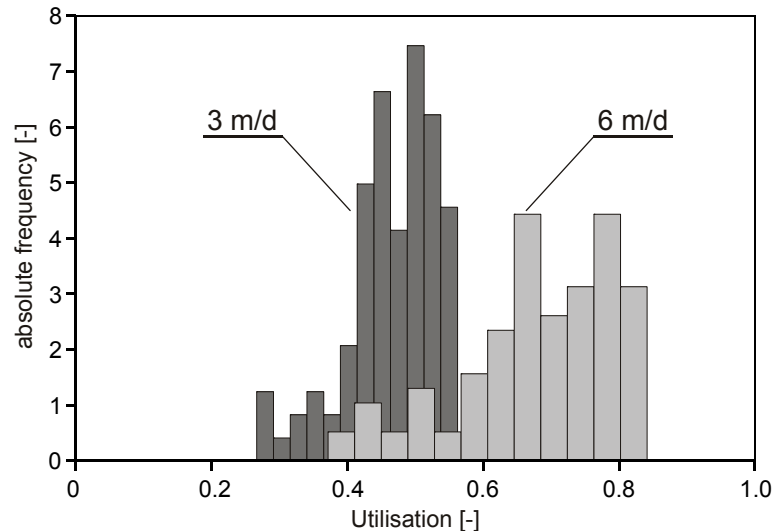
Figure 70. Absolute frequency of the shotcrete utilisation. Light grey: advance rate of 6 m/d, dark grey: 3m/d.

4.3.10 Concluding remarks

The developed method deliberately trades analysis accuracy for calculation speed and simple usage. The issues of longitudinal displacement development and pre-relaxation of a top heading advance have all been treated, resulting in a "closed" calculation methodology allowing dedicated analysis of top heading advance with installed yielding elements. Although easy to use and practical analysis tools are continuously developed (for instance: Phase 2 by RocScience (2009)), the advantages of the approach lie at hand: due to the low calculation effort, both a probabilistic assessment of the system behaviour and a numerical back analysis of ground properties (by coupling it with an optimisation algorithm) are easily possible. Both applications (probabilistic analysis and back analysis) also lay the foundation for well-founded theoretical treatise of system behaviour within the framework of the "observational method" (Peck, 1969; Eurocode 7, 2004). The probabilistic prediction yields an observable value (in most cases displacements) due to spread of anticipated ground conditions (*a priori*); the back analysis can be used to determine rock mass properties from the measurement data gathered during the excavation (*a posteriori*). The data are then used within the framework of Bayes theory (Stille & Holmberg, 2008), updating the probability density distributions with "experience" and assessing the safety anew while paying respect to *measured* data.

In addition, the applied moving least squares method can be coupled with a "full" numerical analysis. If a parameter study is conducted systematically, the response can be used as sampling input for moving least squares approximation. This would enable "filling of the gaps" – yielding an approximate probabilistic prediction of system behaviour. However, the behaviour of the approximation relationship in problems featuring an unsteady response (change of failure mechanism, for instance) has to be examined yet.

4.4 Defining squeezing

As already stated, the occurrence of squeezing is directly associated with the capacity and stiffness of the support. A criterion for squeezing cannot be established solely on ground conditions, since the final result (the observation and experience made during tunnel construction) are always a result of the interaction between the deforming ground and the installed support. In order to address this issue, a novel approach has been taken: the maximum capacity of the shotcrete has been determined by accounting for its rheological behaviour, and put in relation to different ground conditions. Based on the relations presented in chapter 4.3.1, the maximum work envelope of shotcrete can be used to determine whether equilibrium between the rock mass and support is *possible,* while circumventing the issue of exact equilibrium. In the following chapters, the basic considerations and results will be discussed, while a full mathematical treatise and argumentation has been presented in a separate publication (Radoncic & Schubert, 2010).

4.4.1 Work capacity of the support

As already presented in the previous chapters, an exact association of strains with allowable stresses in shotcrete is not a trivial task. The capacity of the shotcrete is not only governed by its strength development, but also by its strain path history (Schubert, 1988; Aldrian, 1991; Hellmich, 1999; Macht, 2002; Schütz, 2010). In order to obtain a reliable final strain limit of shotcrete, a stress analysis using the rheological model after Schubert (1988) and a displacement path after Sulem et al. (1982) has been performed (Figure 71). The final radial strain has been varied between 0.0 and 1.5 % and the strain development shape factor X has been iterated until a shotcrete utilisation factor of 0.75 is reached at any point of the shotcrete stress history. The shotcrete material parameters have been obtained from a long term in situ creep test (Montanuniversität Leoben, 2006).

The maximum utilisation of shotcrete has been capped at 0.75 in order to obtain a safety margin and thus account for loading peaks in the lining caused by the small scale fluctuations of the excavation profile and shear bond between shotcrete and the surrounding ground. An advance rate of 2 m/d has been assumed as a lower boundary for a tunnel advance under adverse conditions. It can be seen that after a final strain of 0.60 %, the required parameter X in order to prevent shotcrete failure rises suddenly and rapidly converges towards highly unlikely values. This is caused by the ongoing hydration of shotcrete. With its aging, the shotcrete becomes stiffer and more sensitive to further strain increments. The range of the observed values of X is based on displacement monitoring data from numerous tunnelling projects in Austria and varies usually

between 6 and 20. Values above 20 can be considered as extremely high and very improbable for homogeneous ground[6].
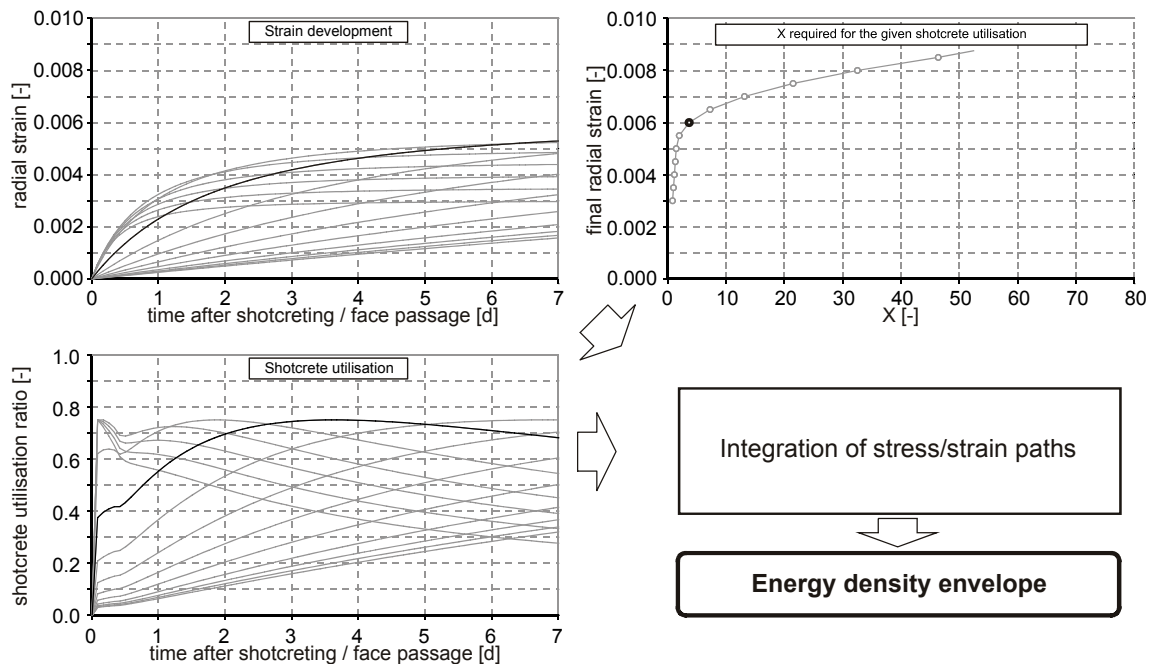
Figure 71. Determination of the allowable stress/strain path of shotcrete. The strain/stress path for the case of final strain equalling 0.006 has been highlighted. The strain path (upper left part) is found by setting the final strain to 0.006 and varying the Sulem's function parameter X in such way that the utilisation ratio does not exceed 0.75 (lower left part). For every final strain value, the parameter X is shown in the upper right diagram.

The maximum energy density envelope is obtained by integrating the stress/strain paths (Figure 72).

---

[6] An extreme example of the influence of ground structure (anisotropy) on the system behaviour is presented by the monitoring data from Strenger tunnel (Schubert, 2011). The foliation was striking largery parallel to the tunnel alignment, causing long-lasting (both due to time and due to excavation) displacement increments and requiring the parameter X in the range above 30.
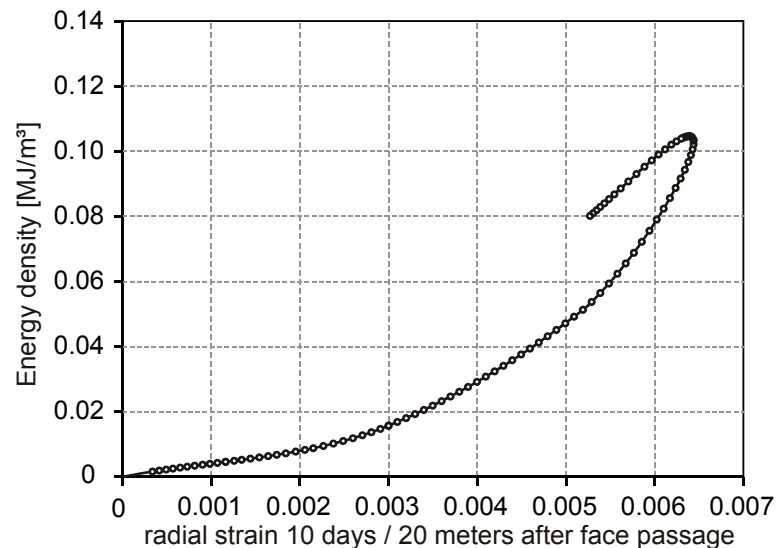
Figure 72. Specific energy density $U_{shot}(\varepsilon)$ attainable by the shotcrete at the given final strain level

As shown, mobilisation of energy densities above 0.11 MJ/m³ are almost impossible, due to the extremely long-stretched strain developments for cases with final strains above 0.65 %. The final maximum value of radial strain has been set to 0.65%, based on the above considerations and experiences from the Inntal tunnel project (Figure 73).
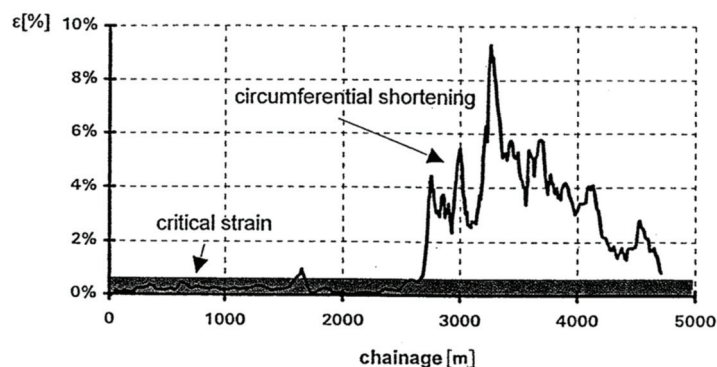
Figure 73. Radial strain distribution in the Inntal tunnel and the critical strain boundary established by evaluating the observed shotcrete damage and respective displacement measurements (Schubert, 1996).

Advance rates higher than the assumed 2 m/d with the same face distance-dependent strain development would inevitably lead to a higher support utilisation and failure (Radoncic et al., 2008). In addition, the rock mass structure and its relative orientation to the excavation have a very high influence both on the displacement distribution and the displacement development. A tunnel advance perpendicular to the foliation results in lower final displacements, but very acute displacement development and high initial strain increments in the lining (Rabcewicz, 1944; Goricki et al., 2005). However, such considerations are beyond the scope of the considerations at hand (aiming at establishing rough boundaries for initial design stages), and should/must be treated in the final design stage. The boundaries of a likely support failure based on the above

assumptions lie on the optimistic side. A shotcrete lining may fail at final strain levels below the stated values under adverse geotechnical conditions. On the other hand, it would definitely fail at final strain levels above the stated values. Due to the intrinsic properties of shotcrete, we have a "window of opportunity" spanning 0 and 0.65 % of radial strain for obtaining an equilibrium with the ground. If no equilibrium can be obtained between these strain boundaries, then there will be no equilibrium and the installed shotcrete liner fails.

4.4.2 Determination of failure boundaries

The determination of ground conditions leading to lining failure has been performed by means of a Monte Carlo simulation. The Mohr-Coulomb parameters of the ground have been sampled from a uniform distribution, and the associated basic Young's modulus has been calculated by multiplying the resulting uniaxial compressive strength with a ratio between 200 and 300 MPa (Equation 65). The overburden has been sampled from a uniform distribution between 100 and 500 meters.

$$E_0 = 200 \div 300 \cdot 2c \cdot \tan(45 + \frac{\varphi}{2}) \qquad \textbf{Equation 63}$$

In order to avoid totally unrealistic ground behaviour with final radial displacements exceeding the tunnel radius, the Young's modulus of the ground has been corrected in accordance with the sampled overburden. The relationship after Janbu (1972) has been found suitable by both Habimana and Kulhawy (Equation 64). p_a is the atmospheric pressure expressed in the same units as E_0 and σ_3 to ensure that n is a unitless number.

$$E_i = E_0 \left(\frac{\sigma_3}{p_a} \right)^n \qquad \textbf{Equation 64}$$

The parameter n has been varied between 0.25 and 0.35, in accordance with the findings of Habimana's work on mechanical properties of severely tectonised rock masses. The thus obtained final value of Young's modulus has been capped at 3000 MPa, in order to avoid analysis of cases featuring irrelevantly low displacement magnitudes.

After the ground conditions have been randomly sampled, the respective ground reaction curves, displacement fields (in case of top heading advance), external work magnitudes and prerelaxation ratios are calculated by using the relationships presented in chapter 1. The maximum work envelope is then added to the energy release of the ground, examining whether equilibrium is possible or not. The cases of full face excavation, top heading with a temporary invert and top heading have been examined separately (Table 9).

Table 9. Parameters used for calculation of work balance
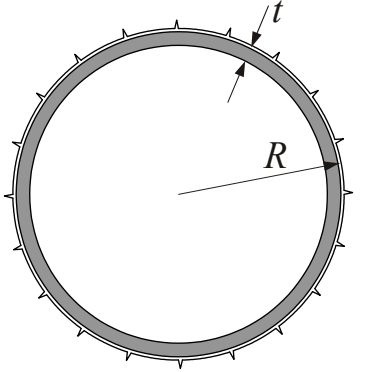
	Full-face excavation	Top heading
External ground work W	$W = 1.00 \cdot W_{full}$	$W = 0.40 \cdot W_{full}$
External support work W_{sup}	$W_{\mathrm{sup}}(\varepsilon) = 2R\pi \cdot t_{shot} \cdot U_{Shot}(\varepsilon)$	$W_{\mathrm{sup}}(\varepsilon) = R\pi \cdot t_{shot} \cdot U_{Shot}(\varepsilon)$
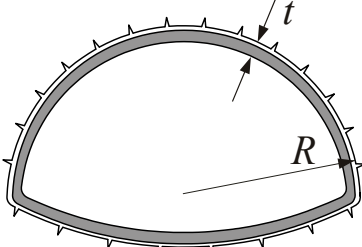
Top heading
w. invert

External ground work W	$W = 0.80 \cdot W_{full}$
External support work W_{sup}	$W_{\mathrm{sup}}(\varepsilon) = (R\pi \cdot t_{shot} + k_{invert} \cdot 2R \cdot t_{shot}) \cdot U_{Shot}(\varepsilon)$

For each considered case, 4000 sampling runs have been performed. In order to correctly depict the influence of the excavation size on the support stiffness, a dimensionless variable called "Support Ratio" has been introduced, defined as lining thickness (in cm) divided by the tunnel radius in meters. The support capacity has been determined by the assumption of the support ratio equalling 4 (thus depicting a rather conventional support with a lining thickness of 20 cm for a tunnel of 10 m diameter). The results of Monte-Carlo sampling for a rock mass with a friction angle of 15° and full face excavation are depicted in Figure 74.
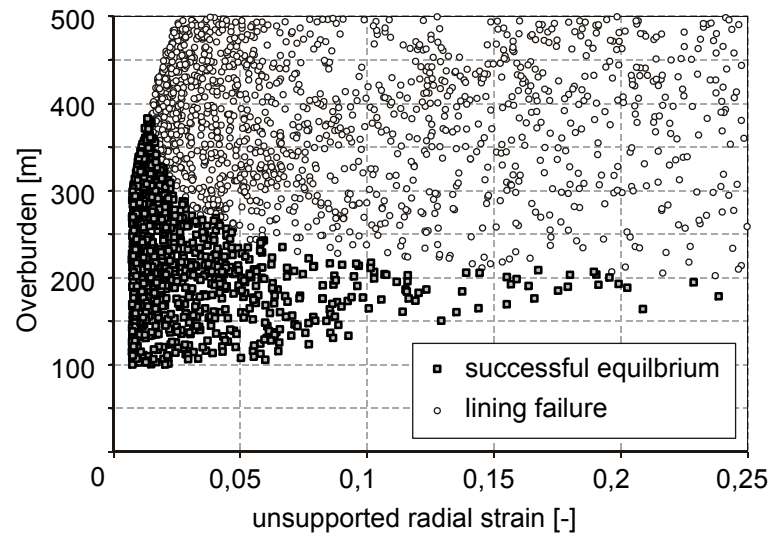
Figure 74. The results of Monte Carlo sampling.

It can be seen that a clear boundary is drawn between lining failure and stable conditions, depicting the influence of the primary stress magnitude. Additional Monte Carlo simulations have been conducted for friction angles between 10° and 30°, thus addressing the usual range for a highly tectonised weak ground.

4.4.3 Results

Analysis of the results has shown that the boundaries between lining failure and successful equilibrium can be described by applying a rational quadratic function (Figure 75). A strong dependency between the results and the assumed friction angle can be observed, featuring a linear increase of the "threshold overburden" with the increase of the friction angle.

$$H_{crit} = H_0 - 75 \cdot \left[1 - \left(\frac{X}{X + \varepsilon - \varepsilon_0} \right)^2 \right]$$
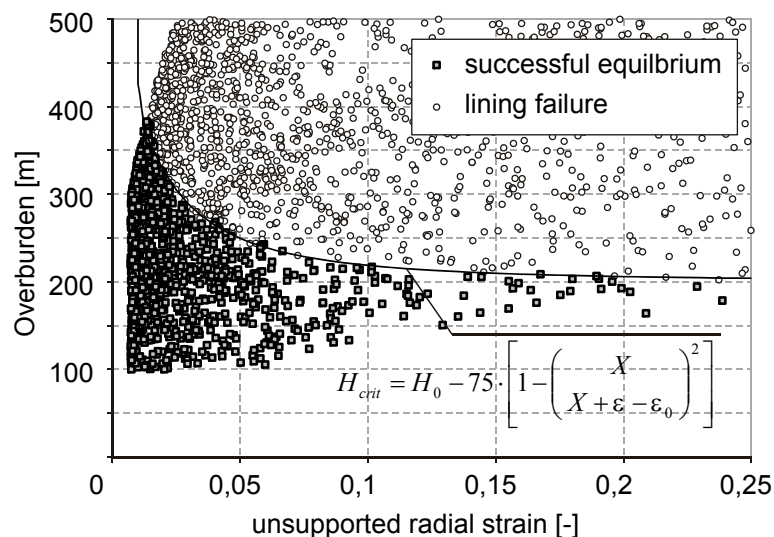
Figure 75. Rational quadratic function defining the boundary between lining failure and successful support installation

After fitting all results, a generalized form of the overburden threshold based on the radial strain has been established, requiring the function parameters φ, H_0, H^*, X and ε_0 (Equation 65). This allows direct calculation of the critical overburden

on the basis of the total radial strain in unsupported conditions and rock mass' friction angle.

$$H_{crit} = (H_0 + H^* \tan\varphi) - 75 \cdot \left[1 - \left(\frac{X}{X + \varepsilon - \varepsilon_0}\right)^2\right]$$

Equation 65

The function parameters associated with the examined cases are given in Table 10.

**Table 10.** Parameters defining the critical overburden H_{crit}

	X [-]	ε_0 [-]	H_0 [m]	H^* [m]
Full-face excavation	0.062	0.035	100	680
Top heading	0.062	0.045	100	680
Top heading w. Invert	0.030	0.030	75	375

As the friction angle approaches 30° the results become increasingly fuzzy, being caused by the capping of the deformability in the assumptions underlying the analysis. The primary stresses, in combination with the assumed elastic properties of the ground, cause displacement magnitudes too high to be sustained by the support disregarding the strength properties of the ground. The issue of determining the likely range of the deformability of the cataclastic material and its dependency on the primary stress state is one of the current research foci at the institute (Pilgerstorfer, 2010). The findings of this work will be used for fine-tuning of the relationships presented herein, decreasing the amount of speculative assumptions with regard to rock mass deformability and strength properties.

All calculations feature a clear and constant lower boundary with regard to the allowable strain. In compliance with the threshold proposed by Hoek and Aydan, no support failure has been observed below 1.0 % of radial strain. This is clear, since the „window of opportunity" for obtaining equilibrium is given within 0 and 0.65 % of radial strain. Assuming that 1/3 of total deformations occur ahead of the face, the maximum radial strain at which no equilibrium problems can be expected has to equal approximately 1.0 %.

The examined top heading advances feature slightly higher allowable displacement/strain magnitudes, caused by the lack of abutment for the top heading feet. This leads to low shotcrete stresses in this area and generally lower overall support stiffness. However, the capacity of a top heading lining for "absorbing" deformations is strongly limited by the stress peaks elsewhere in the cross section and generally high radial displacements in the entire cross section. The installation of the invert has an adverse effect on the support capacity, since the entire work of the ground has to be coped with by a suboptimal lining geometry. This is clearly depicted in the line showing the dependency of the critical overburden on the unsupported radial strain, having a very low threshold (Figure 76).
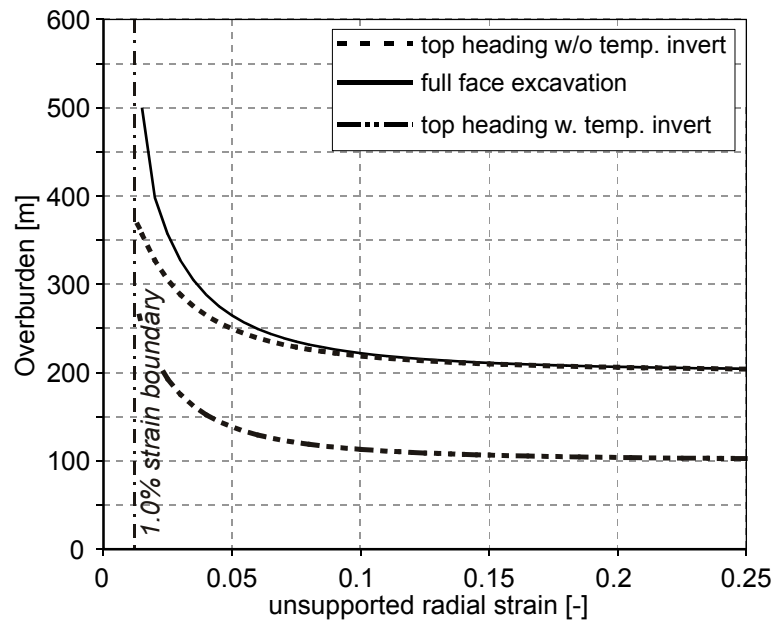
Figure 76. Boundaries of support failure for a friction angle of 15°

The classification of the "magnitude" of squeezing, as proposed by other authors, has been deliberately omitted. This is due to the author's opinion that such classification should be performed along project specific aspects. As already shown, the absolute magnitude of the radial strain in an unsupported case does not fully depict the impact of the ground conditions on the final system behaviour. Radial deformations of 50 cm or more have been successfully coped with when using conventional tunnelling methods. The high magnitude of deformations can easily be handled by applying an appropriate ductile support and performing sufficient overexcavation in order to comply with clearance requirements (John, 1980; Schubert & Marinko, 1989; Schubert, 1993; Schubert, 1996; Moritz, 1999; Schubert, 2008a; Schubert, 2008b; Barla, 2009). On the other hand, a TBM excavation has a highly limited capability for overexcavation and much lower tolerance towards high displacements. In such cases, "squeezing" can have extremely severe consequences even if only a few additional per mil of radial strain occur.

4.4.4 Verification

The established relationship defining the critical overburden in relation to the final radial strain (Equation 65) is tested against observed behaviour of three tunnelling projects in Austria. In case of open deformation gaps, the measured displacements, assumed friction angle and the associated overburden information are used for direct comparison with the above relationships. The unsupported radial displacements for tunnels with installed yielding elements have been obtained by back-analysis of displacement monitoring data.

In order to simplify the interpretation of the results, the difference between the actual overburden H and calculated critical overburden H_{crit} is plotted against the measured radial strain (Figure 77).
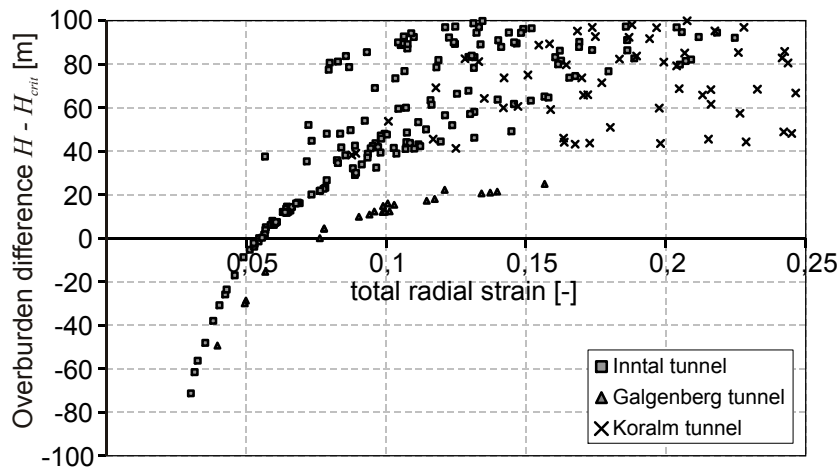
Figure 77. Comparison between predicted critical overburden and observed site data

Each point above the x-axis indicates validity of the found relationship (squeezing behaviour predicted *and* observed). Consequently, points below the x-axis imply that the proposed "squeezing" boundary does not hold true, since the calculated critical overburden is higher than the overburden at which lining damage has been observed and ductile support concept had to be introduced. As depicted, the number of points indicating applicability of the relationship is relatively high.

The measurement data indicating the contrary has been recorded in more competent rock mass portions of the Inntal and Galgenberg tunnels. As already mentioned, no back analysis of the rock mass properties has been performed in these two cases, since the applied support concept featured open gaps. Thus, it has been assumed that the measured final displacements equal the unsupported displacements (after adding one third of pre-displacements). However, the support concept also relies on very dense rock bolt installation, which is most likely to influence the final displacements in the more competent portions. A thorough back analysis of the ground properties in these sections would be required in order to obtain more representative values for the expected unsupported radial strains and allow direct comparison.

4.5 Outlook and recommendations

As presented in this chapter, the two dimensional analysis methods allow a plausible and realistic assessment of system behaviour in preliminary design stages. Further research should be invested in determination of pre-relaxation factors and empirical relationships describing the longitudinal displacement profiles for more sophisticated constitutive laws and anisotropic conditions.

5 Numerical analysis

A numerical parameter study is conducted with the goal of examining the influence of the different yielding elements' types and the excavation sequence on the system behaviour. As already pointed out, such comparison can be conducted only with sound knowledge of the ground properties and appropriate modelling of the excavation sequence and the support measures. With these goals and constraints in mind, the decision was made to generate and consequently calibrate the numerical model on the data gained from displacement monitoring of an already existing tunnel. After the adequacy of the numerical model has been proven by comparing it to the displacement monitoring data, the load-displacement behaviour of the installed yielding elements has been changed in order to examine its influence on the system behaviour.

Due to the abundance of monitoring data, geological documentation, in situ testing and laboratory test data, it was decided to calibrate the model on the system behaviour observed in the exploratory tunnel Paierdorf, Lavanttal fault zone. The examined tunnel section is the same as used in the previous analysis examples (Chapter 4), featuring approximately 480 m of excavation through a major fault zone – starting with chainage 935 and ending at chainage 1425. The fault zone is composed of intermittingly occurring highly fractured rock mass portions combined with tens of meters wide segments composed of coarsely and finely grained cataclastic material (Figure 78).
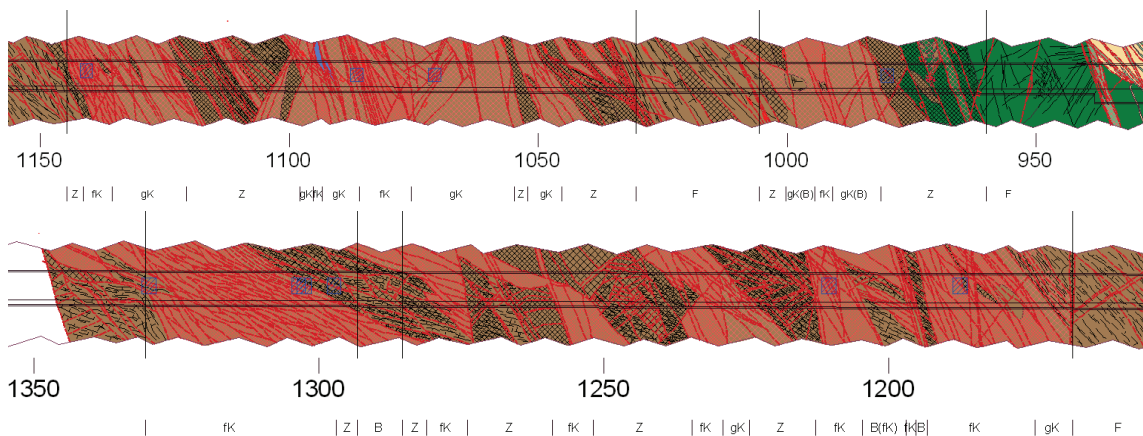
Figure 78. Geological longitudinal section through the Lavanttaler fault zone. Legend: F – competent rock mass, fK – finely grained cataclasite, gK – coarsely grained cataclasite, Z – fractured rock mass, B – Block in matrix. (courtesy of Dipl.-Ing. Florian Fasching, 3G ZT GmbH)

The applied concept of support and excavation sequence has been already presented in chapter 4.3.8. Despite the geological heterogeneity, very similar system behaviour has been recorded in the measurement cross sections MCS 1136.2, MCS 1194.3, MCS 1238.4, MCS 1268.6 and MCS 1304.7. Hence, all of them have been taken as reference cases for the calibration of the numerical model.

5.1 Determination of ground properties

In the initial stages of work, it was intended to use the double-yield model provided by FLAC3D (Itasca, 2009), since it captures both the strength loss under deviatoric loading (strain softening) and the hysteretic material compaction under volumetric loading (volumetric hardening). The ability to capture both mechanisms characteristic for weak geomaterials would have minimised the amount of bias caused by the used constitutive law.

However, the model has shown poor convergence and sometimes even unstable behaviour, resulting in the application of the strain softening constitutive law in the final analysis. Fortunately, the primary stress state and the associated failure mechanism predominantly cause stress paths in the unloading regime (the deep-seated failure of the ground "pushes" the stresses below the primary stress level). This renders the error caused by the lack of differentiation between loading and unloading marginal.

The approach used for finding realistic ground properties is based on drawing information from various "reliable" sources and putting it together into a sound overall picture:

1. The rock mass deformability parameters should (if possible) comply with the findings from the instrumentation adit (in situ load plate tests) and previously published back analysis results (Schubert et al., 2009).
2. The strength mobilisation and its loss are governed by separate mobilisation of friction angle and cohesion (Martin, 1997). They have to be determined by performing numerical back analysis of the direct shear tests on intact specimen. The direct shear tests have to be used since the plastic shear strains occurring in multi-stage triaxial tests span only the range up to the mobilisation of peak strength. By performing a simple Mohr-Coulomb analysis of the ground response to the excavation, it can be shown that the occurring plastic shear strains regularly exceed the ones observed during triaxial testing at least by an order of magnitude. In addition, the interaction between the deforming ground, relatively stiff concrete and the yielding elements can only be captured if the development of a distinct and localised shear band is allowed by the applied constitutive law (chapter 4.1.3)
3. After the ground properties have been determined by the means described above, merely the fine tuning of the ground properties is performed by comparison with the displacement monitoring data. As already stated, not only the amount of final displacements and the orientation of the displacements in the cross section are considered, but also the displacement development due to the ongoing excavation.

5.1.1 Determination of elastic properties

The results from the in-situ plate load tests (Pilgerstorfer, 2011) are doubtlessly the most reliable estimate of the rock mass deformability. Unfortunately, the majority of the test adit was situated in a more competent portion of the rock mass, rendering the thus obtained Young's moduli too optimistic (800 – 3000 MPa) for the conditions encountered in the weaker portions of the fault. The lowest Young's modulus (un/reloading branch) obtained from the test programme was 871 MPa.

The data obtained from triaxial tests varies between 620 MPa and 41000 MPa (3G report, 2010). Needless to say, the triaxial tests are also biased towards better ground, since the retrieval of "undisturbed" specimen and subsequent triaxial testing of coarsely grained, nearly cohesionless cataclasite is currently almost impossible. On the other hand, the two-dimensional back analysis of ground properties conducted by Schubert et al. (2009) state the Young's modulus as between 200 MPa and 300 MPa. These properties have been derived by using the convergence confinement method, utilising a rudimentary calculation method for determining the support characteristic curve and assuming instant ring closure. Hence, the support mobilisation is exaggerated and the back analysis likely yields overly pessimistic ground properties. The Young's modulus for the initial, un-calibrated calculation has been fixed at 450 MPa with a Poisson's ratio of 0.3, representing an average value of the sources mentioned above.

5.1.2 Determination of strength properties

The peak strength properties have been deduced from the triaxial testing of the material retrieved from the instrumentation adit (Table 11). The maximum cohesion values above 0.50 MPa have been discarded as unplausible, since these results have been obtained on specimen retrieved from competent blocks.

Table 11. Overview of the triaxial testing results on the material obtained from the instrumentation adit (Light grey: discarded results).

Lithological description	c [MPa]	φ [°]	E [MPa]	V [MPa]	v [-]
Shale gneiss	6.16	33.2	41650	27220	0.08
Shale gneiss	2.65	29.7	11790	6210	0.02
Shale gneiss	4.58	28.2	17780	8980	0.03
Shale gneiss	2.01	44.4	14390	11560	0.12
Cataclastic shale gneiss	0.20	27.0	620	60	0.29
Cataclastic shale gneiss	0.44	18.9	1340	430	0.46

The strain - dependent mobilisation of cohesion and friction angle has been determined by calibrating the numerical model of the direct shear test (Figure 79) on the respective test results.
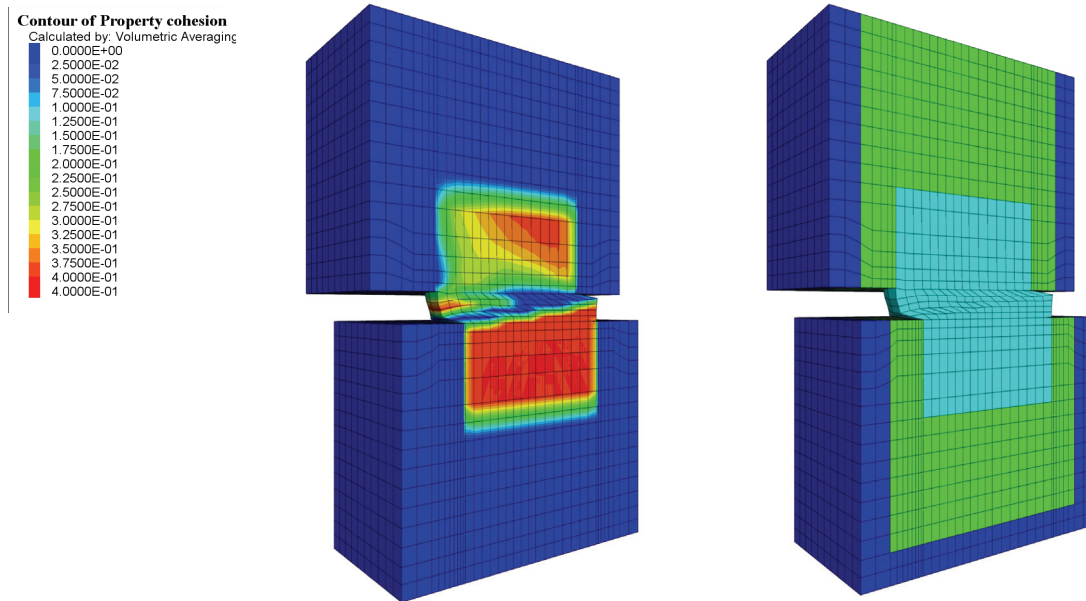
Figure 79. Left: cohesion mobilisation in the grouted specimen (please note the shear band in the middle of the specimen with demobilised cohesion). Right: materials used in the numerical model. Dark blue: steel, green: grout, pale blue: rock specimen.

All laboratory tests have been conducted with infinite external stiffness, which has been simulated by a fixed vertical boundary condition in the numerical model. The material parameters used in the model are listed in the table below.

Table 12. Assumed constitutive laws and respective deformability properties of the modelled materials

Material	Constitutive law	E [MPa]	v [-]
Steel	Linear elastic	210000	0.20
Grout	Linear elastic	20000	0.25
Specimen	Strain softening	450	0.30

Best fit between the numerical model and the test data has been achieved with the strain-strength relationship shown in Figure 80. The friction angle remains relatively constant, while the cohesion has a pronounced peak followed by a rapid drop towards the residual value. Remarkably enough, the calibrated relationship for the weak rock is qualitatively in good agreement with the trends published by Martin (1997) and Hajiabdolmajid et al. (2002). Both papers stress the fact that the cohesion is usually readily available at the beginning of shearing, but strongly drops due to crack development, while the friction may require considerable shear strain in order to attain its peak value.
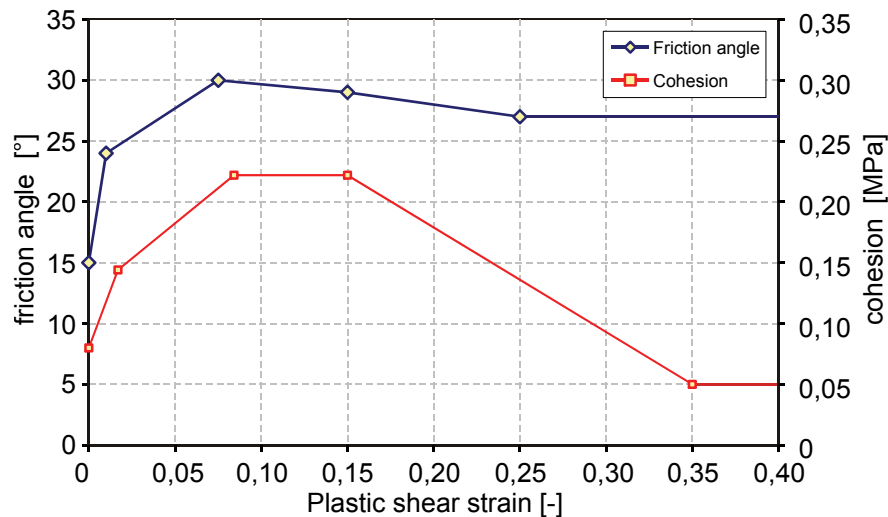
Figure 80. The estimated relationship between friction angle, cohesion and plastic shear strain

The associated shear displacement – shear stress plots and the normal – shear force plots indicate a reasonable fit between the test data and the model (Figure 81). Better fit could not be achieved due to the anisotropy of the test specimen, since the test was conducted with shearing parallel to the foliation. The long lasting decrease in normal forces implies contractant behaviour of the material (negative dilatancy), which clearly conflicts the material appearance and measured unit weight (approx. 2.5 kg/dm³). Such behaviour is usually observed in materials with very high void ratio, with particles/grains "falling into the voids" and leading to the macroscopic volume decrease. In this particular case, the delayed normal force mobilisation is probably caused by the plane of foliation dipping in the direction of shearing, thus causing a downward sliding of the specimen. In addition, the influence of the anisotropy has led to cohesion and friction values not complying with the initial normal loading in certain tests conducted on the same material. If the material was isotropic, then the specimen should have failed during normal load application, clearly contrasting the observed behaviour. The relative orientation of the foliation to the shear direction triggers different failure mechanisms (Button, 2004) and renders the calibration of the isotropic strain softening constitutive law on the test data nearly impossible in some cases.
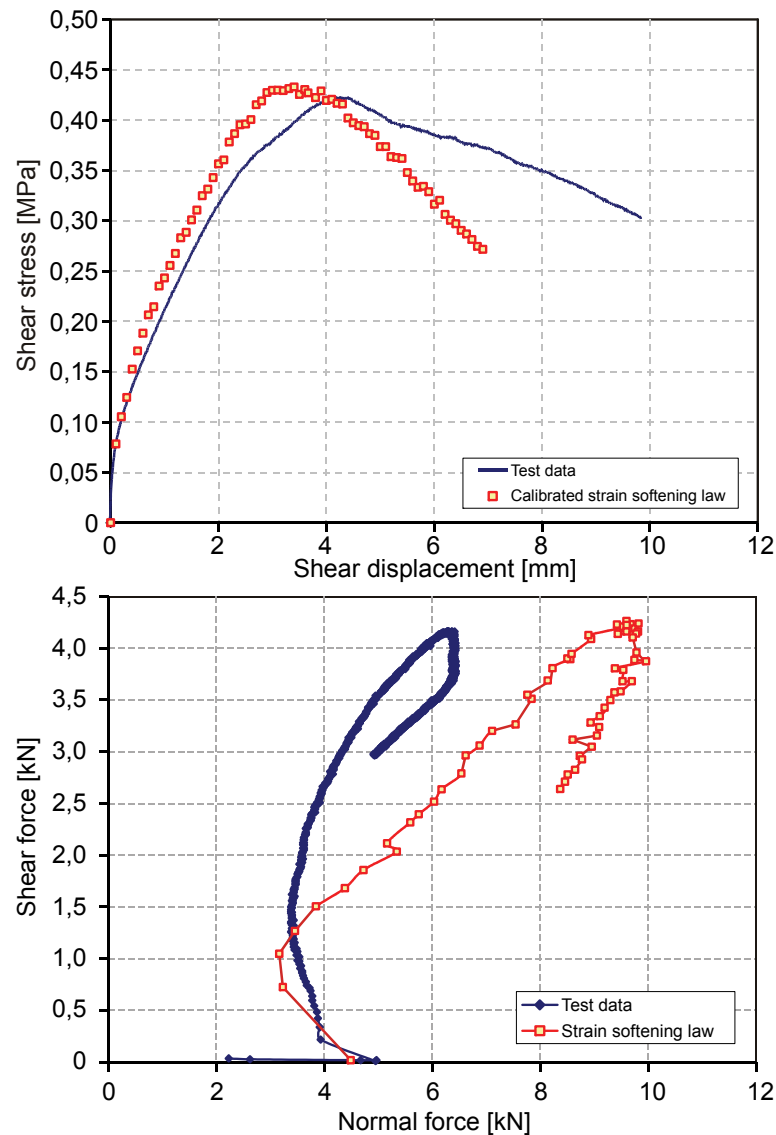
Figure 81. Top: comparison of the shear stress mobilisation depending on the imposed shear displacement. Below: comparison of the normal and shear forces mobilised in reality and in the numerical simulation.

In addition, realistic simulation of the ground / system behaviour while incorporating the effect of dilatancy during shearing is only possible if a dilatancy cut-off is performed, indicating that the state of lowest compaction has been reached in the crushed material around the opening. Unfortunately, the exact relationship between the plastic shear strains and the dilatancy (for an *"intact rock" specimen*) can be directly determined only by driving the triaxial test well into the post failure range, while the specimen volume change is being recorded. This kind of test is currently impossible for certain grain distributions of faulted rock masses. Hence, the value of dilatancy was set to zero in all further calculations.

In the light of the heterogeneity of the rock mass, it was decided not to attempt further fine tuning of the strength properties based on the direct shear test data. The appropriateness of the model can be finally verified only by making a full

analysis of the system behaviour in the ground with the same properties and comparing the results to the measurement data.

5.2 Shotcrete modelling

In order to meet the goal of an objective comparison of the system behaviour with different yielding element types, the rheological time dependent behaviour of shotcrete has to be appropriately captured in the numerical model. For this reason, extensive effort has been invested into developing a FISH code (internal scripting language of FLAC3D, allowing model manipulation) for time dependent shotcrete properties control. It is based on the formulation of flow-rate method published by Schubert (1988), however it generalises its initially uniaxial formulation into a full (albeit still empirical) set of constitutive equations.

5.2.1 Flow-rate method

The flow-rate method is a forward explicit time domain finite-difference calculation method proposed by Schubert (1988). It is based on determining the shrinkage, creep and elastic strains increments from the current time step and past strain and stress history of shotcrete. Assuming a known stress history, the total axial shotcrete strain writes as

$$\varepsilon_2 = \varepsilon_1 + \frac{\sigma_1 - \sigma_2}{E(t)} + \sigma_2 \Delta C(t) + \Delta \varepsilon_d + \Delta \varepsilon_{sh}, \qquad \textbf{Equation 66}$$

With ε_2 - axial strain at the time "2" (end of interval),

   ε_1 - axial strain at the time "1" (begin of interval),

   σ_2 - axial stress at the time "2",

   σ_1 - axial stress at the time "1",

   $E(t)$ - Time – dependent Young's modulus,

   $\Delta C(t)$ - Time – dependent plastic creep rate,

   $\Delta \varepsilon_d$ - Increment of reversible creep strain,

   $\Delta \varepsilon_{sh}$ - Increment of shrinkage strain.

The time-dependent Young's modulus is defined as

$$E(t) = E_{28} \left(\frac{t}{1 + 0.3t} \right)^{0.2}, \qquad \textbf{Equation 67}$$

with E_{28} representing the Young's modulus at 28 days of shotcrete age, and t the current shotcrete age. The plastic creep rate increment $\Delta C(t)$ is given as

$$C(t) = A' \left(t_2^{\frac{1}{3}} - t_1^{\frac{1}{3}} \right), \qquad \textbf{Equation 68}$$

with A' as material parameter. The reversible viscous strain increment $\Delta \varepsilon_d$ is dependent on the already accumulated total viscous strain ε_d and writes as:

$$\Delta \varepsilon_d = (\sigma_2 C_{d\infty} - \varepsilon_d) \left(1 - e^{\frac{-\Delta C(t)}{Q}} \right), \qquad \textbf{Equation 69}$$

having $C_{d\infty}$ and Q as additional parameters. Finally, the shotcrete shrinkage is defined as:

$$\Delta\varepsilon_{sh} = \frac{\varepsilon_{sh\infty}t_2}{B+t_2} - \frac{\varepsilon_{sh\infty}t_1}{B+t_1},$$

Equation 70

having B as curvature parameter and $\varepsilon_{sh\infty}$ as final shrinkage strain. Apart from omitting the shotcrete "swelling" due to hydration heat in the early stages, the above set of equations enables very good assessment of the rheological behaviour of shotcrete (Figure 82).
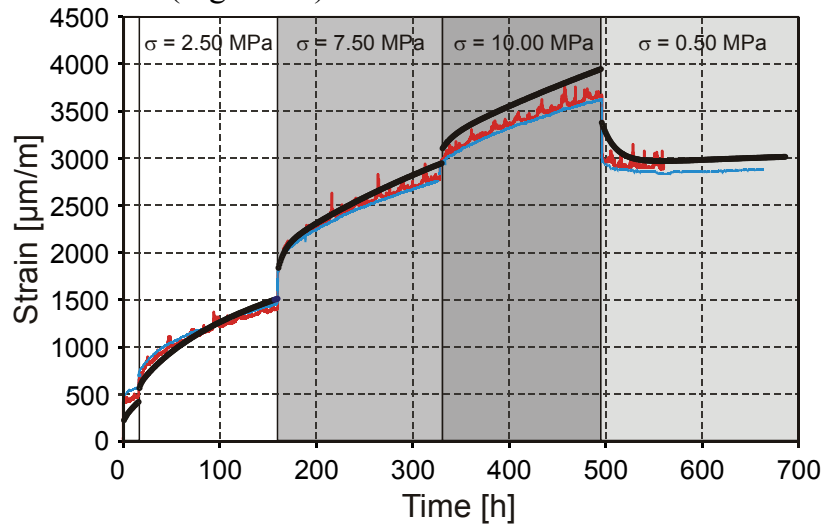

Figure 82. Comparison between the test data obtained from the Plabutsch tunnel (red and blue lines) and the strain development predicted by the flow-rate method.

However, the parameter estimation requires a relatively intense testing programme consisting of a series of shrinkage and creep tests. In addition, the parameters vary depending on the specific composition of shotcrete, rendering renewed testing and parameter calibration for every project indispensable.

5.2.2 Re-formulation for FLAC3D

The flow-rate method is formulated solely for uniaxial loading, thus yielding only the axial strain in the direction of the stress. Since the stress state of shotcrete is in reality somewhere between biaxial in case of thin linings (with one principal stress equalling almost zero) and fully triaxial in case of thick linings, the equations have to be re-formulated in order to capture this behaviour in a FLAC3D analysis.

Assuming that the Poisson's ratio stays constant throughout the aging of concrete, the modelling of the time-dependent change of Young's modulus is trivial (Equation 71 and Equation 72).

$$K(t) = \frac{E(t)}{3(1-2v)}$$

Equation 71

$$G(t) = \frac{E(t)}{2(1+v)}$$

Equation 72

Analogously, the influence of shrinkage is easily incorporated by assuming that the shrinkage strain is isotropic, thus allowing direct calculation of the equivalent change of the hydrostatic stress portion $\Delta\boldsymbol{\sigma}_{sh}$ in the zones representing the shotcrete:

$$\Delta\boldsymbol{\sigma}_{sh} = 3K(t)\Delta\varepsilon_{sh}(t)\mathbf{I} .$$

Equation 73

If the viscous elastic strain increment $\Delta\varepsilon_d$ is assumed to be both volumetric *and* deviatoric, then the Equation 69 can be used as well, provided that the strains and stresses are written in the general matrix form:

$$\Delta\boldsymbol{\varepsilon}_d = \left(\boldsymbol{\sigma}_2 C_{d\infty} - \boldsymbol{\varepsilon}_d\right)\left(1 - e^{\frac{-\Delta C(t)}{Q}}\right).$$

Equation 74

The associated stress corrections are obtained by splitting the viscous strain increment matrix into its respective volumetric and deviatoric parts (Equation 75 and Equation 76).

$$\Delta\varepsilon_{vol} = \frac{1}{3}tr\Delta\boldsymbol{\varepsilon}_d .$$

Equation 75

$$\Delta\boldsymbol{\varepsilon}_{Dev} = \Delta\boldsymbol{\varepsilon}_d - \Delta\varepsilon_{vol}\mathbf{I} .$$

Equation 76

The associated stress correction is easily obtained by using the time-dependent bulk and shear modulus:

$$\Delta\boldsymbol{\sigma}_d = 2G(t)\Delta\boldsymbol{\varepsilon}_{Dev} + 3K(t)\Delta\varepsilon_{vol}\mathbf{I} .$$

Equation 77

The variable of "reversible viscous strain" actually "smears" the pore-water redistribution of the young shotcrete and some kind of viscous material response into one "global variable". The assumption that it is developing in general manner (both the volumetric and the deviatoric stress portion have the same effect) is of course axiomatic and has been made only because of the lack of better information and the simplicity of code implementation. In reality, creep is usually deviatoric (caused only by deviatoric loading), while pore-water pressure redistribution effects are triggered by changes in the volumetric stress. A precise determination of the mechanisms behind the occurrence of "reversible viscous strains" can be obtained only by additional long term triaxial testing of young shotcrete. In this case, the same material should be tested both under drained hydrostatic loading (to determine the pore water pressure influence) and drained deviatoric loading (to "sort out" the creep/viscous strain). The pore-water redistribution of young shotcrete has probably also some influence on the final strength (since the water cement ratio is changed by drainage), rendering the subject of appropriate mechanical description of shotcrete highly complex.

In order to account for the irreversible, plastic creep deformation of shotcrete, the built-in "power law" of FLAC 3D has been used. The reasons lie in the simplicity of the constitutive law and the fact that with certain parameter

manipulation, the model can be forced to cause linear creep strain increments in the calculation. This simplifies the implementation greatly, since the creep strain for every time step can be calculated externally in FISH (just like the other equivalent stress corrections presented above), while the Power Law constitutive law is simply used for causing *exactly these strains* to occur in the model. The power law uses the Mises stress invariant to calculate the associated creep strain rate (Itasca, 2009):

$$\bar{\sigma} = \left(\frac{3}{2}\right)^{\frac{1}{2}} (\sigma_D \sigma_D)^{\frac{1}{2}}.$$ **Equation 78**

The specific creep rate is given by the simple equation:

$$\dot{\varepsilon}_{CR} = A\bar{\sigma}^n.$$ **Equation 79**

The deviatoric creep increment is calculated from the deviatoric stress tensor and the specific creep rate:

$$\Delta\boldsymbol{\varepsilon}_{CR} = \left(\frac{3}{2}\right)^{\frac{1}{2}} \dot{\varepsilon}_{CR} \left(\frac{\boldsymbol{\sigma}_D}{\bar{\sigma}}\right)\Delta t.$$ **Equation 80**

If the parameter *n* is set to 1, then the Equation 80 simplifies to:

$$\Delta\boldsymbol{\varepsilon}_{CR} = \left(\frac{3}{2}\right)^{\frac{1}{2}} A\boldsymbol{\sigma}_D\Delta t.$$ **Equation 81**

Hence, the creep strain increments become linearly bound to the deviatoric stress. The flow-rate method equation of the plastic creep (Equation 68) has to be re-formulated and compared to the equation 80 in order to obtain the information for calculating the power law's parameter *A*. In the first step, the uniaxial stress (scalar) is written in general matrix form and the deviatoric stress portion is determined:

$$\boldsymbol{\sigma}_D = \boldsymbol{\sigma} - \frac{1}{3} tr\boldsymbol{\sigma}\mathbf{I} = ..$$

$$.. = \begin{bmatrix} \sigma & 0 & 0 \\ 0 & 0 & 0 \\ 0 & 0 & 0 \end{bmatrix} - \begin{bmatrix} \frac{1}{3}\sigma & 0 & 0 \\ 0 & \frac{1}{3}\sigma & 0 \\ 0 & 0 & \frac{1}{3}\sigma \end{bmatrix} = \begin{bmatrix} \frac{2}{3}\sigma & 0 & 0 \\ 0 & -\frac{1}{3}\sigma & 0 \\ 0 & 0 & -\frac{1}{3}\sigma \end{bmatrix}.$$ **Equation 82**

The deviatoric stress magnitude in the direction of the measured creep strains equals $2/3\sigma$. Therefore, the "true" creep parameter *C'(t)* has to equal $3/2C(t)$, since the creep strain increment caused by the deviatoric stresses has to equal the "measured" axial creep strain increment associated (wrongly) with the axial stress.

$$\Delta C(t)\sigma = \Delta C'(t)\frac{2}{3}\sigma$$ **Equation 83**

$$\Delta C'(t) = \frac{3}{2}C(t)$$ **Equation 84**

The creep strain increment is hence written as:

$$\Delta\boldsymbol{\varepsilon}_{CR} = \frac{3}{2}\Delta C(t)\boldsymbol{\sigma}_D .$$

Equation 85

By comparing the Equation 81 with Equation 85:

$$\frac{3}{2}\Delta C(t)\boldsymbol{\sigma}_D = \frac{3}{2}A\boldsymbol{\sigma}_D\Delta t ,$$

Equation 86

we obtain the power law's parameter A:

$$A = \frac{\Delta C(t)}{\Delta t} .$$

Equation 87

5.2.3 Calculation scheme

In all further applications of the presented method for shotcrete behaviour assessment, the calculations are performed in the following (repeating) order:

1. Determination of shotcrete age.
2. Assignment of time-dependent Young's modulus.
3. Static equilibrium calculation, yielding stresses induced in the shotcrete.
4. Determination of the increment of the viscous reversible strain tensor $\Delta\boldsymbol{\varepsilon}_d$ and of the respective stress correction tensor $\Delta\boldsymbol{\sigma}_d$, on the basis of the current shotcrete stress state (obtained after finding the equilibrium).
5. Determination of the current creep parameter A.
6. Switch to creep mode in FLAC3D and begin of the creep calculation. After the plastic creep strains have been induced in this manner, the model is switched back into purely mechanic - static mode.
7. Static equilibrium calculation, due to unbalanced forces in the model induced by creep.
8. Stress correction for shrinkage and viscous reversible strains.
9. Final static equilibrium calculation.

In case of uniaxial verification test with constant loading, the results are invariable with regard to the sequence of the above steps, since the loading is kept constant. However, in case of simulated tunnel advance, the sequence becomes very important, since creep depends on the imposed stresses. Therefore, the determination of the irreversible creep strains (via power low, step 5) and reversible viscous strains (step 4) have to be performed directly after determining the stress state associated with the excavation step under consideration. The stress tensor of each zone depicting shotcrete lining can be directly changed (in order to account for viscous reversible strains) first after the creep calculation, since the inverse order would cause stress relaxation in the material, thus underestimating the irreversible plastic creep. The shotcrete shrinkage does not depend on the stress state, so its determination and associated stress release are performed at the end.

When applying this calculation method, each excavation step is associated with three distinct equilibrium calculations, as opposed to a single calculation in case of modelling the shotcrete with a "purely" elasto-plastic model. This renders the calculation of large numerical models highly time consuming.

5.2.4 Verification

The verification has been conducted by modelling a uniaxial long term creep test in FLAC3D and comparing the calculated strains to the strains measured in the long term creep test. The parameter determination has been conducted by using the standard set of empirical relationships for the flow rate method and the test result data from the exploratory tunnel Mitterpichling, part of the Koralm basis tunnel (Montanuniversität Leoben, 2006). The test was conducted with three distinct loading stages with constant axial stress, beginning with 7.8 MPa, increasing to 14.40 MPa and then unloading to 1.40 MPa. As presented in Figure 83, a reasonable fit to the test data can has been obtained, although the deformation of the young shotcrete is somewhat exaggerated.
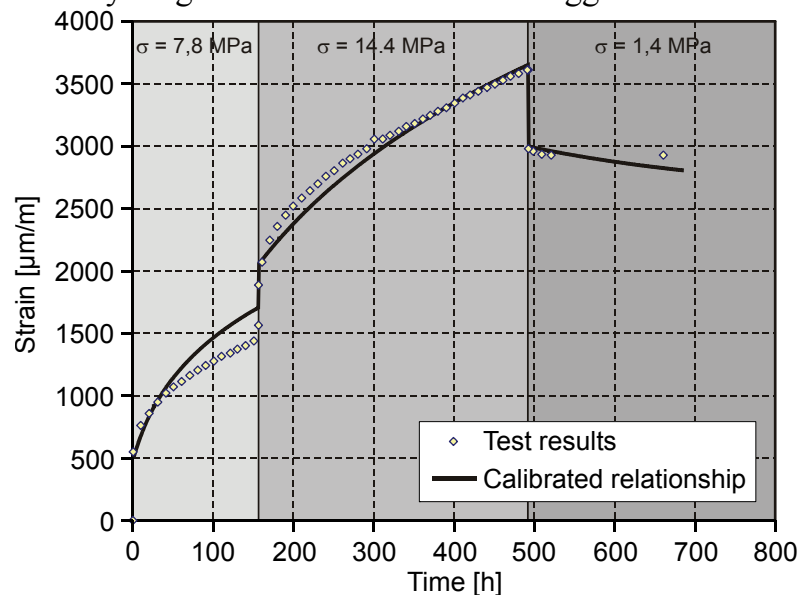
Figure 83. Comparison between the creep test data and the strain development according to the flow rate method (shotcrete age at test begin: 26 h)

The corresponding material parameters are listed below.

Table 13. Shotcrete parameters calibrated on the data from the exploratory tunnel Mitterpichling.

$A^{'}$	0.00010
$C_{d\infty}$	0.00009
Q	0.0001
ε_{sh}	0.00125
B	600
E_{28} [MPa]	15000
β_{28} [MPa]	40

In the next step, the same parameters have been used in the FISH code steering the FLAC3D implementation of the flow rate method, allowing direct verification of the relationships presented in chapter 5.2.2. The results prove that the code behaves flawlessly, and that an excellent fit can be also obtained with a relatively high time increment of 6h between two calculation steps (Figure 84).
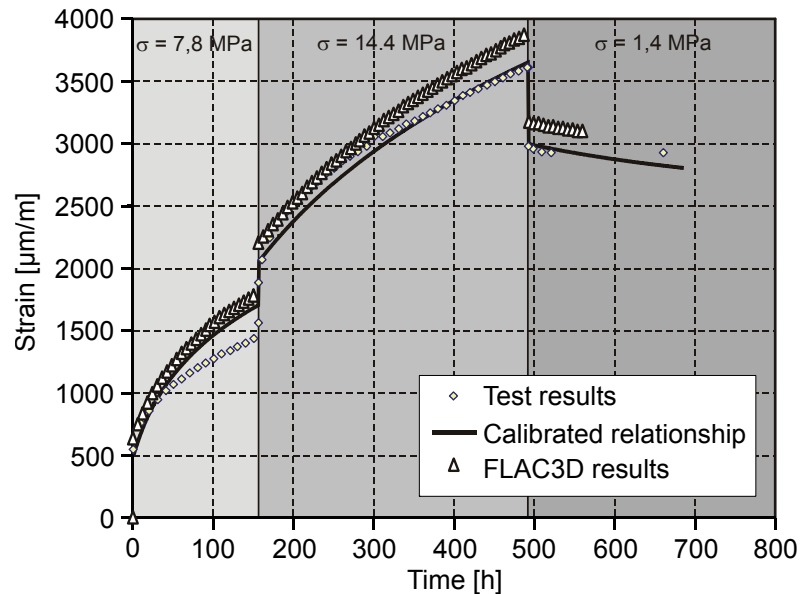
**Figure 84.** Results obtained from the FISH code, compared to the test data and the original relationship after Schubert.

5.3 Numerical model

The numerical model used in the case study is depicted in Figure 85. By the virtue of symmetry, only one half of the real problem is calculated. Since deep-seated overstressing of the ground is anticipated, the model is rather big (50 m x 100 m x 90 m) in order to minimise the interaction between the failure zone and the artificial model boundary. The length of the model (measured in the direction of the excavation) was chosen iteratively, with the goal of being as short as possible and still allowing the middle part of the model to reach a steady state (with final displacements being equal in each cross section).

Primary stress state was assumed to be hydrostatic ($K_0 = 1$) and equalling 6.50 MPa (corresponding to 230 m of overburden). The gravity has been turned off, in order to avoid local instabilities at the excavation face occurring when a strain softening constitutive law and no face support are applied (Leitner, 2005; Volkmann & Schubert, 2009).
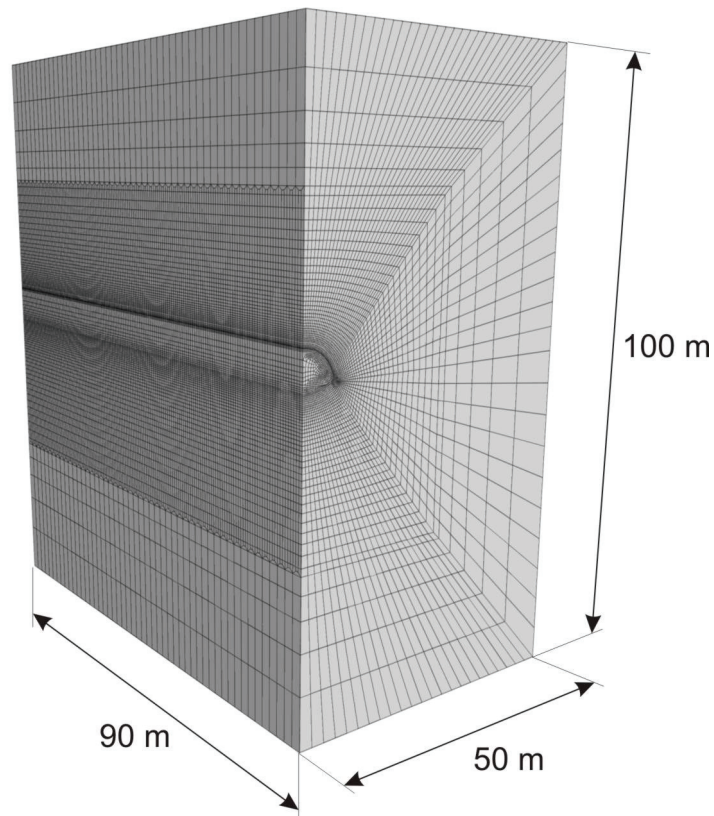
Figure 85. Model dimensions and used discretization

Since no contact elements between the shotcrete and the ground have been used, the model relies on the development of shear bends in the ground to model the occurring slip. Hence, the discretization of shotcrete and ground in its vicinity is very fine, with an element size of approximately 10 cm (Figure 86).
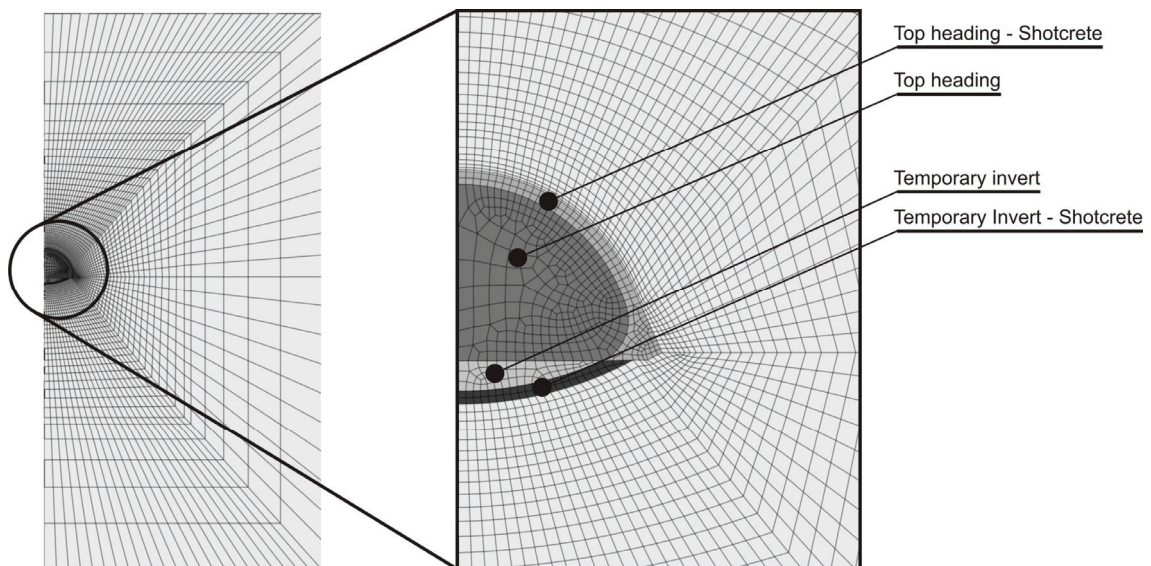
Figure 86. Discretization in the vicinity of the excavation.

The yielding elements installation has been modelled by deleting the zones representing the rock mass and adjacent to the element (Figure 87). This ensures correct force transfer in the model (since yielding elements do not interact with the ground in their vicinity) and realistic kinematical behaviour. The idealised bi-

linear load-displacement behaviour of the yielding elements has been modelled by applying the Mohr-Coulomb constitutive law. The stiffness and strength values have been calculated from the assumed load-displacement relationship of the respective element.
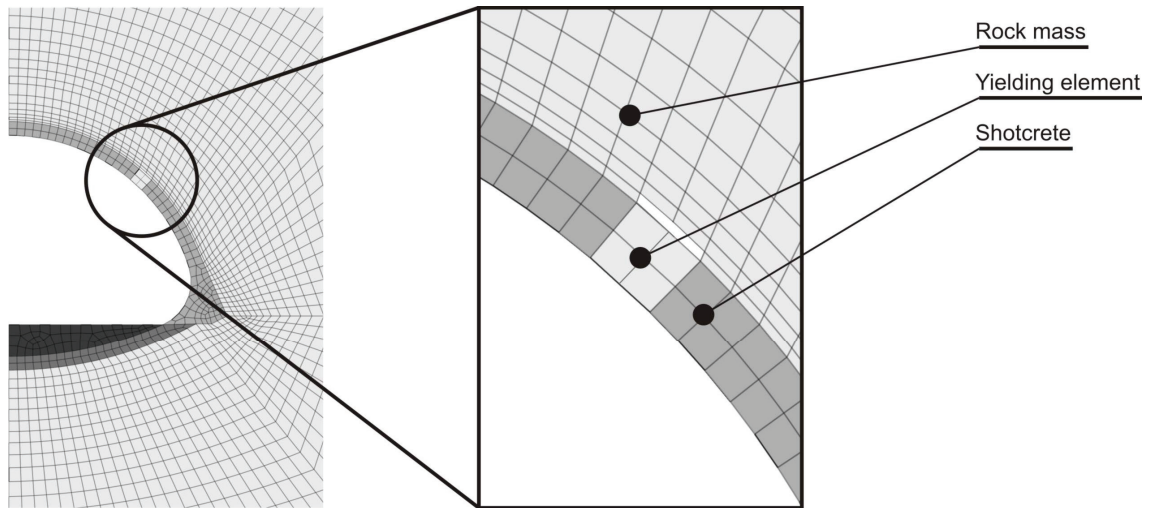
Figure 87. Modelling of yielding elements.

Since the shotcrete age plays a major role during the calculation, the "virtual time" within the model is directly bound to the excavation sequence (Figure 88). After every excavation step, the global model time variable t is incremented by the assumed time interval required for support installation Δt_{sup} and the excavation of the next round Δt_{ex}, respectively. The assumed advance rate is 3.6 m/d (1 round every 8 hours), while the support installation and excavation times are both assumed to equal 4 hours. After every round, the steps presented in chapter 5.2.3 (shotcrete modelling) are executed.
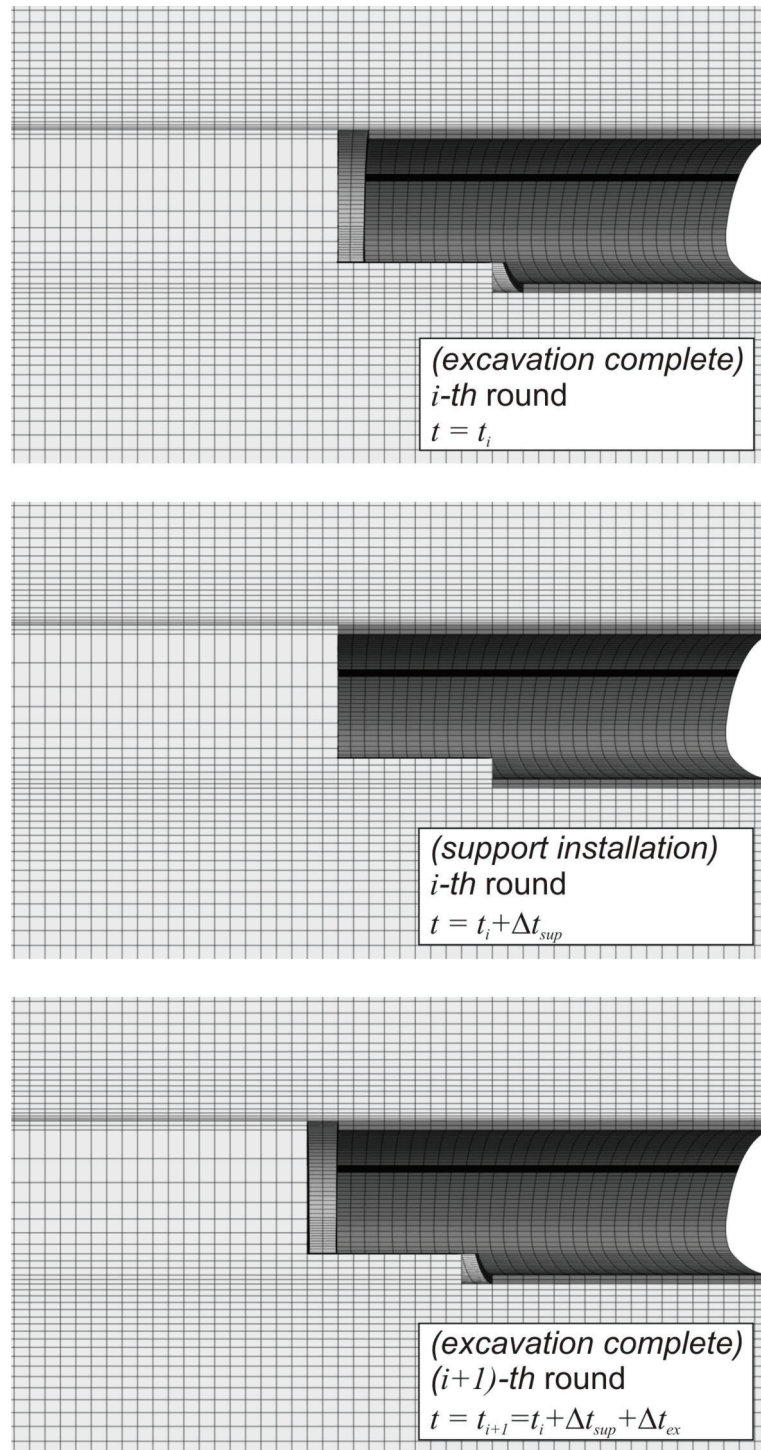
Figure 88. The assumed excavation sequence and time-tracking method.

Shotcrete age is calculated by associating the time of shotcrete "installation" with each respective zone (via FISH), and subtracting it from the global time variable for each subsequent step. For the sake of simplicity, the temporary invert arch is being installed parallel with the top heading advance, in order to have constant distance between the top heading and the temporary invert and simplify the result evaluation. In reality, the distance of the temporary invert and the face usually varies between two threshold values prescribed by the designer, with the construction team constantly switching between top heading and invert construction.

The rock bolt pattern and rock bolt properties used in the model correspond to the systematic rock bolting applied at the site (Figure 89). Instead of using cable elements, pile elements with activated so called "rock bolt logic" have been used (Itasca, 2009), in order to capture the shear resistance of rock bolts in best possible way. In addition, very fine discretization of rock bolt elements was used (20 nodes along the length), also adhering to the goal of correct rock bolt shear resistance mobilisation.
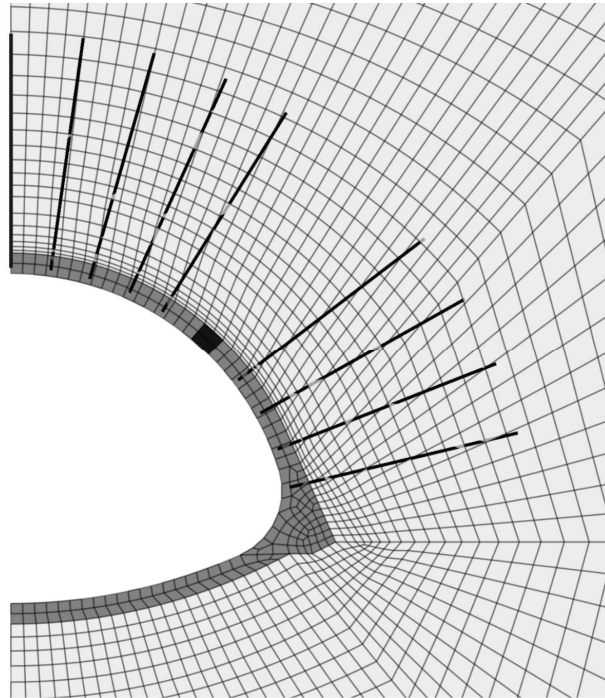
Figure 89. Modelled rock bolting pattern

The required rock bolt properties have been derived from the rock bolt type and the relationships presented in the FLAC3D structural elements manual (Table 14).

Table 14. Properties of the pile elements used to model rock bolts

Rock bolt diameter [mm]	32
Borehole diameter [mm]	51
Rock bolt cross section [mm²]	804
Tensile capacity [MN]	0.48
Moment of inertia [mm^4]	51471
Polar moment of inertia [mm^4]	102943
Grout shear stiffness [MN/m²]	2000
Grout shear strength [MN/m]	0.072
Failure strain [-]	0.20
Young's modulus [MPa]	200000

All calculations (including the calibration of the constitutive law) have been conducted in small-strain mode (geometry update is not being performed). In "large displacements" calculation mode, the strain rates are calculated constantly

on the basis of the *current model configuration*. Since the mobilisation of the strength properties also depends on the accumulated plastic shear strain, this would have led to even less transparent process of numerical calculation and strong tendency towards localised failure development. While this appears to be a desirable behaviour, it also causes additional dependency of results on the used discretization, since FLAC3D 4.0 still has no regularisation algorithm to deal with such phenomena. In addition, small-displacement calculations are considerably faster.

5.4 Overview of the examined cases

After the predictive capability of the numerical model has been proven by comparing the results to the measurement data, further simulations assuming installation of LSC, hiDCon and WABE elements have been conducted. All other boundary conditions (excavation geometry, shotcrete properties, excavation sequence, yielding element position etc.) have been kept constant, in order to examine the influence of the different load-displacement relationships on the system behaviour (Table 15).

Table 15. Assumed mechanical properties of the yielding elements

Element type	Shortening to yield Δl [mm]	Element length l [mm]	Yield load F_y [kN]
Reference case (Strenger-Type)	15	400	1000
4 x Type AII LSC	48	400	2800
hiDCon	14	400	3150[7]
WABE	15	400	1300

As already stated in the previous chapter, the bilinear load-displacement behaviour of the yielding elements has been approximated by using Mohr-Coulomb constitutive law in the respective zones (Table 16). The element strength has been defined by specifying the equivalent cohesion, while the tensile strength and friction angle have been set to 0.1.

Table 16. Equivalent MC-properties used to model yielding element behaviour

Element type	Young's modulus[8] E [MPa]	Poisson's ratio v [-]	Equivalent cohesion c [MPa]
Reference case (Strenger-Type)	63	0.01	1.19
4 x Type AII LSC	55	0.01	3.33
hiDCon	250	0.01	3.75
WABE	82	0.01	1.54

---

[7] Assuming a cross section area of the shotcrete shell to equal 0.42 m² (round length equalling 1.20 meter and shotcrete thickness of 0.35 m), yield stress of 7.50 MPa and yield strain of 3.5 %.
[8] Calculated on the basis of the yield stress, shortening to capacity and element length.

After the yielding elements featuring the "best behaviour" have been identified (along the criteria of support resistance and shotcrete utilisation), two additional calculations with the temporary invert being immediately installed (at the top heading face) and without the temporary invert have been conducted. These results are used to investigate the influence of the excavation sequence on the overall support resistance.

5.5 Results

5.5.1 Calculation of the shotcrete utilisation

The stress state at the innermost surface of the shotcrete shell (free boundary) is always biaxial. Since no reliable data on time dependent shotcrete strength in such conditions is available, the utilisation is calculated by dividing the shell hoop stress σ_θ with the time-dependent shotcrete strength $\beta(t)$:

$$\alpha = \frac{\sigma_\theta}{\beta(t)}. \qquad \qquad \textbf{Equation 88}$$

For each shotcrete zone, all six stress tensor components and their respective zone centroid positions are being recorded during the simulated excavation. Hence, the calculation of the associated hoop stresses is trivial. First a unit vector pointing tangentially to the shotcrete shell is determined from the zone centroid position, and then the hoop stress is calculated by scalar multiplication of the stress tensor (for the given face position) with the unit vector.

5.5.2 Reference case

The first calculation with the ground parameters as presented in chapter 5.1 yielded highly satisfactory results, so no additional effort was invested in fine-tuning the ground properties (Figure 90).
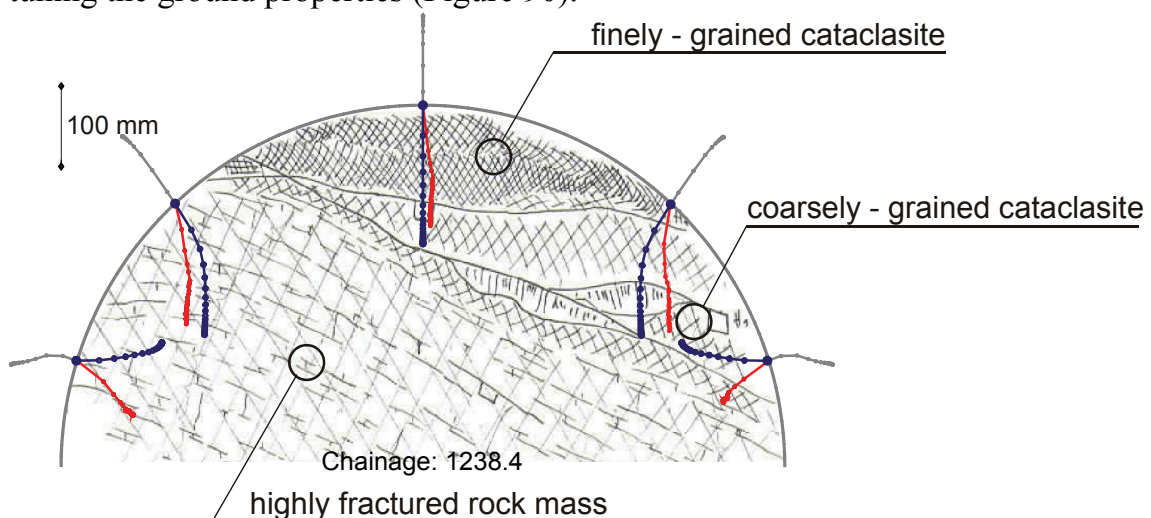

Figure 90. Comparison between measurement data obtained at chainage 1238 (red) and the results of the numerical analysis (grey – displacements ahead of the face, blue – displacements after face passage).

Apart from the displacement path taken by the sidewall points, the crown and shoulder points' displacements agree well with the measurements both in their magnitude as well as the their orientation. The discrepancy in the behaviour of the sidewall points is probably caused by the influence of the construction practice, as already remarked in chapter 4.3.8. It is not unusual for site personnel to cover the ground and the reinforcement of the top heading feet with loose material in order to obtain a clear reinforcement overlap area for the future joint with the bench lining. The inspection of the overall displacement field indicates that the results are in excellent agreement with the assumed kinematical behaviour (chapter 4.1). In addition, not only the final displacements, but also the displacement development due to face advance agree very well with the measurement data (Figure 91).
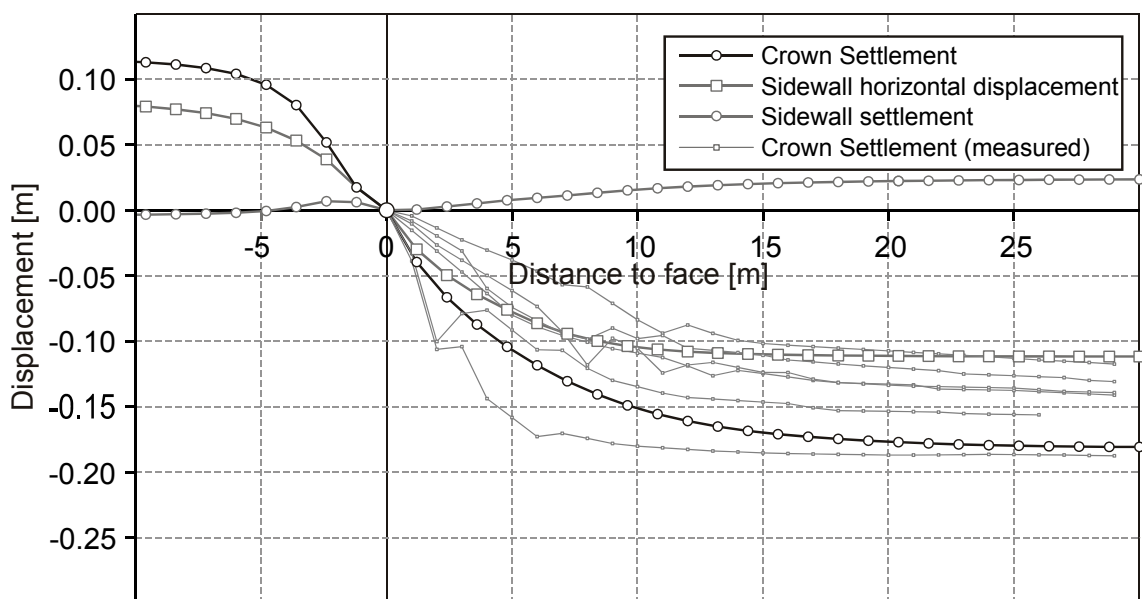
Figure 91. Comparison between displacement monitoring data (Lavanttal fault system) and the displacement development as predicted by the numerical model.

It has to be pointed out that obtaining such good agreement between predictions of the numerical simulation and reality with the first run is usually quite unlikely. In this particular case, both the ground deformability and the general strength properties (albeit "merely" the Mohr-Coulomb parameters) have been exceptionally well known before the analysis was attempted, thus providing a narrow parameter range within which the initial guess had to lie. The presented approach of using direct shear test data to calibrate the strain softening parameters is meaningful, but to draw the conclusion that such approach always leads to a good forward prediction ability of the numerical model would be completely false. Due to the various influences and mechanisms described in chapters 2.1 and 2.2, sometimes even the assessment of basic Mohr-Coulomb strength parameters of a fault zone represents a considerable challenge.

5.5.3 Element comparison

The evaluation of the system behaviour with different yielding elements types has been performed along the lines of the associated displacement development and the peak shotcrete utilisation. The comparison of the crown settlement observed in the reference case with the crown settlements to be anticipated if hiDCon, LSC or WABE elements are installed is shown in Figure 92.
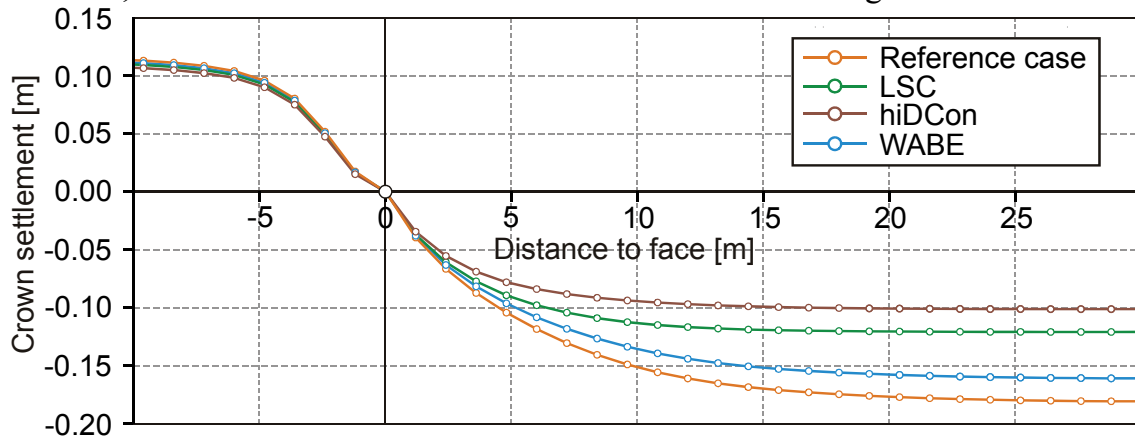

Figure 92. Influence of the yielding element capacity on the displacement development.

The influence of the element capacity is clearly visible, albeit not so pronounced as it would be suggested by the usual convergence confinement method analysis (as presented in Radoncic et al. 2009). In that publication, the mobilised support pressure is calculated merely from the load-displacement relationship of the yielding elements, completely omitting the shear bond between the shotcrete and the ground and the influence of the rock bolts. It is logical that the influence of yielding elements is somewhat decreasing if other additional support measures and load-bearing mechanisms are accounted for. A direct result comparison is possible only in case of LSC elements, since the assumptions regarding the load displacement relationship of the both other types have changed meanwhile, due to additional laboratory testing (Barla, 2010). The 2009 publication by Radoncic et al. suggests that the installation of four LSC Type-II elements would cause a reduction of final displacements from 180 mm to 63 mm, the numerical analysis with more sophisticated constitutive law, rock bolt and excavation sequence suggests a reduction from 180 mm to 120 mm. WABE elements cause a slight reduction to 160 mm caused by their marginally higher yield load than the installed Strengen type elements. The installation of hiDCon elements results in lowest final displacements of 100 mm, due to their yield load of 3150 kN.

The comparison of the shotcrete utilisation draws a more complex picture, since not only the yield load, but also the initial stiffness of the elements has a major influence on the results. Throughout all calculations, the highest hoop stress loading occurred at the fillet of the top heading elephant feet, caused by the influence of the geometry. Since the behaviour of the top heading feet was already deemed as too stiff and unrealistic, these stress peaks have been omitted

in the evaluation, and the tangential stress at the crown has been used for final comparison (Figure 93).
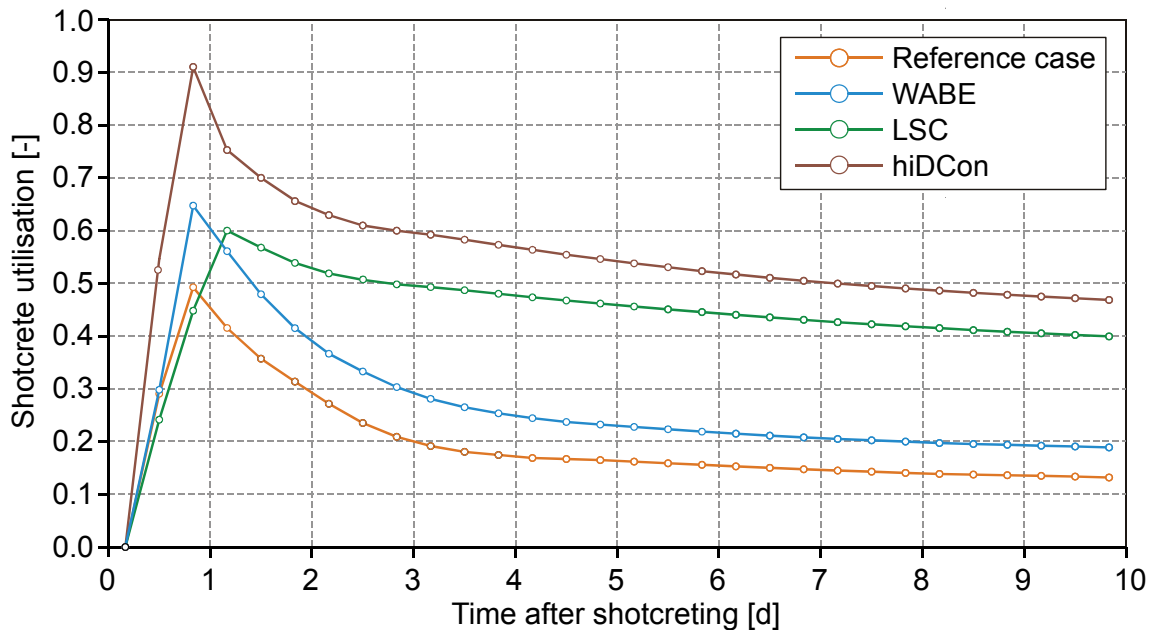
Figure 93. Comparison of the shotcrete utilisation development observed at the crown of the numerical model.

The results are in line with the findings published in Radoncic et al. (2009), albeit the influence of the different load displacement relationships is not so strongly pronounced. This is caused by the full shear bond between the lining "rings" installed in every excavation round, thus smoothing out the occurring lining stresses. In reality, the different age (and thus, stiffness) of the shotcrete applied in each excavation round and the installation of TH beams (or lattice girders) causes additional complexities in the overall material behaviour of the shotcrete shell and probably quite pronounced anisotropy. This places the real behaviour of a shotcrete lining exactly between the range proposed by the results of the 3D numerical analysis (full bond and isotropic conditions in the shotcrete lining) and the 2D analysis presented in Radoncic et al. (2009), assuming no interaction between the adjacent lining rings along the tunnel axis.

However, the basic findings and conclusions regarding the currently available yielding element types at the market remain the same. The WABE and Strengen type elements have a very adverse combination of the relatively high initial stiffness and low final capacity. This combination results in a two-fold problem: on the one hand, the high initial stiffness causes an utilisation peak in the young shotcrete, on the other hand, the low final capacity worsens the behaviour by featuring large final displacements and hence, high initial displacements/strains imposed on the lining. This is best demonstrated by the high discrepancy between the peak and final utilisation of these elements, as shown in Figure 93. While the high initial stiffness causes the utilisation to go up to 65 %, it drops

down rapidly to values below 20%. In other words, merely one fifth of the support capacity of the applied shotcrete is *really* used.

Both the hiDCon elements and the applied LSC element combination result in more reasonable final shotcrete utilization of approx. 40 – 50%. The very high initial stiffness of the hiDCon elements is somewhat counteracted by their high capacity, thus preventing the occurrence of large initial strains in the lining. Nevertheless, a peak utilisation of young shotcrete equalling almost 92% is very high – more adverse ground conditions or more rapid tunnel advance would have shotcrete damage as a result. Simply put, while the hiDCon element capacity is reasonable, it is too stiff in the initial phases of loading. This bounds the hiDCon elements (in their unchanged form, without any attempts to change the load-displacement behaviour by Styrofoam inserts or other means) to application in tunnels with either relatively low advance rate and/or strong time dependent displacement behaviour (swelling or strongly delayed creep deformations).

For the sake of fairness – since the author has the highest experience with the LSC elements and the range of possible thrust magnitudes – the LSC yielding elements have not been fine tuned to the examined ground conditions. However, a short demonstration of possible resistance when an appropriate element combination is used can be performed: according to Table 2, two Type AII elements would surmount to 1400 kN of thrust. Adding two BIIIb (tube diameter approx. 250 mm) would not pose a problem at the lining thickness of 35 cm, thus adding additional 3900 kN to the thrust at yield. In order to avoid shotcrete overstressing, the BIIIb elements could be 50 mm shorter than the AII elements, thus ensuring that the activation of the stiffer and higher capacity elements is delayed and complies with the time dependent shotcrete capacity requirement. The usage of this element combination would result in 5300 kN of thrust at the point of yield *without* shotcrete overstressing.

5.5.4 Influence of the excavation sequence

Despite the fact that the numerical model exaggerates the resistance mobilisation of the elephant feet, two final calculations have been conducted. Both are assuming the installation of 4 x Type AII LSC elements (as in previous calculations), however one calculation features no temporary invert at all, while the other assumes zero distance between the top heading face and temporary invert installation. The results drastically demonstrate the role of the yielding elements in the overall kinematical behaviour of the support: the crown and sidewall displacements (both measured on the shotcrete segment above the yielding elements) are basically unaffected by the moment of the temporary invert installation (Figure 94). On the other hand, the resistance to horizontal movement is greatly increased, as shown by the low horizontal displacements of the sidewalls.
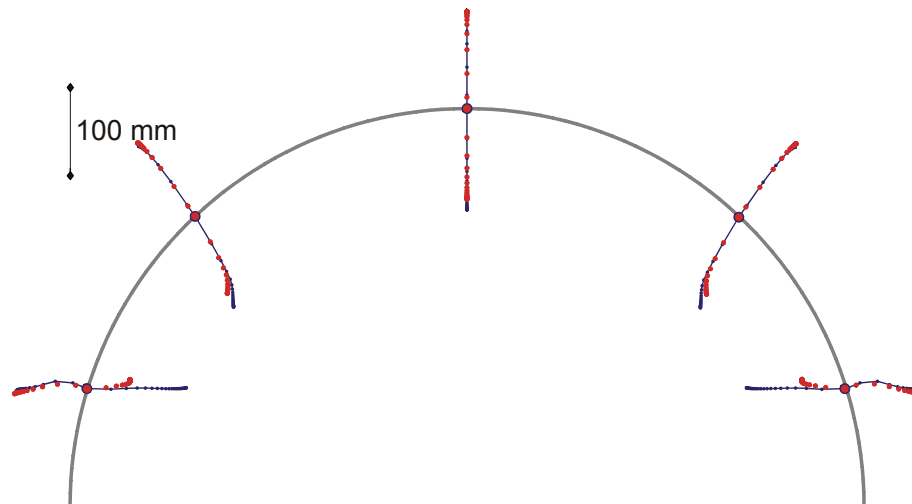
Figure 94. Influence of the temporary invert on the system behaviour. Red dots: immediate invert installation. Blue lines: no temporary invert.

Hence, the overall lining response can only become stiffer if the yielding elements capacity appropriately takes advantage of the stiffer top heading feet abutment. If this is not case, the temporary invert brings merely the advantage of the reduced sidewall movement, while making complications in the joint area between the top heading lining and the invert very likely. Its construction is only meaningful if the yielding element capacity and position within the cross section (in the sidewalls, in order to avoid stress peaks in the joint area) are carefully tuned to its influences. Otherwise, either a "common" top heading advance (if the system is intended to be flexible and an appropriate overexcavation is provided) or a short bench with early ring closure (if high support resistance and more direct control of the resistance mobilisation) should be used.

5.6 Discussion

The presented case study demonstrates that a realistic prediction (and depiction) of the system behaviour in case of integrated yielding elements is possible with numerical methods. However, very fine discretization, the strain softening constitutive law and realistic assessment of the shotcrete stiffness are imperative for plausible predictions. The downside is the extreme calculation time (approx. 4-7 days for a single run), rendering parameter studies quite unwieldy and time consuming. In addition, only a small portion of mechanisms and phenomena taking place in the rock mass and mentioned in chapter 2.2 has been realistically captured by the applied constitutive law. Until more reliable methods of rock mass characterisation and parameter identification are available, it is probably more meaningful to use simpler numerical models.

A very promising idea would be the coupling of the relationships proposed in chapter 4.2.2 with an axisymmetric numerical model. The longitudinal displacement profiles obtained from the numerical model could be used for

calculating the support mobilisation (while accounting for the rheological behaviour of the shotcrete), which can be applied as an external stress at the excavation boundary.

Additional research and development effort should be invested by implementing additional, more complex constitutive laws for the shell and liner elements in FLAC3D. The current state of the development can only handle linear elastic elements, which renders efficient and realistic capturing of the lining behaviour almost impossible.

6 Conclusions

After inspecting the literature review presented in the first chapter and comparing it to the analysis methods shown subsequently, one cannot ignore the fact that the current means of analysis are still lagging behind the experience regarding what the rock mass *can do* and *does*. Nevertheless, the presented methods have been custom-tailored for the tasks of designing ductile linings and making plausible assessment of the system behaviour, thus allowing fast identification of sensitivities and quantifying the influence of the uncertainties in the ground characterisation and influencing factors. As already stressed frequently in the course of the thesis, the level of sophistication in the analysis methods has always to follow the quality and reliability of the rock mass characterisation.

Based on the findings of this thesis, the dialogues with mentors and the knowledge gained from the literature review, following recommendations regarding design of deep tunnels in weak ground lie at hand:

1. Although appearing as a trivial conclusion, the roles of proper investigation, ground characterisation and ground behaviour determination cannot be overstressed. Both the investigation programme and the lab test programme have to be custom-tailored to the envisioned analysis means and identified failure mechanism. This renders the design, especially in the early project stages, an iterative process: after all possible mechanisms of stress re-distribution and displacement development have been identified, additional effort has to be invested into determining reliable parameters for the best-suited calculation model.

2. Proper determination of ground behaviour is an excellent starting point for the basic support design: after the influences of structure, rheological behaviour and water have been determined, the basic layout of lining should follow the anticipated deformation pattern. The layout of the yielding elements within the cross section does NOT have to be symmetrical, but to orientate itself on the kinematics of a ductile lining subjected to unsymmetrical deformation field.

3. The yielding element load-displacement characteristic must comply to the time-dependent development of shotcrete capacity and the displacement development characteristic of the system. Displacement monitoring (especially if including the respective element shortening) should be frequently and systematically conducted and evaluated by competent personnel. A great room for optimisation with regard to overexcavation dimensions, associated support measures and risk miminisation is present when the measurement data are evaluated on time and the right conclusions are drawn.

4. The chosen excavation sequence has to closely follow the envisioned support mobilisation. Advancing a top heading with yielding elements of extreme capacity without taking care about the proper abutment of the top heading feet is basically meaningless. The systematic rock bolting, temporary invert installation and/or elephant feet have a limited effect on the top heading resistance mobilisation. While the temporary invert causes adverse support geometry, the elephant feet and rock bolting are intrinsically bound to the ground properties and can have a strongly varying effect. Above a certain level of thrust required in the lining, a short bench and early ring closure should be envisioned, however this not immediately implies that full-face excavation should be used. It is associated with several operational problems: use of heavy machinery, low accessibility of the crown and shoulders, a great amount of immediate displacement (and energy release) and heavy face support are the usual consequence.

5. The rock bolt pattern has to adhere to the chosen yielding element layout. Long and stiff rock bolts should be either installed far from the yielding elements, or other means of preventing the combined thrust and shear loading should be used. The general rock bolting concept should combine frequent short rock bolts (with the goals of homogenizing the rock mass and increasing its ductility in the vicinity of the excavation, where the strains are highest) and several strong and long rock bolts for the overall stability (thus anchoring the shotcrete segments and the loosened weight of the rock mass).

6. Common sense and engineering judgement have to stay in focus as main tools of an engineer, not tensor calculus and advanced mathematics.

In the end, an inspiring quote which is unfortunately still quite applicable in the field of tunnelling, by a wise and humorous observer of us as a species:
"*Human beings, who are almost unique in having the ability to learn from the experience of others, are also remarkable for their apparent disinclination to do so.*" - Douglas Adams, Last Chance to See

7 References

3G Gruppe Geotechnik Graz ZT GmbH (2010):

> Ergänzendes Erkundungsprogramm für die Hauptstörung des Lavanttaler Störungssystems – Versuchsstollen Endbericht. Internal project communication for the Koralm tunnel. 2010.

Aldrian, W (1991)

> Beitrag zum Materialverhalten von früh belasteten Spritzbeton. PhD thesis. Montanuniversität Leoben, 1991.

Amberg, F. (2009)

> Numerical simulations of tunnelling in soft rock under water pressure In: 2nd international conference on computational methods in tunnelling EURO:TUN 2009, September 9th – 11th, 2009. Bochum, Germany. pp. 353 – 360. Meschke et al. eds. Aedificatio Publishers.

Anagnostou, G. (2009)

> Pore pressure effects in tunnelling through squeezing ground. In: 2nd international conference on computational methods in tunnelling EURO:TUN 2009, September 9th – 11th, 2009. Bochum, Germany. pp. 361 – 368. Meschke et al. eds. Aedificatio Publishers.

Aydan, Ö., Akagi, T. & Kawamoto, T. (1993)

> The squeezing potential of rock around tunnels: theory and prediction. Rock Mechanics and Rock Engineering 2. pp. 137 – 163

Barla, G. (2001)

> Tunnelling under squeezing rock conditions, Eurosummer-School in Tunnel
>
> Mechanics Innsbruck, Politecnico di Torino, Torino. 2001.

Barla, G. (2009)

> Innovative tunnelling construction method to cope with squeezing at the Saint Martin La Porte access adit (Lyon – Turin Base Tunnel). In Rock Engineering in difficult ground conditions – soft rocks and karst. Eurock 2009, 29th – 31st October 2009, Cavtat, Croatia. Vrkljan (ed). Balkema. 2009.

Barla, G. (2010)

> Personal communication with author.

Barla, G., Bonini, M. Debernardi, D., (2007)

> Modelling of tunnels in squeezing rock. In Eberhardsteiner et al. (eds) Computational Methods in tunnelling, EURO:TUN 2007. Digital proceedings.

Barlow, J.P. & Kaiser, P. (1987)

> Interpretation of tunnel convergence measurements. In: Proc. 6th Int. Congress on Rock Mechanics, ISRM, Montreal, Canada 1987. pp 787 – 792. Rotterdam, Balkema.

Barton, N. & Bandis, S. (1990)

Review of predictive capabilities of JRC – JCS model in engineering practice, In: Rock Joints, eds. Barton and Stephansson, (1990), Balkema, Rotterdam

Biot, M. A. (1941)

General theory of three-dimensional consolidation, Journal of applied phyics 12, pp. 155 – 164. 1941

Blümel, M. (1996)

Untersuchungen zum Tragverhalten vollvermörtelter Felsbolzen im druckhaften Gebirge. PhD Thesis. Institute for Rock Mechanics and Tunnelling, Graz University of Technology. 1996.

Bonini, M., Debernardi, D., Barla, M. & Barla, G. (2007)

The mechanical behaviour of clay shales and implications on the design of tunnels. Rock Mechanics and Rock Engineering 42 (2009). pp. 361 – 388. Elsevier, 2009.

Brady, B.H.G. & Brown, E.T. (1985)

Rock mechanics for underground mining. George Allen & Unwin, London. 1985.

Brandtner, M., Moritz, B. and Schubert, P. (2007)

On the challenge of evaluating stresses in a shotcrete lining. Felsbau 25 (2007), No. 5, pp. 93–98.

Brown, E. T., Bray, J.W., Ladanyi, B. and Hoek, E. (1983)

Characteristic line calculations for rock tunnels. J. Geotech. Engineering, Am. Soc. Civ. Engineers 109, pp. 15-39, 1983.

Button, E.A. (2004)

A Contribution to the characterization of Phylittic and Schistose Rock Masses for Tunnelling. PhD Thesis. Institute for Rock Mechanics and Tunnelling, Graz University of Technology. 2004.

Cantieni, L. & Anagnostou, G. (2009)

The effect of the stress path on squeezing behaviour in tunnelling. Rock Mechanics and Rock Engineering 42 (2), pp. 289 – 318. Springer Verlag, 2009.

Carranza – Torres, (2004)

Elasto-plastic solution of tunnel problems using the generalized form of the hoek-brown failure criterion Int. J. of Rock Mech. and Mining Sciences Volume 41, Supplement 1, May 2004, pp 629-639 Proceedings of the ISRM SINOROCK 2004 Symposium

Carranza-Torres, C. & Fairhurst, C. (2000)

Application of the Convergence-Confinement Method of Tunnel Design to Rock Masses That Satisfy the Hoek-Brown Failure Criterion, Tunnelling and Underground Space Technology Vol. 15, No. 2, pp. 187 — 213.

Cristescu, N.D. & Hunsche, U. (1998)

Time effects in rock mechanics. John Wiley & Sons Ltd. London, Great Britain. 1998.

Dalgic, S. (2002)

    Tunnelling in squeezing rock, the Bolu tunnel, Anatolian motorway, Turkey. Engineering geology 67, pp 73 – 96, Elsevier, 2002.

Debernardi, D. & Barla, G. (2009)

    New viscoplastic model for design analysis of tunnels in squeezing conditions. Rock Mechanics and Rock Engineering 42 (2009). pp. 259 – 288. Elsevier, 2009

Diederichs, M. & Hoek, E. (2009)

    Improved longitudinal displacement profiles for convergence confinement analysis of deep tunnels. Rock Mechanics and Rock Engineering 42, pp. 131-146. Springer Verlag, 2009.

Einstein, H.H. (1996)

    Tunnelling in Difficult Ground – Swelling Behaviour and Identification of Swelling Rocks. Rock Mechanics and Rock Engineering 29 (3): pp 113 – 123.

Eurocode 7 (2004)

    Geotechnical design – Part 1: General rules. European Committee for standardisation.

Feder, G. & Arwanitakis, G., (1976)

    Zur Gebirgsmechanik ausbruchsnaher Bereiche tiefliegender Hohlraumbauten (unter zentralsymmetrischer Belastung), Berg- und Hüttenmännische Monatshefte, Jahrgang 121, Heft 4.

Fenner, R. (1938)

    Untersuchungen zur Erkenntnis des Gebirgsdrucks. PhD Thesis. Technische Hochschule zu Breslau. Verlag Glückauf Essen. 1938. Essen.

Gamper, C., Knapp, M. & Fiest, T. (2009)

    Jenbach tunnel – a shallow hydroshield drive. Geomechanics and Tunnelling 2 (2009) No. 5. pp. 494 – 501. Ernst & Sohn Verlag, Berlin. 2009.

Goel, R.K., Jethwa, J.L. & Paithakan, A.G. (1995)

    Tunnelling through the young Himalayas – a case history of the Maneri – Uttarkashi power tunnel. Engineering Geology 39. pp. 31-44

Golser, H. (2001)

    The Application of Finite Element and Boundary Element Methods in Tunnelling. PhD thesis, Institute for Rock Mechanics and Tunnelling, Graz University of Technology, Austria

Gonzales – Nicieza, C., Alvarez-Vigil, A.E., Menendez-Diaz, A. & Gonzales – Palacio, C. (2008)

    Influence of the depth and shape of a tunnel in the application of the convergence-confinement method. Tunnelling and Underground Space Technology 23 (2008), Pp. 25 – 37. Elsevier, 2008.

Goricki, A., Button, E.,Schubert, W., Pötsch, M. & Leitner, R., (2005)

    The Influence of Discontinuity Orientation on the Behaviour of Tunnel. Felsbau 23/05. pp. 12-18, VGE Verlag

Gradsack, O. (2010)

Influence of sub-horizontal faults on the system behaviour. Institute for Rock Mechanics and Tunnelling, Graz University of Technology. 2010.

Gresovnik, I. (2006):

Deliverable 1.3.1.1: Specifications for software to determine sensitivities for optimisation of the design of underground construction as part of IOPT. TunConstruct Deliverable, Sixth Framework Programme of the European Union. C3M, 2006.

Gschwandtner, G. (2010)

Analytische Berechnungsansätze zum Kennlinienverfahren, Diploma Thesis, Department of Sub-Surface Engineering, Montanuniversität Leoben, 2010.

Habimana, J., Labiouse, V. & Descoeudres, F. (2002)

Geomechanical characterisation of cataclastic rocks: experience from the Cleuson-Dixence project. Int. Journal Rock Mech. & Mining Sci., Vol. 39, pp. 677 – 693.

Hajiabdolmajid, V., Kaiser, P.K. & Martin, C.D. (2002)

Modelling brittle failure of rock. International Journal of Rock Mechanics & Mining Sciences 39 (2002). Pp. 731 – 741. Elsevier, 2002.

Hellmich, C. (1999)

Shotcrete as part of the New Austrian Tunnelling Method: from thermochemomechanical material modelling to structural analysis and safety assessment of tunnels. Doctoral thesis Technische Universität Wien, 1999.

Hoek, E. (2001)

Big tunnels in bad rock. 36th Karl Terzaghi Lecture, ASCE Journal of Geotechnical and Geoenvironmental Engineering. ASCE. Seattle. 2001

Hoek, E. (2007)

Practical rock engineering. Electronic manuscript.
http://www.rocscience.com/hoek/PracticalRockEngineering.asp

Hoek, E. (2009)

Overcoming squeezing in the Yacambu – Quibor Tunnel, Venezuela. RocNews Spring 2009.
electronic publication: http://www.rocscience.com/library/rocnews/ spring2009/Top-Project-Venezuela.pdf

Hoek, E., Carranza-Torres, C., Diederichs, M. & Corkum, B. (2008)

Integration of geotechnical and structural design in tunnelling. 2008 Kersten Lecture. Proceedings University of Minnesota 56th Annual Geotechnical Engineering Conference. Minneapolis. 2008.

Irfan, T.Y. & Tang, K.Y. (1993)

Effect of the coarse Fractions on the shear strength of colluvium. Geo Report No. 23, Geotechnical Engineering Office, Civil Engineering Department, Hong Kong.

Itasca Consulting Group Inc. (2004)
UDEC 4.00 Manual: Theory and Background. Itasca Consulting Group Inc. Minneapolis, 2004.

Itasca Consulting Group Inc. (2009)
FLAC 3D 4.00 Manual. Itasca Consulting Group Inc. Minneapolis, 2009.

Jethwa, J.L., Singh, B. & Singh, B. (1984)
Estimation of ultimate rock pressure for tunnel linings under squeezing rock conditions – a new approach. Design and Performance of Underground Excavations, ISRM Symposium, Cambridge. E.T. Brown and J.A. Hudson eds. pp. 231 – 238

John, M. & Mattle, B. (2007)
Auswirkungen stark druckhafter Gebirgsverhältnisse auf den TBM-Vortrieb. Felsbau 25 (2007), No. 6, pp. 14–21. Verlag Glückauf Essen. 2007.

John, M. (1980)
Construction of the Arlberg expressway tunnel tube 3. Tunnels and Tunnelling International 12 (1980), No. 5, pp. 45–50.

Kastner, H. (1962)
Statik des Tunnel- und Stollenbaus. Berlin, Springer Verlag.

Kilic, A., Yasar, E. & Celik, A.G. (2002)
Effect of grout properties on the pull-out load capacity of fully grouted rock bolt. Tunnelling and Underground Space Technology 17, pp. 355 – 362. Elsevier, 2002.

Kovari, K., Ehrbar, H. and Theiler, A. (2005)
Druckhafte Strecken im TZM Nord: Projekt und bisherige Erfahrungen. In Löw (ed): Geologie und Geotechnik der Basistunnels am Gotthard und am Lötschberg. Vdf. Hochschulverlag an der ETH Zürich, 2005.

Kulhawy, F.H. (1975)
Stress deformation properties of rock and rock discontinuities. Engineering Geology 9, pp. 327 – 350.

Leber, C. (2010)
Personal communication with regard to the influence of geological structure on the system behaviour. Upcoming PhD Thesis, Institute for Rock Mechanics and Tunnelling, Graz University of Technology. *In work*.

Leitner, R. & Müller, H. (2007)
Numerische Modellierung von Wasserzutritten für tiefliegende Tunnel. Christian Veder Kolloqium, Graz University of Technology, 2007.

Leitner, R. (2005)
Numerical investigation on Failure Mechanisms and Function of Tunnel Support Systems, Diploma Thesis, Institute for Rock Mechanics and Tunnelling, Graz University of Technology, 2005.

Lenk, K. (1930)

Der Ausgleich des Gebirgsdruckes in großen Teufen beim Berg- und Tunnelbau. Julius Springer Verlag, 1930. Berlin.

Levin, D. (1998)

The approximation power of moving least squares. Mathematics of Computation 67, Number 224, Pp. 1217 – 1531. American mathematical society. 1998.

Lindquist, E.S. & Goodman, R.E, (1994)

Strength and deformation of a physical model melange. Rock Mechanics – Models and Measurements Challenges from Industry, Nelson & Laubach (eds). Balkema, Rotterdam, 843 - 850

Macht, J. (2002)

Hybrid analysis of shotcrete tunnel linings: assessment and online monitoring of the level of loading. Doctoral thesis Technische Universität Wien, 2002.

Mahmutoglu, Y., Vardar, M., Kocak, C. & Sans, G. (2006)

Tunnelling difficulties under squeezing and flowing conditions at Ayas tunnel. Felsbau 24 (2006) No. 5. pp. 44 – 50. Verlag Glückauf Essen. 2006.

Martin, D. (1997)

The effect of cohesion loss and stress path on brittle rock strength. Canadian Geotechnical Journal Vol. 34, No. 5, 1997.

MathWorks (2004):

MatLab. Electronic User Manual, Non-linear optimisation toolbox. MathWorks, Natick, 2004.

Medley, E. & Goodman, R.E. (1994)

Estimating the block volumetric proportions of melanges and similar block-in-matrix rocks (bimrocks). Rock Mechanics – Models and Measurements Challenges from Industry, Nelson & Laubach (eds). Balkema, Rotterdam, 851 - 858.

Mitchell, J.K., Campanella, R. G. & Singh, A. (1968)

Soil Creep as a rate process, ASCE Journal SMFD, V. 94, N.1. 1968.

Montanuniversität Leoben (2006)

Ermittlung der rheologischen Parameter für Spritzbetonproben aus dem Koralmtunnel. Lehrstuhl für Geomechanik, Tunnelbau und konstruktiven Tiefbau. Montanuniversität Leoben. Leoben 2006.

Moritz, A.B.(1999)

Ductile Support System for Tunnels in Squeezing Rock. In Riedmüller, Schubert & Semprich (eds.): Schriftenreihe Gruppe Geotechnik Graz, Heft 5, Graz University of Technology, 1999.

Mösslacher, A. (2006)

Numerische Untersuchung des Einflusses einer Störungszone auf Verschiebungen während des Tunnelvortriebes. Diploma Thesis, Institute for Rock Mechanics and Tunnelling, Graz University of Technology, Austria

Nealen, A. (2009)
　　An As-Short-As-Possible introduction to the least squares, weighted least squares and moving least squares methods for scattered data: approximation and interpolation. Electronic script/note.
　　http://www.nealen.net/projects/mls/asapmls.pdf

OEGG (2008)
　　Guideline for the geotechnical design of underground structures with cyclic excavation. 2nd revised edition. Salzburg: The Austrian Society for Geomechanics

Oreste, P. (2008)
　　Distinct analysis of fully grouted bolts around a circular tunnel considering the congruence of displacements between the bar and the rock, International Journal of Rock Mechanics & Mining Sciences 45 (2008) pp. 1052–1067

Pacher, F. (1964)
　　Deformationsmessungen im Versuchsstollen als Mittel zur Erforschung des Gebirgsverhaltens und zur Bemessung des Ausbaus, Felsmechanik (1964).

Pan, X.F., Zhang, X. & Lu, M.W. (2004):
　　Meshless Galerkin least-squares method. Computational mechanics 35 (2005), Pp. 182 – 189. Elsevier, 2005.

Pan, Y.W., Hsieh, M.H. & Liao, J.J.(2008)
　　Mechanical Properties of Virtual Block-in matrix Colluvium. In: Proc. of 42nd US Rock Mechanics Symposium, San Francisco, June 29 - July 2, 2008.

Panet, M. & Guenot, A. (1982)
　　Analysis of convergence behind the face of a tunnel, Tunnelling 1982, The Institution of Mining and Metallurgy, pp. 197 – 204

Patton, F. D. (1966)
　　Multiple modes of shear failure in rock. In Proc. 1st Congr. International society of rock mechanics, Volume 1., 509 – 513, Lisboa.

Peck, R.B. (1969)
　　Advantages and limitations of the observational method in applied soil mechanics. Geotechnique 19. No. 2

Peck, R.B., (1969)
　　Advantages and limitations of the observational method in applied soil mechanics, Geotechnique 19, No. 2, 171-187. The Institution of Civil Engineers, London

Pellet, F. & Egger, P. (1996)
　　Analytical model for the mechanical behaviour of bolted rock joints. Rock Mechanics and Rock Engineering 29 (2), pp. 73 – 97. Springer Verlag, 1996.

Peltham, P. (1973)
　　A stochastic model of crystal plasticity, J. Phys. D: Appl. Phys. Vol. 6, 1973.

Pichler, B., Scheiner, S., Hellmich, C. & Eberhardsteiner, J. (2009)
Micromechanics-based models for elasticity and strength of shotcrete, for hybrid analyses of NATM tunnel shells. In: 2nd international conference on computational methods in tunnelling EURO:TUN 2009, September 9th – 11th, 2009. Bochum, Germany. pp. 353 – 360. Meschke et al. eds. Aedificatio Publishers.

Pilgerstofer, T. (2010)
Personal communication with regard to the geomechanical characterisation of the tectonical fault zones. Upcoming PhD Thesis, Institute for Rock Mechanics and Tunnelling, Graz University of Technology. *In work.*

Pilgerstorfer, T. (2008)
Prediction of displacement development using closed form solutions. Diploma Thesis. Institute for Rock Mechanics and Tunnelling. Graz University of Technology. 2008. Austria.

Pilgerstorfer, T., Schubert, W., Moritz, B. & Goricki, A. (2011):
In-situ test program for fault zone characterisation. In: Proceedings of WTC 2011, 21st – 26th May 2011, Helsinki, Finnland.

Pöchhacker, H. (1974):
Moderner Tunnelvortrieb in sehr stark druckhaftem Gebirge. Porr Nachrichten 57/58, 1974.

Pötsch, M. (2001)
Parametric studies with UDEC for the quantification of the influence of joint set properties on the tunnel deformations, Projekt Geotechnik, Institute for Rock Mechanics and Tunnelling, Graz University of Technology. 2001. Austria

Pöttler, R. (1996)
Über die Wirkungsweise einer geschlitzten Spritzbetonschale. Felsbau 15 (1996), No. 6, pp. 422–428.

Pusch, R., Zhang, L., Adey, R. & Kasbohm, J. (2009)
Rheology of an artifical smectitic clay, Applied Clay Science 47 (2010), pp. 120 – 126, Elsevier, 2010.

Rabcewicz, L.v. (1944)
Gebirgsdruck und Tunnelbau, Springer Verlag, 1944.

Rabcewicz, L. v. (1950)
Die Hilfsgewölbebauweise. Dissertation, TH – Graz, 1950. Graz

Radoncic, N. & Schubert, W. (2010)
Defining squeezing: the support oriented approach. Under review and to be published in: Rock Mechanics and Rock Engineering, Elsevier.

Radoncic, N., Moritz, A.B. & Schubert, W. (2009)
Ductile lining design. Geomechanics and tunnelling 2 (2005). pp. 561 – 577. Ernst & Sohn Verlag, Berlin. 2009.

Radoncic, N., Pilgerstorfer, T. & Schubert, W. (2008)
Prediction of displacements in tunnels. 5th Asian Rock Mechanics Symposium. November 24th – 26th 2008. A. Majdi & A.Ghazvinian eds. pp. 809 – 819

Ramoni, L. & Anagnostou, G. (2010)

The interaction between shield, ground and tunnel support in TBM tunnelling through squeezing ground. Rock Mechanics and Rock Engineering, available online since 14th May 2010. Springer Verlag, 2010.

Reinhold, C. & Kudla, W. (2007)

Großödometerversuche und spannungsabhängige Steifemoduli bei hohen Überlagerungsspannungen für nicht-bindige, tertiäre Grundwasserleiter des Lausitzer Tagebaureviers. Geotechnik 30, Nr. 3, pp. 170 – 178.

Riedmüller, G., Brosch, F. J., Klima, K. and Medley, E.W. (2001):

Engineering geological characterisation of brittle faults and classification of fault rocks. Felsbau 19, No. 4. pp 13 – 18, Verlag Glückauf GmbH, 2001. Essen.

RocScience (2009)

Phase 2, v. 7.0. http://download.rocscience.com/products/Phase2.asp. 2009.

Rokahr, R.; Zachow, R. (1997)

Ein neues Verfahren zur täglichen Kontrolle der Auslastung einer Spritzbetonschale. Felsbau 15 (1997), No. 6: 430-434. Essen: VGE

Rupnig, M. (2008)

Einfluss der Gefügeorientierung auf das räumliche Verschiebungsverhalten im Tunnelbau. Diploma Thesis, Institute for Rock Mechanics and Tunnelling, Graz University of Technology. 2008. Austria

Salamon, M.D.G. (1984)

Energy considerations in rock mechanics: fundamental results. J.S.Afr. Inst.Min.Metall., 84(8), Pp. 2333 – 246. 1984.

Schneider, E., Rotter, K., Saxer, A. and Röck, R. (2005)

Compex Support System – Komprimierbarer Ringspaltmörtel zur Bewältigungdruckhafter Gebirgsbereiche bei TBM-Vortrieben mit starrem Tübbingausbau. Felsbau 23 (2005), No. 5, pp. 95–101. Verlag Glückauf Essen, 2005.

Schubert, P (1988)

Beitrag zum rheologischen Verhalten vom Spritzbeton. Felsbau 6 (3), pp. 150–153. Verlag Glückauf Essen, 1988.

Schubert, P. (1984)

Das Tragvermögen des mörtelversetzten Ankers unter aufgezwungener Verschiebung. Bericht Nr. 4/84, Insitut für Konstruktiven Tiefbau, Montanuniversität Leoben, 1984.

Schubert, P. and Marinko, T. (1989)

Vortrieb des Karawankentunnels im tektonisch stark beanspruchten Südabschnitt. Felsbau 7 (1989), No. 2, pp. 65–68. Verlag Glückauf Essen. 1989.

Schubert, P., Hölzl, H., Sellner, P. & Fasching, F. (2009)
Geomechanical knowledge gained from the Paierdorf investigation tunnel in the section through the Lavanttal main fault zone. Geomechanics & Tunnelling 3 (2), Pp. 163 – 173. Ernst & Sohn Verlag, Berlin. 2010.

Schubert, W. & Riedmüller, G. (1995)
Geotechnische Nachlese eines Verbruches – Erkenntnisse und Impulse. Proc. 10. Christian Veder Kolloqium, 1995. Graz

Schubert, W. (1993)
Erfahrungen bei der Durchörterung einer Großstörung im Inntaltunnel. Felsbau 11 (6). pp. 287-290. Verlag Glückauf Essen. 1993.

Schubert, W. (1996)
Dealing with squeezing conditions in alpine tunnels. Rock Mechanics and Rock Engineering 29 (3). Springer-Verlag. 1996.

Schubert, W. (2002)
Displacement Monitoring in Tunnels – an Overview. Felsbau 20 (2002), No. 2. pp. 7-15. Verlag Glückauf Essen, 2002.

Schubert, W. (2008a)
Design and construction of tunnels in poor and faulted rock masses. 5th Asian Rock Mechanics Symposium. November 24th – 26th 2008. A. Majdi & A.Ghazvinian eds. pp. 827 – 835

Schubert, W. (2008b)
Design of ductile tunnel linings. 42nd Us Rock Mechanics Symposium and 2nd U.S. – Canada Rock Mechanics Symposium, San Francisco, June 29th – July 2nd, 2008. Paper code ARMA 08-146. Digital proceedings.

Schubert, W.; Budil, A. (1996)
The importance of longitudinal deformations in tunnel excavation. In Fuji, T. (ed.), Proc. 8th int. Congress on Rock Mechanics, Vol. 3, Tokyo, Japan, 1995: 1411-1414. Rotterdam: A.A. Balkema

Schubert, W. (2011):
Experience from Tunnel Construction in weak Ground, Geomechanics and Tunnelling 3/2011. Ernst & Sohn Verlag, 2011.

Schütz, R. (2010)
Numerical modelling of shotcrete for tunnelling. PhD Thesis. Department of civil and environmental engineering, Imperial College London. 2010.

Schwieger, H. & Nasekhian, A. (2010)
Random Set Finite Element Method - Application to Tunnelling. Proceedings of the 4th international workshop on reliable engineering computing, robust design – coping with hazards, risk and uncertainty. Beer, Muhanna & Mullen (eds.). 3rd – 5th March, 2010. Singapur, Singapur. Research Publishing, 2010.

Sibson, R.H. (1977)
Fault rocks and fault mechanisms. J. Geol. Soc. London 133, pp. 191 – 231, 1977.

Singh, B. Jethwa J.L., Dube, A.K. & Singh, B. (1992)
Correlation between observed support pressure and rock mass quality. Tunnelling and Underground Space Technology 7, pp 59 – 74.

Singh, B., Goel, R.K., Jethwa, J.L. & Dube, A.K. (1997)
Support pressure assessment in arched underground openings through poor rock masses. Engineering Geology 48, pp. 59 – 81

Solak, T. (2006)
Influence of the geological features block size, shape and joint strength on the ground behaviour, PhD Thesis, Institute for Rock Mechanics and Tunnelling, Graz University of Technology, 2006.

Sönmez, H., Gokceoglu, C., Tuncay, E., Medley, E.W. & Nefeslioglu, H. (2004)
Relationships between volumetric block proportions and overall UCS of a volcanic Bimrock. Felsbau 22 (5). Pp. 27 – 34. Verlag Glückauf Essen. 2004.

Spang, K. (1988)
Beitrag zur rechnerischen Berücksichtigung vollvermörtelter Anker bei der Sicherung von Felsbauwerken in geschichtetem oder geklüftetem Gebirge. PhD Thesis. Ecole Polytechnique Federale de Lausanne, 1988.

Steindorfer, A.F. (1996)
Short Term Prediction of Rock Mass Behaviour in Tunnelling by Advanced Analysis of Displacement Monitoring Data. PhD thesis, Graz University of Technology, Austria. In Riedmüller, Schubert & Semprich (eds.): Schriftenreihe der Gruppe Geotechnik Graz, Heft 1. Graz, 1996

Sterpi, D. & Gioda, G. (2009)
Visco-plastic behaviour around advancing tunnels in squeezing rock, Rock Mechanics and Rock Engineering 42 (2009), Pp. 319 – 339. Elsevier, 2009

Stille, H. & Holmberg, M. (2008)
Observational method in rock engineering. 5th Asian Rock Mechanics Symposium, Majdi & Ghazvinian (eds.). 24th – 26th Novemver 2008, Teheran Iran. Pp. 156 – 166.

Sulem, J., Panet, M. & Guenot, A. (1987)
An analytical solution for time-dependent displacements in a circular tunnel, Int. J. Rock Mech. Min. Sci. & Geomech. Abstr. Vol 24, No. 3, pp. 155-164

Test report MUL (2006)
Ermittlung der rheologischen Parameter für Spritzbetonproben aus dem Koralmtunnel. Lehrstuhl für Geomechanik, Tunnelbau und konstruktiven Tiefbau. Montanuniversität Leoben. Leoben 2006.

Vigl, A., Schubert,W., Posch, P.,Walter, A. and Blümel, M. (2007)
Investigations for a convergence compatible lining system. Felsbau 25 (2007), No. 6, pp. 48–53. Verlag Glückauf Essen, 2007.

Volkmann, G. & Schubert, W. (2009)

Effects of Pipe Umbrella Systems on the Stability of the Working Area in Weak Ground Tunnelling. In Tham et al. (eds): Sinorock 2009: Rock characterization, Modelling and Engineering Design Methods, $19^{th} - 22^{nd}$ May 2009, Hong Kong.

Wagner, H., Handke, D., Matter, J., Fabbri, D. & Kaiper, K. (2009)

Concepts to overcome squeezing geological conditions at the Koralm tunnel. Geomechanics and Tunnelling 2 (2005). pp. 601 – 611. Ernst & Sohn Verlag, Berlin. 2009.

Yang, S. & Jiang, Y. (2010)

Triaxial mechanical creep behaviour of sandstone, Int. J. of Min. Sci and Technology 20 (2010), pp. 339 – 349. Elsevier. 2010.

Zienkiewicz, O.C. & Taylor, R.L. (2006)

The finite element method for solid and structural mechanics. Elsevier Butterworth – Heinemann, Amsterdam. 2006.